RAINFALL–RUNOFF PROCESSES
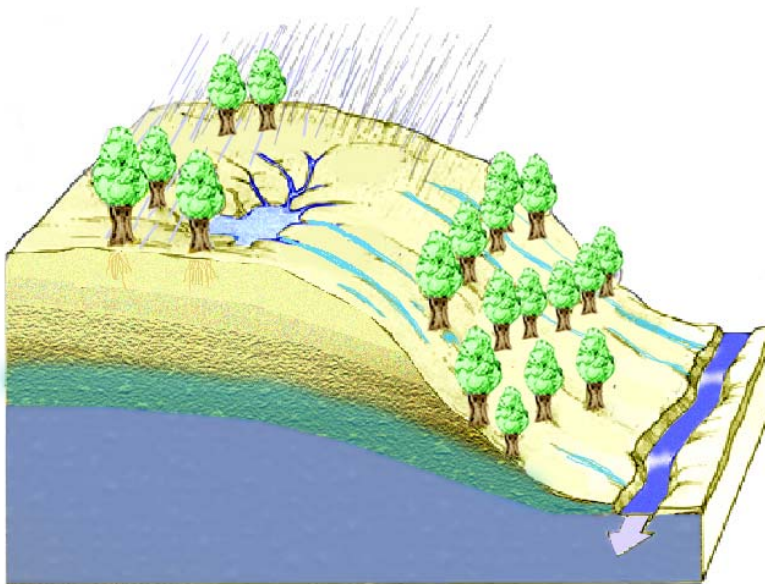
David G. Tarboton

A workbook to accompany the Rainfall-Runoff Processes Web
module.

http://www.engineering.usu.edu/dtarb/rrp.html

CONTENTS

PREFACE

This workbook accompanies an online module on Rainfall Runoff Processes developed for the National Weather Service COMET outreach program. The complete module includes:

- This workbook.
- Streaming video and slide presentations.
- Visualizations and computer animations to convey key concepts.
- Powerpoint presentations.
- Online quizzes serving as exercises where the user needs to respond to multiple choice questions or enter numeric answers to problems.
- An online final exam.

This module is designed to provide a comprehensive and quantitative understanding of infiltration and runoff generation processes. The module should take in 6-15 hours to complete depending on your quantitative background and a priori knowledge in this area. This module is targeted at students with a scientific or engineering background such professionals with a college degree in science or engineering, or seniors or graduate students in a hydrologic science or engineering program. No prior knowledge on Rainfall Runoff Processes is required.

This module consists of six sections each corresponding to a chapter in this workbook. This workbook is designed to be used in conjunction with the online resources and we recommend that you print out this work book to have on hand for reference as you work through the online resources in each section. The online material focuses on key graphics, visualizations and animations, with the substantive material given as text in this workbook. Resource links in the margin indicate where there is an online resource associated with the adjacent material.

See Online Resource

View the
Welcome Video

Resource link example

There is a quiz at the end of each chapter designed to reinforce your knowledge of the material covered in the section. The online quiz resource compares answers to the solution and provides feedback. There is also an online final exam accessible once each chapter quiz has been attempted.

The material in the early parts of the module is qualitative introducing the terminology and conceptual models involved in describing Rainfall Runoff processes. The latter parts of the module require users to perform quantitative calculations using a spreadsheet program such as Excel or an advanced engineering or scientific calculator.

The module is intended to be accessible to users with any current internet browser. Software used includes Adobe Acrobat Reader, Macromedia Flash Reader and Windows Media Player so the online resources are best accessed using a personal computer that has this software. The online module includes web links to obtain this software

Some of the animations and video use large files so a high speed internet connection is recommended.

Acknowledgements

CHAPTER 1
OVERVIEW AND RUNOFF PROCESSES

CHAPTER 1: OVERVIEW AND RUNOFF PROCESSES

An important question in hydrology is how much stream flow occurs in a river in response to a given amount of rainfall. To answer this question we need to know where water goes when it rains, how long does water reside in a watershed, and what pathway does water take to the stream channel. These are the questions addressed in the study of rainfall – runoff processes, or more generally surface water input – runoff processes. The term, "surface water input" is used in preference to rainfall or precipitation to be inclusive of snowmelt as a driver for runoff.

Answering the question of how much runoff is generated from surface water inputs requires partitioning water inputs at the earth surface into components that infiltrate and components that flow overland and directly enter streams. The pathways followed by infiltrated water need to be understood. Infiltrated water can follow subsurface pathways that take it to the stream relatively quickly, in which case it is called interflow or subsurface stormflow. Infiltrated water can also percolate to deep groundwater, which may sustain the steady flow in streams over much longer time scales that is called *baseflow*. Infiltrated water can also remain in the soil to later evaporate or be transpired back to the atmosphere. The paths taken by water determine many of the characteristics of a landscape, the occurrence and size of floods, the uses to which land may be put and the strategies required for wise land management. Understanding and modeling the rainfall – runoff process is therefore important in many flood and water resources problems. Figure 1 illustrates schematically many of the processes involved in the generation of runoff.

The rainfall – runoff question is also at the heart of the interface linking meteorology and hydrology. Quantifying and forecasting precipitation falls into the realm of meteorology and is part of the mission of the National Weather Service. Meteorological forcing is also a driver of snowmelt surface water inputs. River forecasting involves the use of meteorological variables as driving inputs to the surface hydrology system to obtain streamflow. The temporal and spatial scales associated with surface water inputs, given as output from meteorological processes have profound effects on the hydrological processes that partition water inputs at the earth surface. High intensity short duration rainfall is much more likely to exceed the capacity of the soil to infiltrate water and result in overland flow than a longer less intense rainfall. In arid climates with deep water

See Online Resource

View the
Welcome Video

See Online Resource

See how to use this
module

See Online Resource

View the
Learning Goals

tables, spatially concentrated rainfall on a small area may generate local runoff that then infiltrates downriver, whereas a more humid area with shallow water tables is less likely to be subject to stream infiltration losses and even gentle rainfall when widespread and accumulated over large areas may lead to large stream flows.
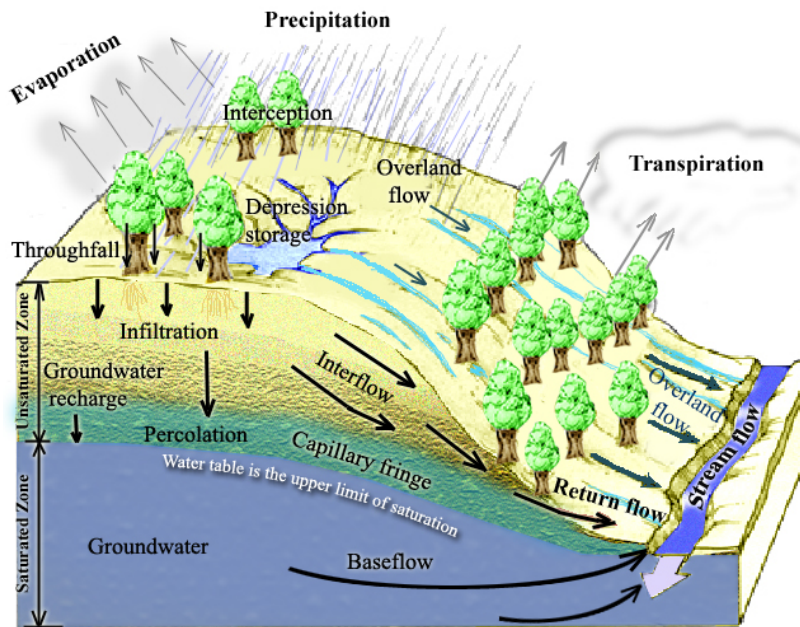
Figure 1. Physical Processes involved in Runoff Generation.

This module will provide an elementary quantitative understanding of the processes involved in the transformation of surface water input to runoff at the earth surface. We will review the mechanisms involved in runoff generation and the pathways water takes moving to streams in different settings. Much of this review will provide the language and terminology used by hydrologists as a basis for qualitative understanding and description of the runoff processes. We will then consider the physical factors at the land surface that affect runoff, and present in depth the current understanding of runoff processes. Soils and soil properties are fundamental to the partitioning of water inputs at the earth surface, so we focus on quantification of soil attributes important for understanding infiltration and runoff generation processes. Quantifiable soil properties serve as the basis for a variety of mathematical models for the calculation of infiltration given surface water inputs, and for the partitioning of surface water input into runoff components. A

section of this module focuses on these at a point infiltration models. Soil properties and at a point infiltration models are the most quantitative part of this module and the equations and exercises are provided for the implementation and reinforcement of these concepts. Practical hydrologic models can rarely represent the at a point detail of rainfall – runoff processes, and tend to average or lump hydrologic response over large areas or watersheds. This lumping is at the heart of the scale problem that has received much attention in hydrologic research recently. Averaging is necessary for computational reasons as well as because it is difficult to measure and quantify the full spatial heterogeneity of soil properties involved in runoff generation. In practice rainfall runoff models rely on numerical and conceptual representations of the physical rainfall – runoff processes to achieve continuous runoff generation simulations. This module ends with a brief review of the simulation of runoff generation in hydrologic models using TOPMODEL (Beven et al., 1995) and the National Weather Service River Forecast System (NWSRFS) as examples.

The student needs to recognize that rainfall – runoff processes in hydrology are an active and deep area of research with continually emerging new understanding. Entire books (e.g. Kirkby, 1978; Anderson and Burt, 1990) have been devoted to the subject, as well as recent conferences (AGU Chapman conference on Hillslope Hydrology, 2001, Sun River, Oregon, http://www.agu.org/meetings/cc01ecall.html) and journals (Uhlenbrook et al., 2003). The student is referred to good texts that include sections on rainfall – runoff processes for a deeper understanding (Dunne and Leopold, 1978; Linsley et al., 1982; Chow et al., 1988; Bras, 1990; Beven, 2000; Dingman, 2002).

Runoff Processes

The paths water can take in moving to a stream are illustrated in Figure 1. Precipitation may be in the form of rain or snow. Vegetation may *intercept* some fraction of precipitation. Precipitation that penetrates the vegetation is referred to as *throughfall* and may consist of both precipitation that does not contact the vegetation, or that drops or drains off the vegetation after being intercepted. A large fraction of intercepted water is commonly evaporated back to the atmosphere. There is also flux of water to the atmosphere through transpiration of the vegetation and evaporation from soil and water bodies. The surface water input available for the generation of runoff consists of throughfall and snowmelt. This

See Online Resource

Further Study

See Online Resource

Runoff Process Puzzle

surface water input may accumulate on the surface in *depression storage*, or flow overland towards the streams as *overland flow*, or *infiltrate* into the soil, where it may flow laterally towards the stream contributing to *interflow*. Infiltrated water may also *percolate* through deeper soil and rock layers into the *groundwater*. The *water table* is the surface below which the soil and rock is saturated and at pressure greater than atmospheric. This serves as the boundary between the saturated zone containing groundwater and unsaturated zone. Water added to the groundwater is referred to as *groundwater recharge*. Immediately above the water table is a region of soil that is close to saturation, due to water being held by capillary forces. This is referred to as the *capillary fringe*. Lateral drainage of the groundwater into streams is referred to as *baseflow*, because it sustains streamflow during rainless periods. Subsurface water, either from interflow or from groundwater may flow back across the land surface to add to overland flow. This is referred to as *return flow*. Overland flow and shallower interflow processes that transport water to the stream within the time scale of approximately a day or so are classified as *runoff*. Water that percolates to the groundwater moves at much lower velocities and reaches the stream over longer periods of time such as weeks, months or even years. The terms quick flow and delayed flow are also used to describe and distinguish between runoff and baseflow. Runoff includes *surface runoff* (overland flow) and *subsurface runoff* or *subsurface stormflow* (interflow).

Exercises

1. Label the Rainfall-Runoff processes depicted in the figure
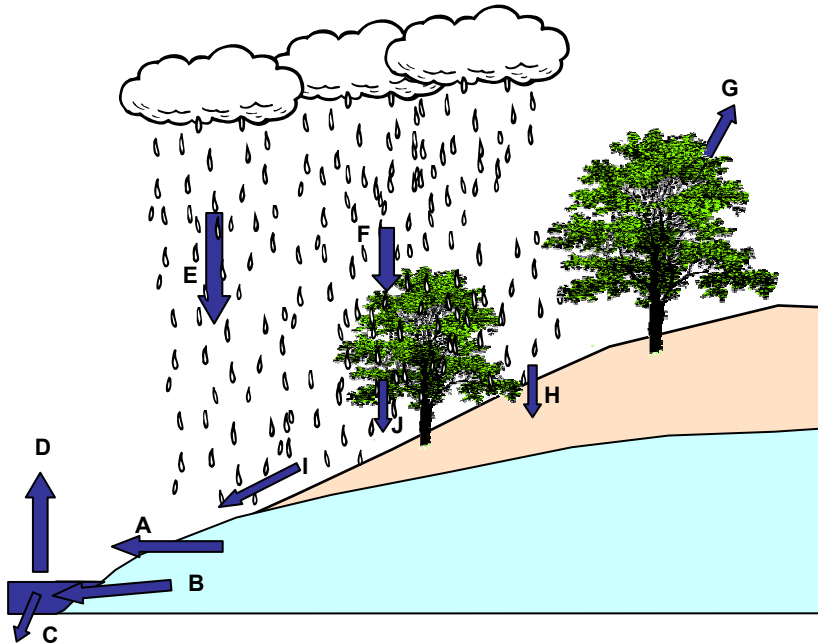
Infiltration	
Return flow	
Overland flow	
Base flow	
Interception	
Throughfall	
Precipitation	
Evaporation	
Transpiration	
Streamflow	

2. Label the locations depicted in the figure associated with runoff generation processes
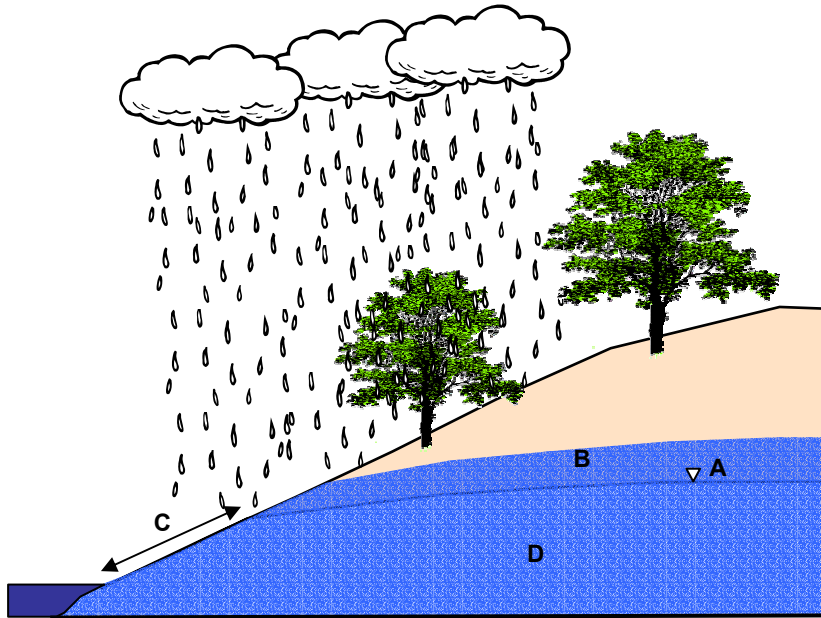
Water Table	
Groundwater	
Capillary Fringe	
Variable Source Area for saturation excess overland flow	

References

Anderson, M. G. and T. P. Burt, ed. (1990), <u>Process Studies in Hillslope Hydrology</u>, John Wiley, Chichester.

Beven, K., R. Lamb, P. Quinn, R. Romanowicz and J. Freer, (1995), "Topmodel," Chapter 18 in <u>Computer Models of Watershed Hydrology</u>, Edited by V. P. Singh, Water Resources Publications, Highlands Ranch, Colorado, p.627-668.

Beven, K. J., (2000), <u>Rainfall Runoff Modelling: The Primer</u>, John Wiley, Chichester, 360 p.

Bras, R. L., (1990), <u>Hydrology, an Introduction to Hydrologic Science</u>, Addison-Wesley, Reading, MA, 643 p.

Chow, V. T., D. R. Maidment and L. W. Mays, (1988), <u>Applied Hydrology</u>, McGraw Hill, 572 p.

Dingman, S. L., (2002), <u>Physical Hydrology</u>, 2nd Edition, Prentice Hall, 646 p.

Dunne, T. and L. B. Leopold, (1978), <u>Water in Environmental Planning</u>, W H Freeman and Co, San Francisco, 818 p.

Kirkby, M. J., ed. (1978), <u>Hillslope Hydrology</u>, John Wiley, Chichester, 389 p.

Linsley, R. K., M. A. Kohler and J. L. H. Paulhus, (1982), <u>Hydrology for Engineers</u>, 3rd Edition, McGraw-Hill, New York, 508 p.

Uhlenbrook, S., J. McDonnell and C. Leibundgut., ed. (2003), <u>Runoff Generation and Implications for River Basin Modelling</u>, Hydrological Processes Special Issue 17(2), 197-493.

Chapter 2
Runoff Generation Mechanisms

CHAPTER 2: RUNOFF GENERATION MECHANISMS

Figure 2 depicts a cross section through a hillslope that exposes in more detail the pathways infiltrated water may follow. Infiltrated water may flow through the matrix of the soil in the inter-granular pores and small structural voids. Infiltrated water may also flow through larger voids referred to as *macropores*. Macropores include pipes that are open passageways in the soil caused by decaying roots and burrowing animals. Macropores also include larger structural voids within the soil matrix that serve as preferential pathways for subsurface flow. The permeability of the soil matrix may differ between soil horizons and this may lead to the build up of a saturated wedge above a soil horizon interface. Water in these saturated wedges may flow laterally through the soil matrix, or enter macropores and be carried rapidly to the stream as subsurface stormflow in the form of interflow.

See Online Resource

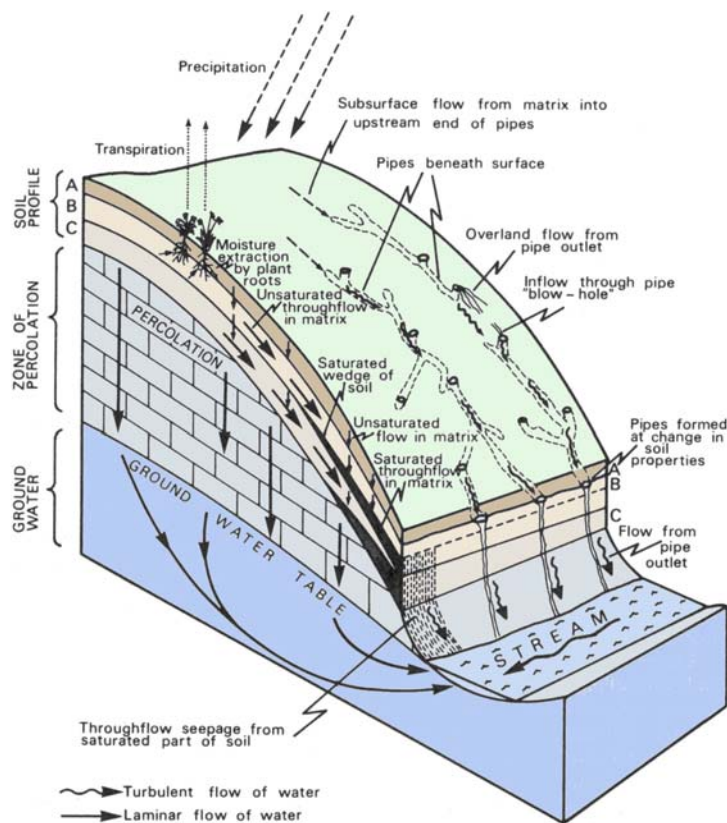Overview of processes involved in runoff generation

Figure 2. Pathways followed by subsurface runoff on hillslopes. (From Kirkby, 1978)

Recent research in hillslope hydrology involving tracers, especially in humid catchments has found that the dominant contributor to stormflow in the stream is pre-event water (averaging 75% world wide, Buttle, 1994). Pre-event water is water that was present in the hillslope before the storm as identified by a distinct isotopic or chemical composition. Another consensus emerging from recent research is that interflow involving preferential flow through macropores is a ubiquitous phenomenon in natural soils. Rapid lateral flow through a network of macropores and the effusion of old water into stream channels is the primary mechanism for runoff generation in many humid regions where overland flow is rarely observed. This mechanism has been linked to nonlinear threshold type behavior in hillslope runoff response. Figure 3 shows how runoff ratio, the fraction of precipitation that appears as runoff, is dependent upon soil moisture content. Soil moisture content needs to exceed a threshold before any significant runoff occurs. Figure 4 shows the relationship between depth to groundwater and runoff at two different hillslope locations (Seibert et al., 2003) that also shows threshold behavior, with runoff being more tightly related to depth to groundwater near the stream than further up a hillslope.
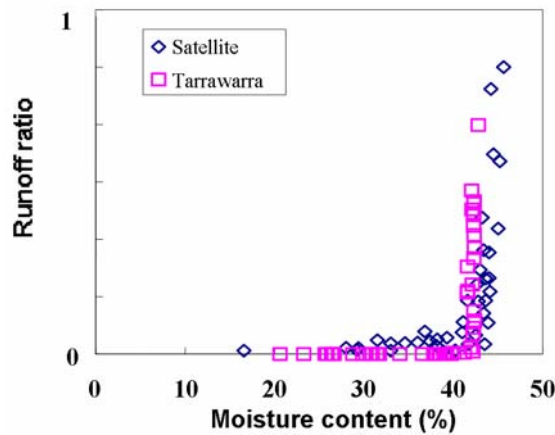
Figure 3. Relationship between runoff ratio and soil moisture content (Woods et al., 2001, Copyright, 2001, American Geophysical Union, reproduced by permission of American Geophysical Union).

See Online Resource

Animation of Preferential
Pathway Infiltration

Natural soils contain heterogeneities that lead to variability in the infiltration process itself. Infiltrating water follows preferential pathways and macropores and may result in increases in moisture content at depth before saturation or similar increases in moisture content higher in the soil profile. Figure 5a shows a photograph of a

soil where dye has been used to trace infiltration pathways in experiments reported by Weiler and Naef (2003). Figure 5b shows the dye intensity objectively classified from the photograph following excavation of the plot following a dye sprinkling experiment. Figure 5c shows moisture content over time measured at a range of depths using time domain reflectometry in these sprinkler experiments.
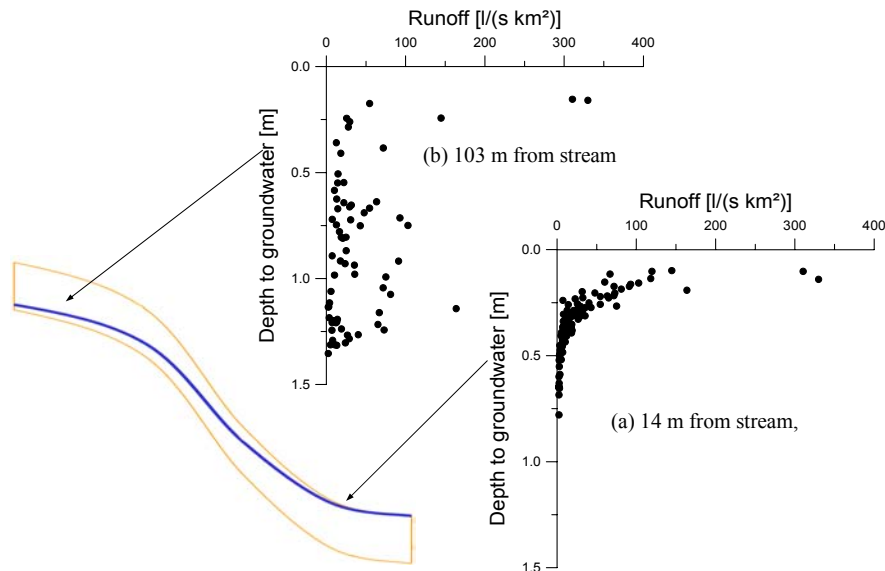
Figure 4. Relation between runoff and depth to groundwater for two different locations in the Svartberget catchment (Seibert et al., 2003, Copyright, 2003, American Geophysical Union, reproduced by permission of American Geophysical Union)

With this background on the pathways followed by infiltrated water we can examine the mechanisms involved in the generation of runoff (Figure 6). Each mechanism has a different response to rainfall or snowmelt in the volume of runoff produced, the peak discharge rate, and the timing of contributions to streamflow in the channel. The relative importance of each process is affected by climate, geology, topography, soil characteristics, vegetation and land use. The dominant process may vary between large and small storms.

Figure 5. (a) Photograph of cross section through soil following dye tracing experiment (Courtesy of Markus Weiler).
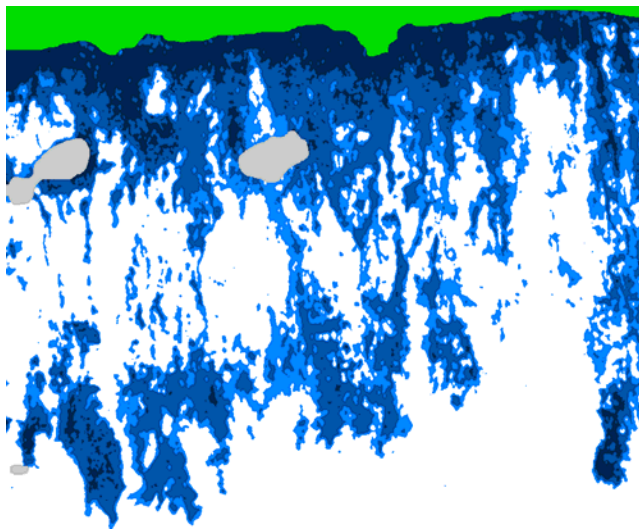
Figure 5. (b) Objectively classified dye intensity following sprinkler experiment. (Courtesy of Markus Weiler)
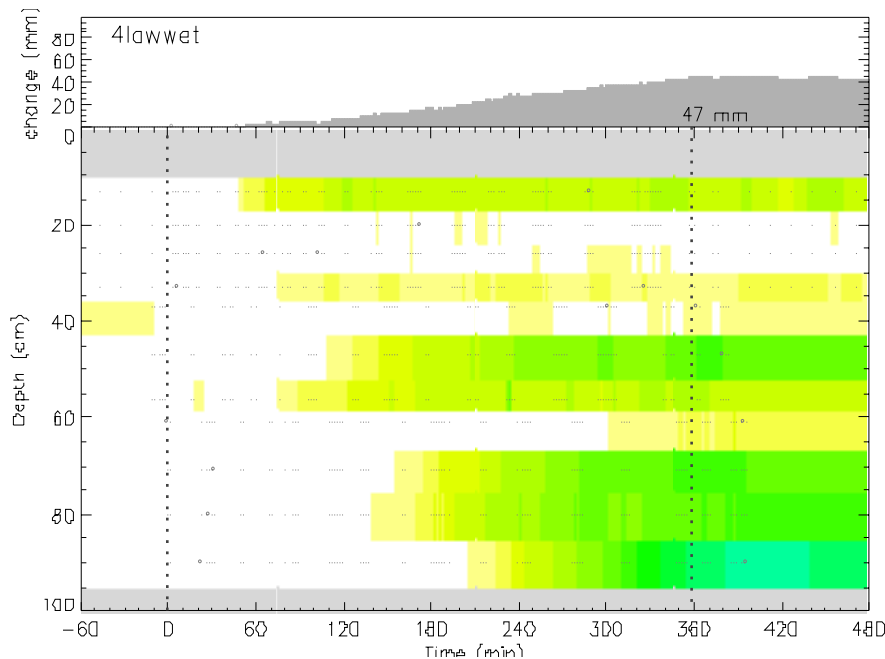
Figure 5. (c) Moisture content change measured using time domain reflectometry during sprinkler experiment. (Courtesy of Markus Weiler)

In Figure 6a the *infiltration excess* overland flow mechanism is illustrated. There is a maximum limiting rate at which a soil in a given condition can absorb surface water input. This was referred to by Robert E. Horton (1933), one of the founding fathers of quantitative hydrology, as the *infiltration capacity* of the soil, and hence this mechanism is also called Horton overland flow. Infiltration capacity is also referred to as *infiltrability*. When surface water input exceeds infiltration capacity the excess water accumulates on the soil surface and fills small depressions. Water in depression storage does not directly contribute to overland flow runoff; it either evaporates or infiltrates later. With continued surface water input, the depression storage capacity is filled, and water spills over to run down slope as an irregular sheet or to converge into rivulets of overland flow. The amount of water stored on the hillside in the process of flowing down slope is called *surface detention*. The transition from depression storage to surface detention and overland flow is not sharp, because some depressions may fill and contribute to overland flow before others. Figure 7 illustrates the response, in terms of runoff from a hillside plot due to rainfall rate exceeding infiltration capacity with the filling of depression storage and increase in, and draining of, water in

See Online Resource

Animations of Infiltration Excess Runoff Generation

surface detention during a storm. Note, in Figure 7, that infiltration capacity declines during the storm, due to the pores being filled with water reducing the capillary forces drawing water into pores.

Due to spatial variability of the soil properties affecting infiltration capacity and due to spatial variability of surface water inputs, infiltration excess runoff does not necessarily occur over a whole drainage basin during a storm or surface water input event. Betson (1964) pointed out that the area contributing to infiltration excess runoff may only be a small portion of the watershed. This idea has become known as the *partial-area* concept of infiltration excess overland flow and is illustrated in Figure 6b.

Infiltration excess overland flow occurs anywhere that surface water input exceeds the infiltration capacity of the surface. This occurs most frequently in areas devoid of vegetation or possessing only a thin cover. Semi-arid rangelands and cultivated fields in regions with high rainfall intensity are places where this process can be observed. It can also be seen where the soil has been compacted or topsoil removed. Infiltration excess overland flow is particularly obvious on paved urban areas.

In most humid regions infiltration capacities are high because vegetation protects the soil from rain-packing and dispersal, and because the supply of humus and the activity of micro fauna create an open soil structure. Under such conditions surface water input intensities generally do not exceed infiltration capacities and infiltration excess runoff is rare. Overland flow can occur due to surface water input on areas that are already saturated. This is referred to as *saturation excess* overland flow, illustrated in Figure 6c. Saturation excess overland flow occurs in locations where infiltrating water completely saturates the soil profile until there is no space for any further water to infiltrate. The complete saturation of a soil profile resulting in the water table rising to the surface is referred to as *saturation from below*. Once saturation from below occurs at a location all further surface water input at that location becomes overland flow runoff.

See Online Resource

Animation of Saturation Excess Runoff Generation
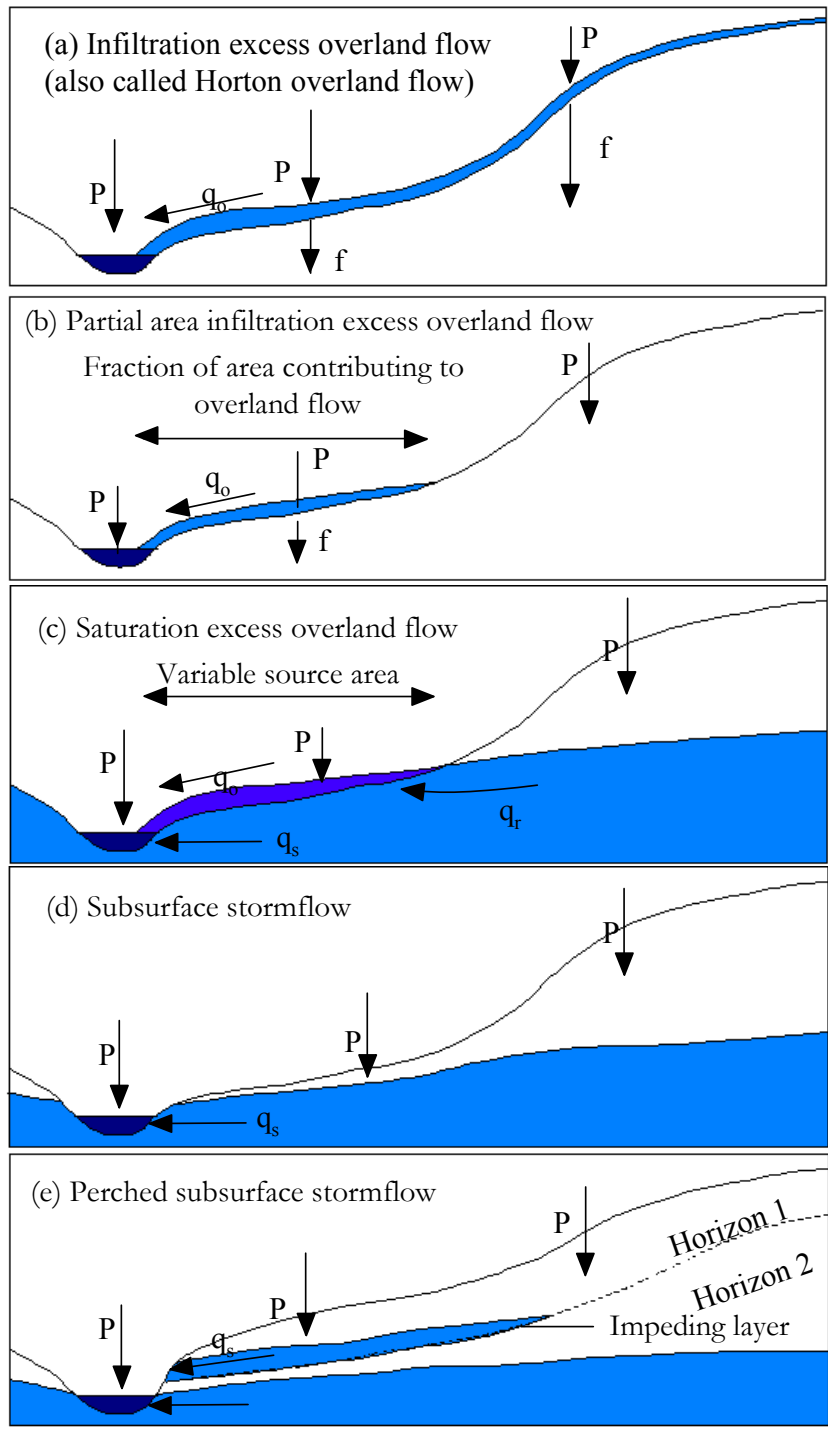
Figure 6. Classification of runoff generation mechanisms
(following Beven, 2000)
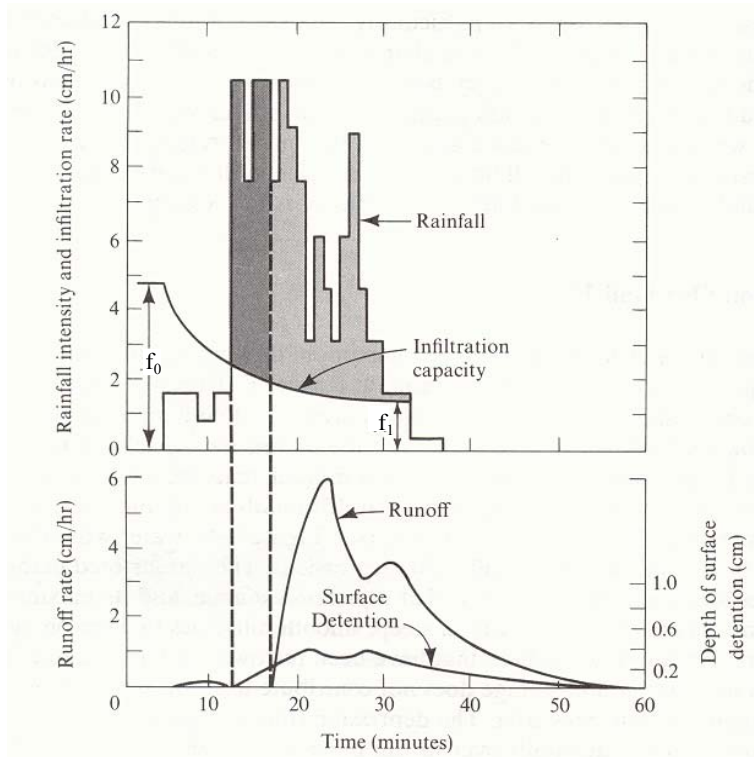
Figure 7. Rainfall, runoff, infiltration and surface storage during a natural rainstorm. The shaded areas under the rainfall graph represent precipitation falling at a rate exceeding the infiltration rate. The dark grey area represents rainfall that enters depression storage, which is filled before runoff occurs. The light grey shading represents rainfall that becomes overland flow. The initial infiltration rate is f_0, and f_1 is the final constant rate of infiltration approached in large storms (from Water in Environmental Planning, Dunne and Leopold, 1978).

In humid areas streams are typically gaining streams (gaining water by drainage of baseflow from the groundwater into the stream) with the groundwater table near the surface coincident or close to the stream water surface elevation. This means that the water table near streams is close to the ground surface, especially in flat topography, making these near stream areas in flat topography particularly susceptible to saturation from below. The extent of the area subject to saturation from below varies in time, both at seasonal and event time scales due to fluctuations in the depth to the shallow water table. This variability of the extent of surface saturation is referred to as the *variable source area* concept (Hewlett and Hibbert, 1967) and is illustrated in Figures 8 and 9.

Geometrical considerations dictate that near stream saturated zones will be most extensive in locations with concave hillslope profiles and wide flat valleys. However, saturated overland flow is not restricted to near-stream areas. Saturation from below can also occur (1) where subsurface flow lines converge in slope concavities (hillslope hollows) and water arrives faster than it can be transmitted down slope as subsurface flow; (2) at concave slope breaks where the hydraulic gradient inducing subsurface flow from upslope is greater than that inducing down slope transmission; (3) where soil layers conducting subsurface flow are locally thin; and (4) where hydraulic conductivity decreases abruptly or gradually with depth and percolating water accumulates above the low-conductivity layers to form perched zones of saturation that reach the surface.
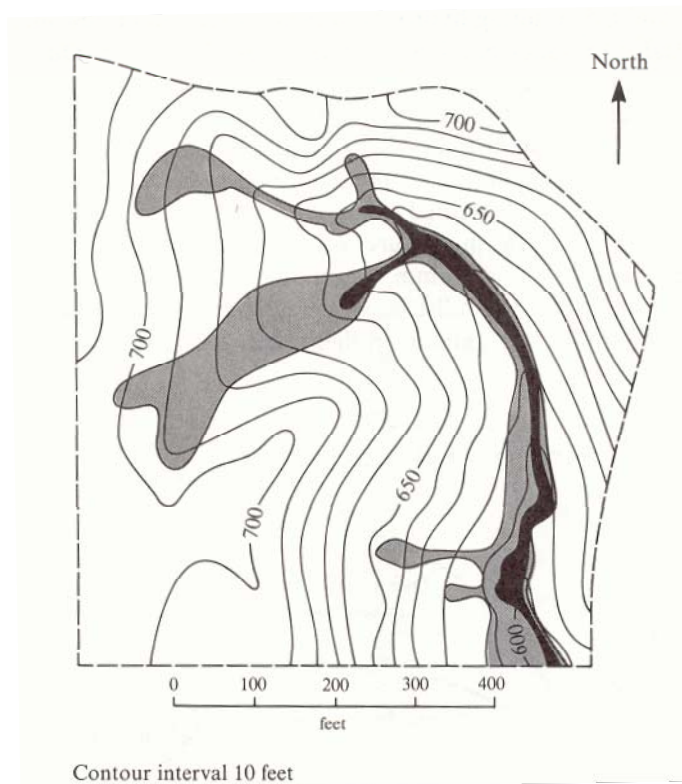
Figure 8. Map of saturated areas showing expansion during a single rainstorm. The solid black shows the saturated area at the beginning of the rain; the lightly shaded area is saturated by the end of the storm and is the area over which the water table had risen to the ground surface (from Water in Environmental Planning, Dunne and Leopold, 1978)

Return flow (q$_r$ in Figure 6c) is subsurface water that returns to the surface to add to overland flow. Return flow also occurs at places where the soil thins, for example rock outcrops and may manifest in the form of springs.

In areas with high infiltration capacities, interflow, or subsurface storm flow is usually the dominant contributor to streamflow, especially on steeper terrain or more planar hillslopes where saturation excess is less likely to occur. A number of processes are involved in rapid subsurface stormflow. These include *transmissivity feedback*, *lateral flow at the soil bedrock interface* and *groundwater ridging*.

See Online Resource

Animation of Subsurface Stormflow

Contour interval 10 feet

■ Summer ▨ Immediately after snowmelt period

▨ Autumn
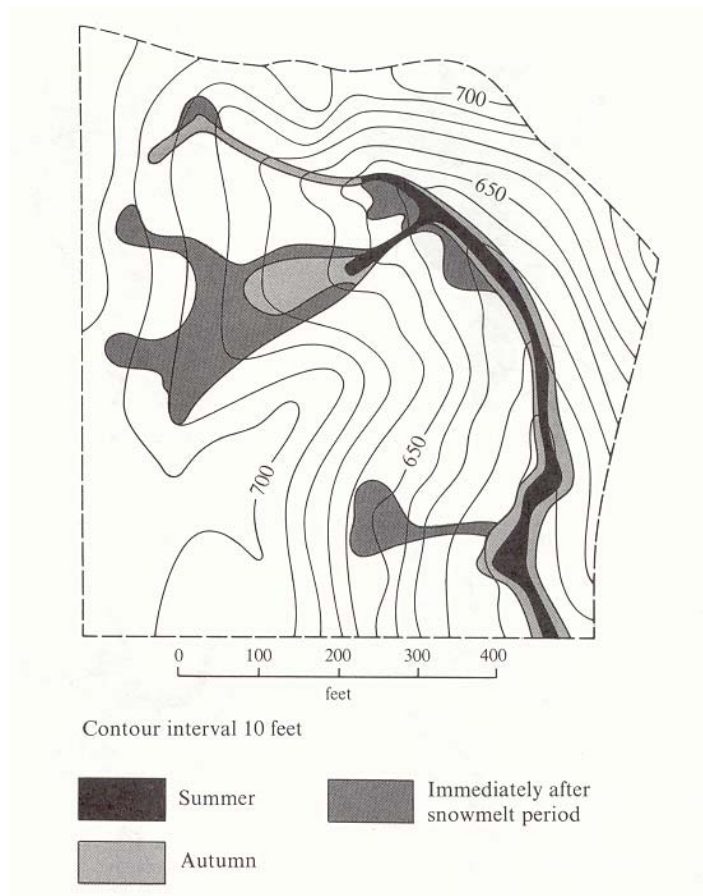
Figure 9. Seasonal variation in pre-storm saturated area (from Water in Environmental Planning, Dunne and Leopold, 1978)

Transmissivity feedback (Weiler and McDonnell, 2003) is illustrated in Figure 10 and occurs when water infiltrates rapidly along preferential pathways and causes the groundwater to rise to the point where highly permeable soil layers or macropore networks become activated and transmit water rapidly downslope. Much of the water that drains from the soil matrix into the macropore network is pre-event water. This mechanism results in a nonlinear threshold like response as illustrated in Figures 3 and 4.
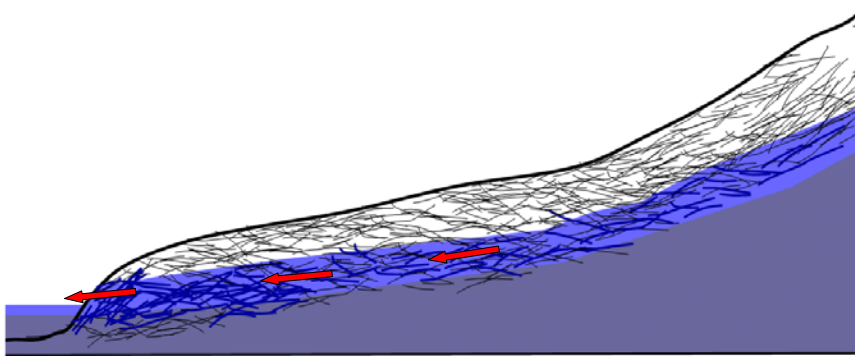
Figure 10. Schematic illustration of macropore network being activated due to rise in groundwater resulting in rapid lateral flow.

Lateral flow at the soil bedrock interface (Weiler and McDonnell, 2003) illustrated in Figure 11, occurs in steep terrain with relatively thin soil cover and low permeability bedrock, where water moves to depth rapidly along preferential infiltration pathways and perches at the soil-bedrock interface. Since moisture content near the bedrock interface is often close to saturated, the addition of only a small amount of new water (rainfall or snowmelt) is required to produce saturation at the soil-bedrock or soil-impeding layer interface. Rapid lateral flow occurs at the permeability interface through the transient saturated zone. Once rainfall inputs cease, there is a rapid dissipation of positive pore water pressures and the system reverts back to a slow drainage of matrix flow.

See Online Resource

Animation of Perched layer stormflow
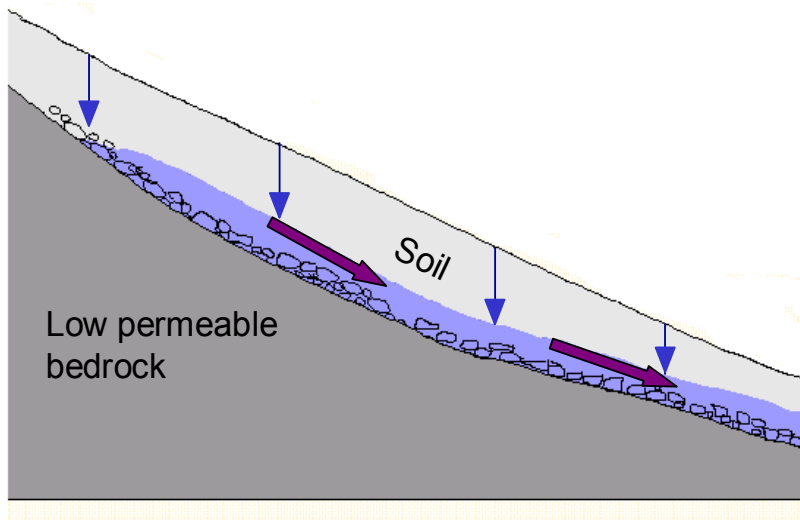
Figure 11. Rapid lateral flow at soil bedrock interface.

The processes involved in the generation of subsurface stormflow by groundwater ridging are illustrated in Figure 12. An idealized cross section of a valley with a straight hillslope is shown. In a simplified situation with uniform soils the water table has an approximately parabolic form, and soil moisture content decreases with increasing height above the water table. The shaded areas represent graphs of soil moisture at the base, middle and near the top of the hillslope (a) before the onset of rainfall; (b) as an initial response to rainfall; and (c) after continuing rainfall. Because (in a) before the onset of water input the water table slopes gently towards the channel there will be a slow flow of groundwater to maintain the baseflow of the stream. With the onset of surface water input, water that infiltrates near the base of the hillslope will quickly reach the water table and cause the water table near the stream to rise, early in a storm. Further upslope the soil is dryer and distance to the water table greater. It therefore takes longer for infiltrating water to reach the water table and where the water table is deep all the infiltrating water may go into storage in the unsaturated zone and not reach the water table for many days after the storm. The initial response to water input is therefore as depicted in Figure 12b, where the water table has risen near the stream but remained unchanged further upslope. The rising water table near the stream causes an increase in the hydraulic gradient between the groundwater and stream, and increased subsurface flow into the stream results. This is subsurface stormflow, and is frequently seen to be groundwater that has been displaced by the infiltrating water, and is thus old or pre-storm water bearing the

chemical and isotopic signature of water in the hillslope prior to the storm, which may be different from the chemical and isotopic signature of overland flow from rainwater that has not infiltrated. Measurement of chemical and isotopic signatures of stream water, ground water and rain water is commonly used in hydrology as a way of inferring hillslope flow pathways. After continuing rain (Figure 12c), the water table has risen to the surface over the lower part of the hillslope and the saturated area is expanding uphill. Some water emerges from this saturated area and runs down slope to the stream. This is termed *return flow*. Direct precipitation onto the saturated zone (DPS) forms saturation excess runoff as described above.
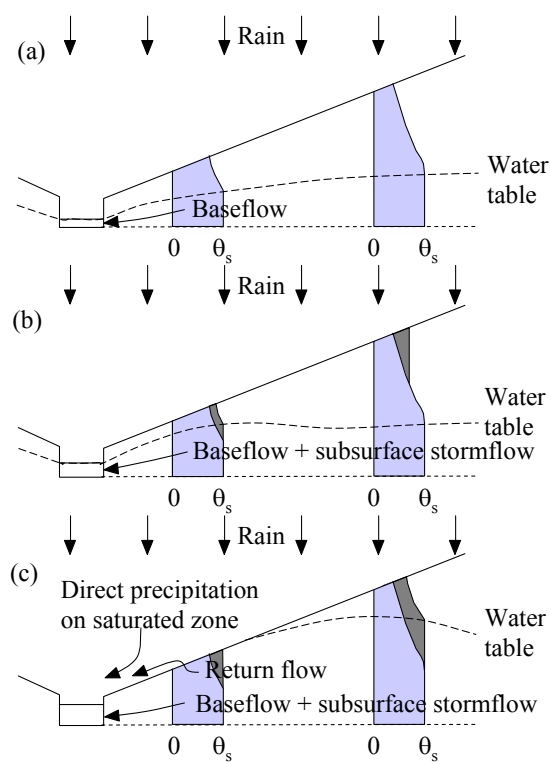
Figure 12. Groundwater ridging subsurface stormflow processes in an area of high infiltration rate. (redrawn following Water in Environmental Planning, Dunne and Leopold, 1978)

Figure 12 illustrates a region just above the water table that was close to saturation. This is known as the *capillary fringe*, and can play an important role in runoff generation in certain situations. Capillary forces due to the surface tension between water and soil particles act to pull water into the soil matrix above the water table and maintain the capillary fringe at moisture content very close to saturation. The

addition of a small amount of water can saturate this soil and cause the water table to rise quite rapidly, resulting in subsurface stormflow, surface saturation and saturation excess overland flow. The moisture content in the capillary fringe can also be affected by the history of wetting and drying of the soil, a phenomenon known as *hysteresis*. When soil has been draining the moisture content tends to remain above what it would be if it were filling at the same pressure. The addition of a small amount of water can switch the soil from draining to filling mode, enhancing the effect of the capillary fringe on the rise of the water table and subsurface stormflow response. The capillary fringe and hysteresis are discussed in more detail in Chapter 4.

The discussion thus far has focused on the main processes involved in runoff generation on a hillslope. To complete the discussion on runoff generation processes it is necessary to mention briefly some other processes and factors involved. Interception of precipitation by vegetation can play a significant role in reducing runoff, especially in forested environments. Much intercepted water is eventually evaporated back to the atmosphere (Figure 1). In some hydrologic models, interception is sometimes modeled as an *initial abstraction* that is subtracted from precipitation inputs before they are used in infiltration or runoff calculations. In other hydrologic models detailed representations of the interception, storage of water in the canopy, throughfall or stem flow are used (e.g. Rutter et al., 1972).

Direct precipitation onto a stream or water body also contributes to runoff as indicated in Figure 6. This is important in areas where the water surface is extensive, as with lakes, reservoirs and floodplains that are flooded, because in these situations runoff generation is not delayed by the usual hillslope processes.

The freezing state of the soil, in regions where freezing occurs, also plays a role in runoff generation. Infiltration capacity is reduced due to frozen ground, depending upon the soil moisture content at the time of freezing.

Fire results in water repellency by soils which reduces infiltration capacity. One cause for water repellency is chemicals released during a fire that are absorbed in the soil, and can make it water repellent for months to years following a fire. The heat from fire also removes the thin films of irreducable water adhered to soil particles by capillary forces, disconnecting potential flow paths. Penetration of water into macropores following a fire is limited due to this effect. High temperatures in deserts have the same effect, adding to the tendency

for infiltration capacities to be lower in arid regions making them more subject to infiltration excess runoff generation processes. This water repellency due to fire has been implicated in many floods following severe bush or forest fires.

Many of the runoff generation processes described depend on the soil moisture status of the soil. This is referred to as the *antecedent conditions*. Between storms (surface water input events), processes of evaporation, transpiration, percolation and drainage serve to set up the soil moisture antecedent conditions. Runoff generation mechanisms and processes therefore depend not only on conditions during storms, but conditions in advance of storms and a complete understanding or representation of all the land surface hydrologic processes is required to quantify the generation of runoff. Recognition of this has led to the development of continuous simulation models, such as the National Weather Service Sacramento soil moisture accounting model that keeps continuous track of the state of different soil moisture components for the modeling of runoff. Detailed presentation of these models is beyond the scope of this module, although key ideas are reviewed at the end of this model.

The discussion above has reviewed, in a conceptual way many of the processes and mechanisms involved in runoff generation. These can be quite complex, and when efforts are made to perform quantitative calculations the devil is in the details. Each watershed or hillslope is different, with different topography, soils and physical properties. The challenge for hydrologic modelers is to balance practical simplifications with justifiable model complexity and the knowledge that many specific physical properties required for detailed hydrologic modeling are physically unknowable. Our understanding of runoff generation involves the movement of water through soil pores and macropores. These flows follow the physical laws governing fluid flow (Navier Stokes equations) but we can never know in sufficient detail the flow geometry to make use of fluid flow theory and ultimately have to resort to simplifications or parameterizations of the runoff generation processes. In the remainder of this module the astute reader will note discrepancies between the physical understanding given above and mathematical descriptions used to perform practical calculations. The mathematical descriptions, although frequently complex, incorporate significant simplifications relative to the field based conceptual understanding of how runoff processes work. This gap between field based and model based representations makes the subject of rainfall – runoff processes a

fertile area for research to learn how to better model rainfall runoff processes.

Figure 13 summarizes the main processes involved in runoff generation, showing the interaction between infiltration excess, saturation excess and groundwater flow pathways. Most rainfall runoff models are organized around a representation similar to Figure 13 involving partition of surface water input into infiltration or overland flow, either due to infiltration excess or saturation excess. Infiltrated water enters the soil regolith where it contributes to interflow, percolates to deeper groundwater or is evaporated or transpired back to the atmosphere. The quantity of water in the soil affects the variable source area involved in the generation of saturation overland flow. The deeper groundwater contributes to baseflow and affects interflow through groundwater rise.

Figure 13. Hydrological Pathways involved in different runoff generation processes. Infiltration excess pathways are shown in red. Saturation excess and subsurface stormflow pathways are shown in blue. Groundwater and baseflow pathways in black and Evapotranspiration is green. (Courtesy of Mike Kirkby)
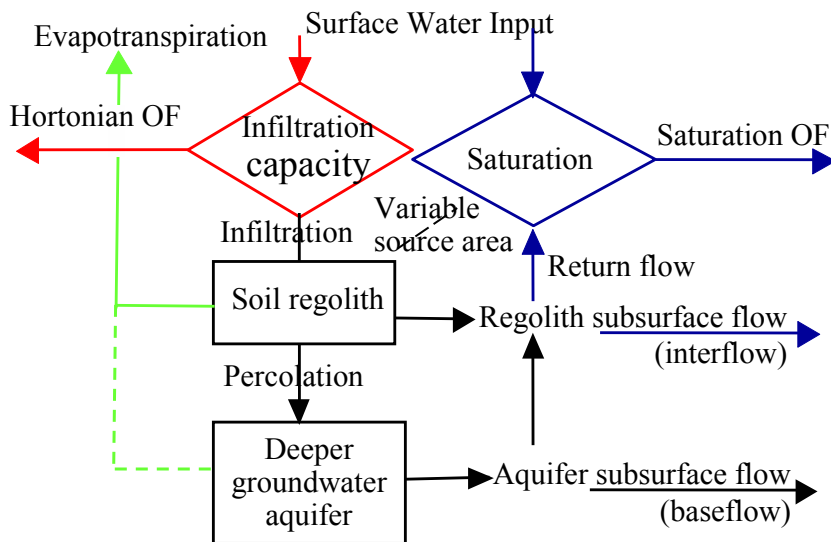
See Online Resource

View the Chapter 2 Summary

Exercises

1. Given the topographic map from Logan Canyon below, indicate the location where saturation excess overland flow is most likely to be generated during rainfall (from labeled locations, A, B, C, D, E): _____
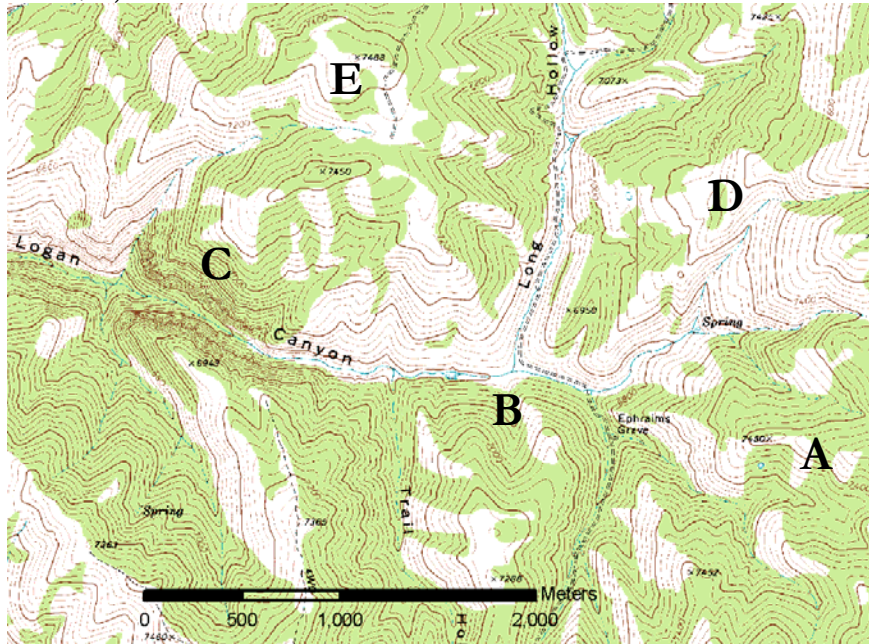
2. Infiltration capacity is:
   A. The number of foreign spies that a country can tolerate
   B. The rate of water input to a stream by subsurface flow
   C. The fraction of watershed area contributing to overland flow
   D. The maximum rate at which water can be absorbed into soil
   E. The water holding capacity of surface depressions

3. Subsurface stormflow is likely to be larger in:
   A. A steep narrow valley
   B. A wide flat valley

References

Betson, R. P., (1964), "What Is Watershed Runoff?," <u>Journal of Geophysical Research</u>, 68: 1541-1552.

Beven, K. J., (2000), <u>Rainfall Runoff Modelling: The Primer</u>, John Wiley, Chichester.

Buttle, J. M., (1994), "Isotope Hydrograph Separations and Rapid Delivery of Pre-Event Water from Drainage Basins," <u>Progress in Physical Geography</u>, 18(1): 16-41.

Dunne, T. and L. B. Leopold, (1978), <u>Water in Environmental Planning</u>, W H Freeman and Co, San Francisco, 818 p.

Hewlett, J. D. and J. R. Hibbert, (1967), "Factors Affecting the Response of Small Watersheds to Precipitation in Humid Areas," in <u>Forest Hydrology</u>, Edited by W. E. Sopper and H. W. Lull, Pergamon Press, New York, p.275-291.

Kirkby, M. J., ed. (1978), <u>Hillslope Hydrology</u>.

Rutter, A. J., K. A. Kershaw, P. C. Robins and A. J. Morton, (1972), "A Predictive Model of Rainfall Interception in Forests, 1. Derivation of the Model from Observations in a Plantation of Corsican Pine," <u>Agricultural Meteorology</u>, 9: 367-384.

Seibert, J., K. Bishop, A. Rodhe and J. J. McDonnell, (2003), "Groundwater Dynamics Along a Hillslope: A Test of the Steady State Hypothesis," <u>Water Resources Research</u>, 39(1): 1014, doi:10.1029/2002WR001404.

Weiler, M. and J. J. McDonnell, (2003), "Virtual Experiments: A New Approach for Improving Process Conceptualization in Hillslope Hydrology." Journal of Hydrology, in review.

Weiler, M. and F. Naef, (2003), "An Experimental Tracer Study of the Role of Macropores in Infiltration in Grassland Soils," <u>Hydrological Processes</u>, 17: 477-493, DOI: 10.1002/hyp.1136.

Woods, R. A., R. B. Grayson, A. W. Western, M. J. Duncan, D. J. Wilson, R. I. Young, R. P. Ibbitt, R. D. Henderson and T. A. McMahon, (2001), "Experimental Design and Initial Results from the

Mahurangi River Variability Experiment: Marvex," in <u>Observations and Modelling of Land Surface Hydrological Processes</u>, Edited by V. Lakshmi, J. D. Albertson and J. Schaake, Water Resources Monographs, American Geophysical Union, Washington, DC, p.201-213.

Chapter 3
Physical Factors Affecting Runoff

CHAPTER 3: PHYSICAL FACTORS AFFECTING RUNOFF

The general climatic regime controls the total volume of runoff in any region through its effect on the water balance. In a broad sense, over a time scale long enough that storage changes average out (are negligible), and over a region large enough or with boundary defined so that inflows (surface and subsurface) are negligible, the water balance may be stated as

$$P = Q + E \tag{1}$$

where P is the precipitation rate, Q the runoff rate, and E the evapotranspiration rate. This equation indicates that the precipitation input is disposed of either into runoff or evapotranspiration. In general the climatic regime controls the overall proportioning. Here groundwater recharge supplying baseflow is included in Q. Because the quantities in equation (1) must be positive, this equation places limits on the values of Q and E given any specific P. Both Q and E are constrained to be less than P. This may be visualized in a space where E is plotted versus P (Figure 14).
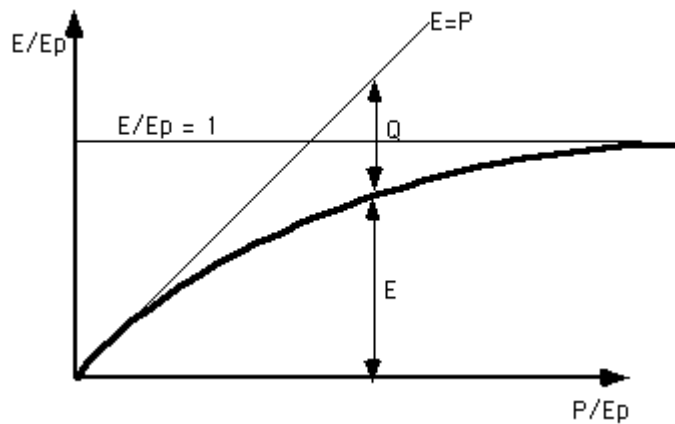
Figure 14. Water balance constraints on runoff and evaporation.

The domain of valid solutions is below the 1:1 line E=P. There is in general an upper limit on the possible evapotranspiration, due to the energy inputs required to evaporate water. This limit is related to the solar radiation inputs as well as the capacity of the atmosphere to transport evaporated water away from the surface (related to wind and humidity). This limit has been denoted as Ep (potential evapotranspiration) in Figure 14. The line E=Ep provides another upper limit to the domain of valid solutions. In general if

precipitation is large (P >> Ep) water is not going to be limited at the earth surface so E will approach Ep asymptotically for P tending to infinity. Also, if precipitation is small (P << Ep) water is very limited at the earth surface and may all evaporate, so E will approach the line E=P asymptotically as P tends to 0 approaching the origin. These constraints suggest a solution for the E versus P function of the form indicated in Figure 14. In Figure 14 the axes have been scaled by Ep to make them dimensionless. A nonlinear increase in Q with P as P/Ep increases is suggested, and the index P/Ep serves as an index of regional humidity or aridity, with P/Ep large (>1) in humid regions and small (<1) in arid regions.
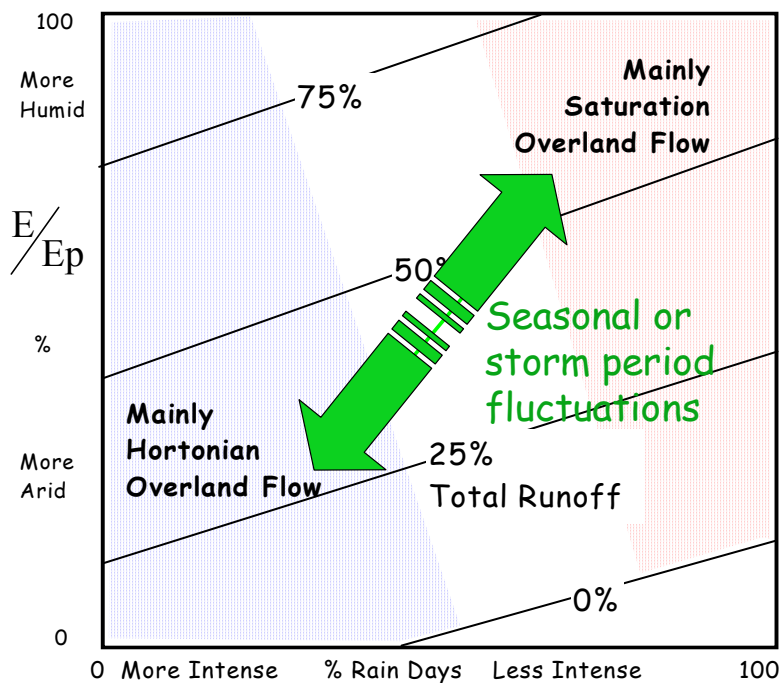
Figure 15. Generalised dependence of Runoff Coefficient and Style of Overland Flow on Arid-Humid scale and on Storm Rainfall Intensities (Courtesy of Mike Kirkby)

These regional water balance considerations based on climatic regime serve as first order controls on the generation of runoff. However data plotted in the form of Figure 14, shows scatter due to other effects. Precipitation intensity is also important. Figure 15 shows the interplay between humidity/aridity and precipitation intensity on runoff processes and the runoff coefficient. In this figure, similar to P/Ep the ratio E/Ep serves as a measure of aridity, with E/Ep

approaching 1 for humid regions. The runoff coefficient is defined as the ratio Q/P and expresses the percentage of total precipitation that becomes runoff.

There is also a scale affect associated with the regional water balance that is different for humid and arid regions. Figure 16, collated by David Goodrich (personal communication 2003) shows data for four different areas in the U.S. In semi-arid regions like Arizona the mean annual runoff decreases with drainage area due to channel transmission losses. Most runoff is infiltration excess and the opportunity for infiltration increases as water progresses down the channel network. Figure 17 shows an advancing flood wave over a dry channel bed in the Walnut Gulch experimental watershed where channel transmission losses are considerable. Walnut Gulch, the San Pedro and Reynolds Creek in Idaho are all semi-arid watersheds where transmission losses increase with drainage area. In contrast to this in humid regions, such as the Coshocton watershed in Ohio, mean annual runoff increases with drainage area due to groundwater flow. Basically water that infiltrates and recharges groundwater in small watersheds adds to the baseflow of larger watersheds.
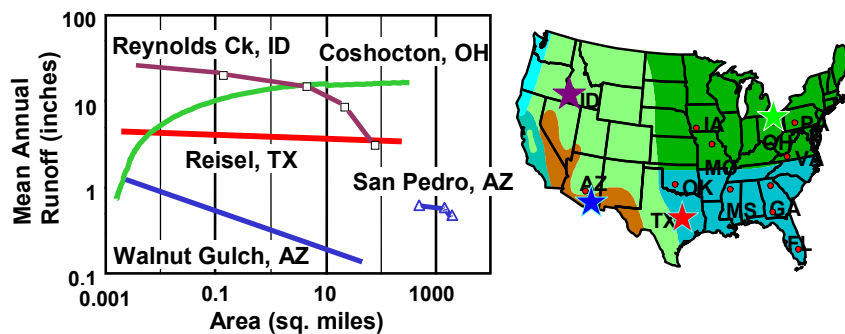
Figure 16. Scale dependence of mean annual runoff for different geographic locations in the U.S. (Courtesy of David Goodrich, USDA–ARS).

Following regional climatic regime and precipitation intensity, vegetation, land use, topography and soils, also exert controls on runoff processes. The following discussion based on Dunne and Leopold (1978) reviews these controls. Figure 18 summarizes the major controls on the various runoff processes. These vary with climate, vegetation, land use, soil properties, topography and rainfall characteristics. In arid and semi-arid regions and those disturbed by humans (through agriculture, urbanization and mining) infiltration

capacity is a limiting factor and infiltration excess is the dominant storm runoff process. In most humid regions where infiltration is not a limiting factor the variable source model of storm runoff is appropriate. There are important differences within and between humid regions in the relative importance of the two major runoff processes at work: subsurface stormflow and saturation overland flow.

Figure 17. Flood wave advancing over a dry streambed in Walnut Gulch experimental watershed where channel transmission losses are considerable (Courtesy of David Goodrich, USDA-ARS).

Where soils are well-drained, deep and very permeable, and cover steep hillsides bordering a narrow valley floor, subsurface stormflow dominates the volume of storm runoff. The saturated zone is more or less confined to the valley floor, and saturation overland flow is limited, though even in such situations, it frequently generates the peak rates of runoff from small catchments. Subsurface stormflow achieves its greatest importance in areas such as forested highlands; in deep permeable forested soils on volcanic tuffs and sandstones; and in deep, permeable volcanic ash deposits. In most other humid regions, where the saturated and near-saturated valley bottoms are more extensive, and where foot slopes are gentler and soils thinner, the saturated area is more extensive before and throughout a storm or snowmelt period. Although subsurface stormflow occurs in such regions, it is less important to the storm hydrograph than are return flow and direct precipitation onto saturated areas, which produce saturation overland flow from limited areas of the catchment. A range of topographic and pedologic conditions exist between those

that tend to produce a preponderance of subsurface stormflow and those that favor the occurrence of saturation overland flow. The saturated zones do not often cover more than half of a catchment, and usually cover much less. They are extremely important, however, for the generation of storm runoff and processes related to storm runoff.
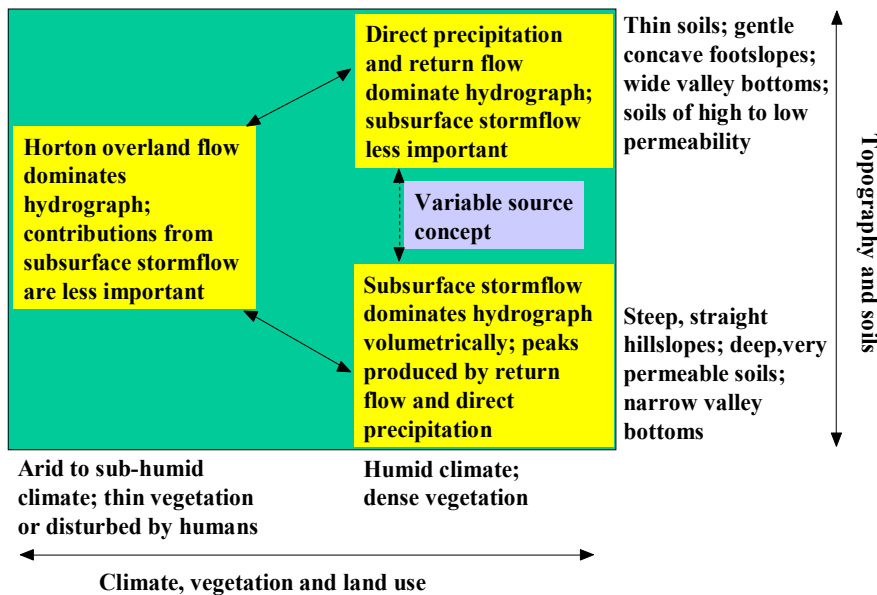
Figure 18. Runoff processes in relation to their major controls (following Dunne and Leopold, 1978).

The variable source area concept related to the occurrence of saturation excess indicates that saturation overland flow originates, not over the whole watershed, but over a fraction of it due to local saturation. This occurrence of local saturation is related to topography, because water generally flows downhill, either over or below the surface. The most fundamental topographic property used in hydrology is *contributing area*. Contributing area is the area upslope of any point on a watershed or topographic surface. Contributing area may be concentrated as in distinct river valleys, or dispersed as on smooth surfaces such as hillslopes. In the dispersed smooth surface case the area contributing to a point may be a line that theoretically has an area of zero. In such cases the contributing area concept is better defined as contributing area per unit contour width, in which case it is called *specific catchment area*. Contributing area and specific catchment area are illustrated in Figure 19. Contributing area is denoted 'A' whereas specific catchment area 'a'. Contributing area

has units of area [m²] and specific catchment area has units of length [m].
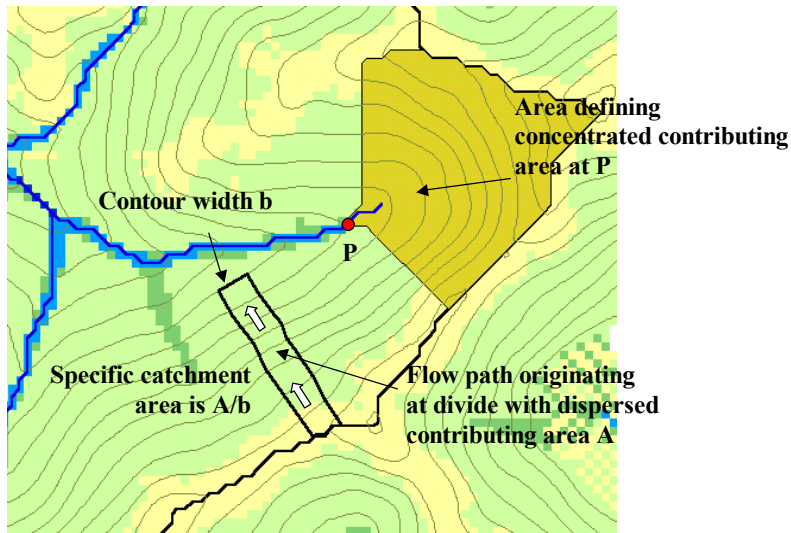
Figure 19. Topographic definition of contributing area, concentrated at a point or dispersed (specific catchment area) on a hillslope.

Given the general tendency of water to flow downhill, specific catchment area serves as a useful surrogate for the subsurface lateral moisture flux comprised of interflow and groundwater flow at a location. This is related to the wetness of the soil profile at the location, quantified as

$$q = r\,a \tag{2}$$

Here q represents the lateral moisture flux across a unit contour width [m²/hr], and r is a proportionality constant, which can be thought of, under steady state, as a constant rainfall, infiltration, or recharge, rate with units of depth/time [m/hr]. The soil profile has a maximum lateral flow capacity that is related to the hydraulic conductivity and depth of the soil as well as the slope, S, because lateral flow is driven by the topographic gradient. Slope is generally represented as either the tangent, or sin of the slope angle β. The lateral flow capacity is

$$q_{cap} = T\,S \tag{3}$$

Here q_{cap} represents the lateral flow capacity of the soil profile per unit width [m²/hr] and T is called the transmissivity [m²/hr] and is the integral over depth of the hydraulic conductivity. (Hydraulic conductivity is defined and discussed in section 4 below.) The slope S is dimensionless. The relative wetness of a soil profile is related to the ratio of the lateral moisture flux to the lateral flow capacity from equations (2, 3), namely

$$w = \frac{r\,a}{T\,S} \qquad\qquad (4)$$

This is based on the idea that for a soil profile to transport water laterally at capacity, it needs to approach saturation; however when the lateral flow is less than capacity the profile can be less wet. The topographic component of the wetness expression (4) is just a/S, which is commonly used as a *topographic wetness index*. More commonly this is written ln(a/S) or ln(a/tan β) because this is the way it was first expressed (Beven and Kirkby, 1979) in the definition of TOPMODEL (which will be discussed below) where there was an assumption of exponential decrease of hydraulic conductivity with depth that led to the logarithm in the definition. On steep slopes the distance over which flow occurs is the length along the slope, i.e. the hypotenuse of the triangle, so S is better defined as sin β. For most practical angles the difference between tan and sin is indistinguishable given the uncertainty in other quantities involved in these equations. The topographic wetness index is readily calculated using geographic information systems (GIS) from digital elevation models (DEMs) which are also now readily available. The topographic wetness index provides a way to identify and model locations likely to generate runoff by saturation excess and to quantify the variable source area concept. When the lateral water flux (equation 2) exceeds the lateral flow capacity (equation 3) the soil profile becomes completely saturated, so the variable source areas contributing to saturation excess overland flow can be identified as those locations where

$$a/S > T/r \qquad\qquad (5)$$

The supply of water to soil drainage (r in equation 2), or specific catchment area proportionality constant, quantifies the general antecedent wetness of the watershed. Under an assumption of steady state, r is also the per unit area baseflow. Higher r values result in a smaller threshold in equation (5) and larger variable source area. The

wetness index and saturated area for two different T/r thresholds evaluated from a DEM is illustrated in Figure 20.
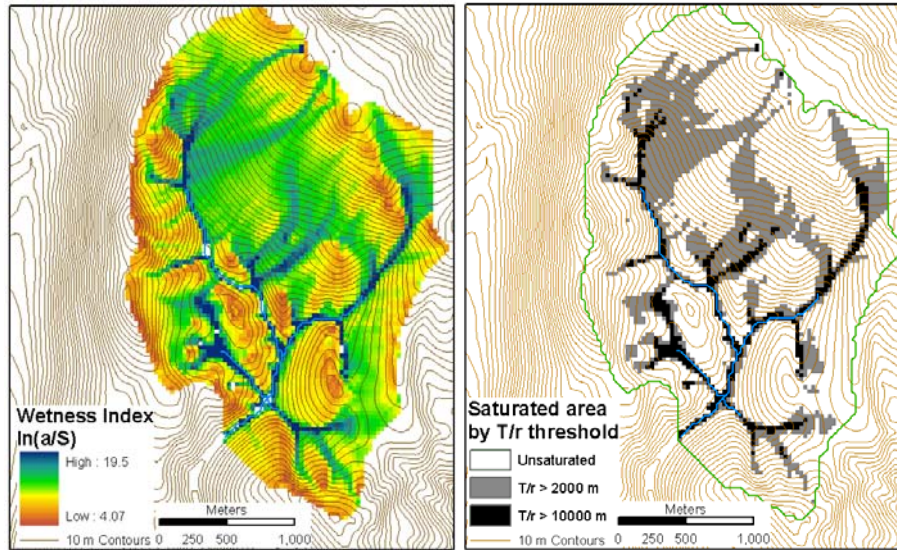
Figure 20. (a) ln (a/S) wetness index for a small watershed evaluated from a 30 m Digital Elevation Model. The gaps within the wetness index are where the slope is 0 and wetness index is formally undefined. (b) Saturated area based on this wetness index for two different T/r thresholds.

Exercises

1. Saturation excess overland flow is most likely to occur in:
   A. Gently sloping areas where the water table is shallow
   B. Steep forested hillsides
   C. Urban areas
   D. Arid regions with compacted crusted soil surfaces

2. Infiltration excess overland flow is most likely to occur in:
   A. Gently sloping areas where the water table is shallow
   B. Steep forested hillsides
   C. Arid regions with compacted crusted soil surfaces
   D. Urban areas

3. Infiltration excess overland flow is more likely to occur in:
   A. A short gentle rainstorm
   B. A short intense rainstorm
   C. A long gentle rainstorm
   D. A snow blizzard

4. Saturation excess overland flow is more likely to occur in:
   A. A short intense rainstorm with moderate total rainfall amount
   B. A short gentle rainstorm with small total rainfall amount
   C. A snow blizzard with all precipitation in the form of snow
   D. A long gentle rainstorm with large total rainfall amount

5. Saturated areas that contribute to saturation excess overland flow are most likely larger
   A. At the end of a long dry spell
   B. At the end of the wet season

6. Interception is most likely to
   A. Result in a large capillary fringe
   B. Increase the infiltration capacity
   C. Reduce the infiltration capacity
   D. Increase erosion
   E. Occur in an urban area
   F. Lead to increased infiltration excess overland flow
   G. Reduce the amount of runoff generated in a forested area

7. The area contributing to saturation excess overland flow is likely to be larger:
   A. At the end of a rainstorm
   B. At the beginning of a rainstorm
   C. Midway through a rainstorm when the rainfall intensity is highest
   D. Midway through a dry interstorm period

8. Following are annual precipitation and potential evaporation estimates for five watersheds.

	P	Ep	Q	E
	mm	mm	mm	mm
A	200	700		
B	500	900		
C	800	700		
D	1200	900		
E	2000	800		

Fill in the missing Q and E values from the selections below:
Q: 20, 100, 300, 400, 1350;   E: 800, 650, 500, 400, 180

9. In a typical storm in a humid catchment the saturated area is:
   A. less than 50% of the area
   B. between 50% and 75% of the area
   C. greater than 75% of the area

References

Beven, K. J. and M. J. Kirkby, (1979), "A Physically Based Variable Contributing Area Model of Basin Hydrology," <u>Hydrological Sciences Bulletin</u>, 24(1): 43-69.

Dunne, T. and L. B. Leopold, (1978), <u>Water in Environmental Planning</u>, W H Freeman and Co, San Francisco, 818 p.

Chapter 4
Soil Properties

CHAPTER 4: SOIL PROPERTIES

Infiltration is the movement of water into the soil. This is possible, because soil is not solid matter; instead it is a porous medium comprising a matrix of solid granular particles and voids that may be filled with air or water (Figure 21). Flow in a porous medium may be unsaturated when some of the voids are occupied by air, or saturated when all the voids are occupied by water. Considering the cross section of a porous medium illustrated in Figure 21, the *porosity* is defined as

$$n = \frac{\text{volume of voids}}{\text{total volume}} \tag{6}$$
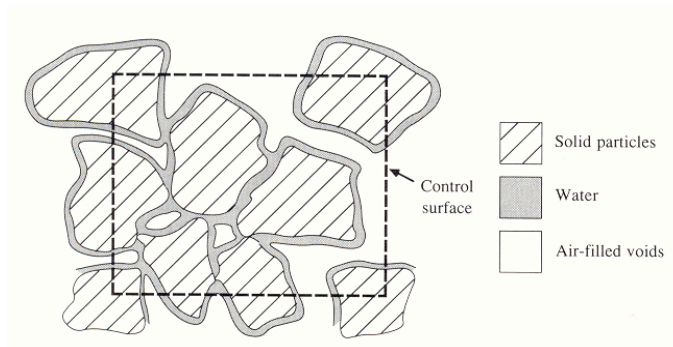
Figure 21. Cross section through an unsaturated porous medium (from Chow et al., 1988).

The range of n for soils is approximately 0.25 to 0.75 depending upon the soil texture. A part of the voids is occupied by water, and the remainder by air. The volume occupied by water being measured by the *volumetric soil moisture content* is defined as

$$\theta = \frac{\text{volume of water}}{\text{total volume}} \tag{7}$$

Hence $0 \le \theta \le n$; the soil moisture content is equal to the porosity when the soil is saturated. Soil moisture content is also sometimes characterized by the degree of saturation, defined as

$$S_d = \theta/n \tag{8}$$

The degree of saturation varies between 0 and 1.

Referring to Figure 21, the soil particle density, ρ_m, is the weighted average density of the mineral grains making up a soil

$$\rho_m = M_m / V_m \tag{9}$$

where M_m is the mass and V_m the volume of the mineral grains. The value of ρ_m is rarely measured, but is estimated based on the mineral composition of the soil. A value of 2650 kg/m³, which is the density of the mineral quartz, is often assumed. The bulk density, ρ_b, is the dry density of the soil

$$\rho_b = \frac{M_m}{V_s} = \frac{M_m}{V_a + V_w + V_m} \tag{10}$$

where V_s is the total volume of the soil sample which is the sum of the volume of the air, V_a, liquid water, V_w, and mineral components, V_m, of the soil respectively. In practice, bulk density is defined as the mass of a volume of soil that has been dried for an extended period (16 hr or longer) at 105 °C, divided by the original volume. The porosity (6) is given by

$$n = \frac{V_a + V_w}{V_s} = \frac{V_s - V_m}{V_s} = 1 - \frac{M_m / V_s}{M_m / V_m} = 1 - \frac{\rho_b}{\rho_m} \tag{11}$$

and n is usually determined by measuring ρ_b and assuming an appropriate value for ρ_m. Laboratory determination of volumetric moisture content θ is by first weighing a soil sample of known volume, oven drying it at 105 °C, reweighing it and calculating

$$\theta = \frac{M_{swet} - M_{sdry}}{\rho_w V_s} \tag{12}$$

Here M_{swet} and M_{sdry} are the masses before and after drying, respectively, and ρ_w is the density of water (1000 kg/m³). This method for determining soil moisture is referred to as the gravimetric method. In the field moisture content can be measured in a number of other ways. Electrical resistance blocks use the inverse relationship between water content and the electrical resistance of a volume of porous material (e.g. gypsum, nylon or fiberglass) in equilibrium with the soil. Neutron probe moisture meters are combined sources and detectors of neutrons that are inserted into

access tubes to measure the scattering of neutrons by hydrogen atoms, which is a function of moisture content. Gamma-ray scanners measure the absorption of gamma rays by water molecules in soil between a source and a detector. Capacitance and time-domain reflectometry (TDR) techniques measure the dielectric property of a volume of soil, which increases strongly with water content. Nuclear magnetic resonance techniques measure the response of hydrogen nuclei to magnetic fields. Remote sensing and specifically, microwave remote sensing can provide information about surface soil water content over large areas. Both active and passive microwave systems exist, with active systems (radar) having higher resolution. Because of the importance of soil moisture in hydrologic response, as well as land surface inputs to the atmosphere, the relationship of soil moisture to remote sensing measurements is an area of active research. The assimilation of remote sensing measurements of soil moisture into hydrologic and atmospheric forecasting models is one exciting aspect of this research that holds the potential for improving hydrologic and atmospheric model forecasts. For details on these methods for soil moisture measurement the reader is referred to soil physics texts, or the research literature (e.g., Hillel, 1980)

The flow of water through soil is controlled by the size and shape of pores, which is in turn controlled by the size and packing of soil particles. Most soils are a mixture of grain sizes, and the grain size distribution is often portrayed as a cumulative-frequency plot of grain diameter (logarithmic scale) versus the weight fraction of grains with smaller diameter (Figure 22). The steeper the slopes of such plots, the more uniform the soil grain-size distribution.

For many purposes the particle size distribution is characterized by the *soil texture,* which is determined by the proportions by weight of clay, silt and sand. Clay is defined as particles with diameter less than 0.002 mm. Silt has a particle diameter range from 0.002 mm to 0.05 mm and sand has particle diameter range from 0.05 to 2 mm. Figure 23 gives the method developed by the U.S. Department of Agriculture for defining textures based on proportions of sand, silt and clay. Larger particles with grain sizes greater than 2 mm are excluded from this proportioning in the determination of texture. Grain size distributions are obtained by sieve analysis for particles larger than 0.05 mm and by sedimentation for smaller grain sizes. Sieve analysis is a procedure where the soil is passed through a stack of successively finer sieves and the mass of soil retained on each sieve is recorded. Because soil grains are irregular shapes, the practical

definition of diameter then amounts to whether or not the soil grain passes through a sieve opening of specified size. Sedimentation is a procedure whereby the settling rate in water of soil particles is measured. For details see a soil physics reference (e.g. Hillel, 1980).
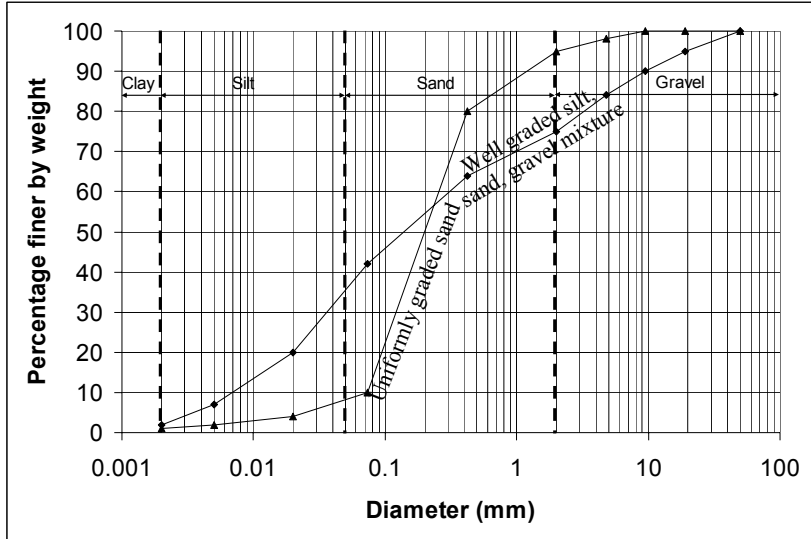
Figure 22. Illustrative grain–size distribution curves. The boundaries between size classes designated as clay, silt, sand and gravel are shown as vertical lines.

Following are the grain sizes used for the determination of texture for the soils illustrated in Figure 22.

Diameter (mm)	A. % Finer	B. % Finer	A. % Finer < 2mm only	B. % Finer < 2mm only
50	100	100		
19	95	100		
9.5	90	100		
4.76	84	98		
2	75	95	100	100
0.42	64	80	85.3	84.2
0.074	42	10	56	10.5
0.02	20	4	26.7	4.2
0.005	7	2	9.3	2.1
0.002	2	1	2.7	1.1
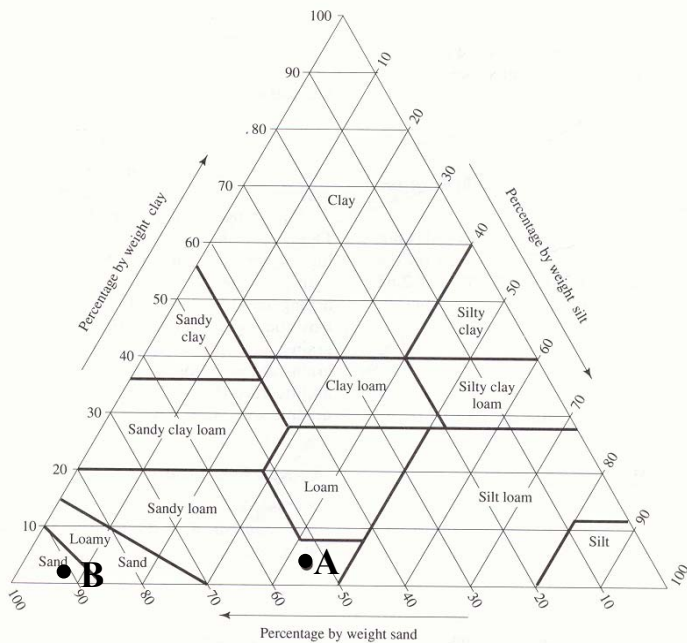
Figure 23. Soil texture triangle, showing the textural terms applied to soils with various fractions of sand, silt and clay (Dingman, Physical Hydrology, 2/E, © 2002. Electronically reproduced by permission of Pearson Education, Inc., Upper Saddle River, New Jersey)

Soil A is a well-graded mixture comprising gravel, silt and sand in roughly equal proportions. The majority of grains in soil B are all from the same sand size class. It is therefore described as uniformly graded sand. The percentages of Sand, Silt and Clay, for these soils determine the texture as indicated by the dots in Figure 23

	A	B
% Sand	52.8	91.4
% Silt	44.5	7.6
% Clay	2.7	1.1
Texture (Figure 23)	Sandy Loam	Sand

The soil properties, porosity, moisture content, bulk density are defined in terms of averages over a volume referred to as the representative elementary volume (Bear, 1979). It is not meaningful, for example, to talk about these quantities as a very small scale where we are looking at individual soil grains or particles. These properties

(and others such as hydraulic conductivity and specific discharge to be defined below) represent averages over the representative elementary volume and are referred to as continuum properties of the porous medium. The macroscopic continuum representation of flow through a porous medium relies on this concept to overlook the complexity of the microscopic flow paths through individual pores in a porous medium (see Figure 24). Typically the representative elementary volume is about 1 to 20 cm^3. Where heterogeneity exists in a porous medium at all scales, the definition of macroscopic continuum properties can be problematic.

At the macroscopic scale, flow through a porous medium is described by *Darcy's equation*, or *Darcy's law*. The experimental setup used to define Darcy's equation is illustrated in Figure 25. A circular cylinder of cross section A is filled with porous media (sand), stoppered at each end, and outfitted with inflow and outflow tubes and a pair of piezometers. (A piezometer is a tube inserted to measure fluid pressure based on the height of rise of fluid in the tube.) Water is introduced into the cylinder and allowed to flow through it until such time as all the pores are filled with water and the inflow rate Q is equal to the outflow rate. Darcy found that the flow rate Q is proportional to cross sectional area A, the piezometer height difference Δh, and inversely proportional to the distance between piezometers, Δl. This allows an equation expressing this proportionality to be written

$$Q = -KA \frac{\Delta h}{\Delta l} \qquad (13)$$

where the negative sign is introduced because we define $\Delta h = h_2 - h_1$ to be in the direction of flow. K, the proportionality constant is called the hydraulic conductivity. Hydraulic conductivity is related to the size and tortuousity of the pores, as well as the fluid properties of viscosity and density. Because the porous medium in this experiment is saturated, K here is referred to as the saturated hydraulic conductivity. The *specific discharge*, q, representing the per unit area flow through the cylinder is defined as

$$q = \frac{Q}{A} \qquad (14)$$

Q has dimensions $[L^3/T]$ and those of A are $[L^2]$ so q has the dimensions of velocity $[L/T]$. Specific discharge is sometimes known

as the *Darcy velocity*, or *Darcy flux*. The specific discharge is a macroscopic concept that is easily measured. It must be clearly differentiated from the microscopic velocities associated with the actual paths of water as they wind their way through the pores (Figure 24).

Figure 24. Macroscopic and microscopic concepts of porous medium flow (Freeze/Cherry, Groundwater, © 1979. Electronically reproduced by permission of Pearson Education, Inc., Upper Saddle River, New Jersey).

The proportion of the area A that is available to flow is nA. Accordingly the average velocity of the flow through the column is (Bear, 1979)

$$V = Q/nA = q/n \qquad (15)$$

Using specific discharge, Darcy's equation may be stated in differential form

$$q = -K\frac{dh}{dl} \qquad (16)$$

In equation (16) h is the *hydraulic head* and dh/dl is the *hydraulic gradient*. Since both h and l have units of length [L], a dimensional analysis of equation (16) shows that K has the dimensions of velocity [L/T]. Hydraulic conductivity is an empirical porous medium and fluid property. We discuss later how it can be related to pore sizes and the viscosity of water. In Figure 25, the piezometers measure hydraulic head. The pressure in the water at the bottom of a piezometer (location 1 or 2 in Figure 25) is given by

$$p = (h\text{-}z)\gamma = (h\text{-}z)\rho_w g \qquad (17)$$

where $\gamma = \rho_w g$ is the specific weight of water, the product of the density and gravitational acceleration, g (9.81 m/s^2). The hydraulic head h is comprised of elevation z above any convenient datum and a *pressure head* term $\psi = p/\gamma$.

$$h = z + p/\gamma = z + \psi \qquad (18)$$

Pressure head represents the pressure energy per unit weight of water. The elevation z above the datum is also termed *elevation head*, and represents the potential energy, relative to the gravitational field, per unit weight of water. It is important to note that equations (13) and (16) state that flow takes place from a higher hydraulic head to a lower hydraulic head and not necessarily from a higher pressure to a lower pressure. The pressure at location 2 can still be higher than the pressure at location 1, with flow from 1 to 2. The hydraulic head difference Δh in (13) represents a hydraulic energy loss due to friction in the flow through the narrow tortuous paths (Figure 24) from 1 to 2. Actually, in Darcy's equation, the kinetic energy of the water has been neglected, as, in general, changes in hydraulic head due to pressure and elevation along the flow path are much larger than changes in the kinetic energy.
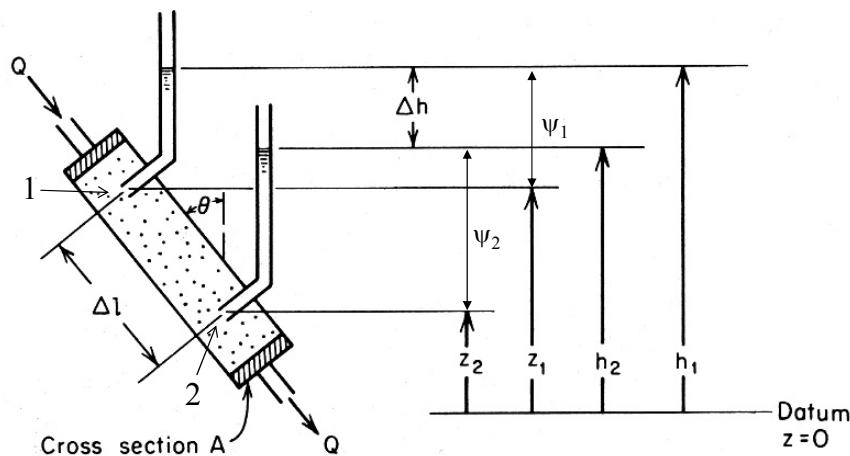
Figure 25. Experimental apparatus for the illustration of Darcy's equation (Freeze/Cherry, Groundwater, © 1979. Electronically reproduced by permission of Pearson Education, Inc., Upper Saddle River, New Jersey).

Darcy's equation, as presented here, is for one dimensional flow. Flow in porous media can be generalized to three dimensions in which case the hydraulic gradient, becomes a hydraulic gradient vector, and the hydraulic conductivity becomes a hydraulic conductivity tensor matrix in the most general case of an anisotropic medium. Refer to advanced texts (e.g. Bear, 1979) for a discussion of this.

One conceptual model for flow through a porous media is to represent the media as a collection of tiny conduits with laminar flow in each (Figure 26). The average velocity in each conduit is given by the Hagen-Poiseville equation (Bras, 1990, p291)

$$v_i = -\frac{\gamma d_i^2}{32\mu}\frac{dh}{dl}$$
(19)

where d_i is the conduit diameter and μ the dynamic viscosity (which for water at 20 °C is 1.05×10^{-3} N s m^{-2}).
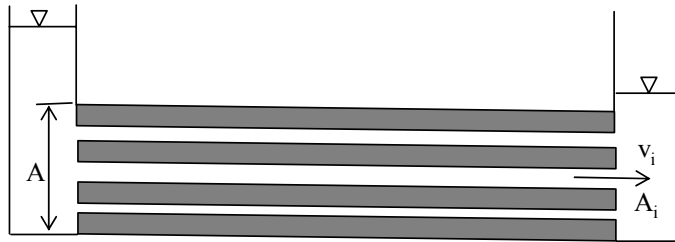
Figure 26. Parallel conduit conceptual model for porous media flow.

The flow in each conduit may be expressed as $v_i A_i$ where A_i is the cross sectional area of each conduit. Summing these and expressing flow per unit area, the specific discharge is

$$q = \frac{\sum v_i A_i}{A} = -\frac{1}{A}\sum A_i \frac{\gamma d_i^2}{32\mu}\frac{dh}{dl}$$
(20)

By comparison with (16) the hydraulic conductivity is

$$K = \frac{1}{A}\sum A_i \frac{\gamma d_i^2}{32\mu} = \frac{\gamma}{\mu}\underbrace{\left(\frac{1}{A}\sum A_i d_i^2 / 32\right)}_{\text{medium property k}} = \frac{\gamma}{\mu}k$$
(21)

Here hydraulic conductivity K has been expressed in terms of fluid properties (γ/μ) and medium properties grouped together into the

quantity k, which is called the medium's *intrinsic permeability*. Intrinsic permeability has units of area [L^2] and (21) suggests this should be related to the average pore area. Equation (21) represents a conceptual model useful to understand the intrinsic permeability of porous media. Real soils are more complex than straight tiny conduits. Nevertheless, experiments with fluids with different viscosity and density, and a porous media comprising glass beads of different diameter have supported the extension of Darcy's equation to

$$q = -\frac{Cd^2\gamma}{\mu}\frac{dh}{dl} \qquad (22)$$

where d is effective grain diameter and $k=Cd^2$. C is a constant of proportionality that accounts for the geometry and packing in the porous media. Effective grain diameter d may be taken as mean grain diameter, or d_{10}, the diameter such that 10% by weight of grains are smaller than that diameter. Differences in these definitions of d are absorbed in the constant C. The intrinsic permeability quantifies the permeability of a porous medium to flow of any fluid (e.g. air, oil, water) and is more general than the concept of hydraulic conductivity. The viscosity of water is temperature and salinity dependent, and this can be accounted for using (21), although this is rarely done in practice in infiltration and runoff generation calculations.

The conceptual model above relied on laminar flow and the linear relationship in Darcy's equation is a consequence of the flow through porous media being laminar. Limits to this linearity have been suggested. For fine grained materials of low permeability some laboratory evidence (see discussion in Bear, 1979; Freeze and Cherry, 1979) has suggested that there may be a threshold hydraulic gradient below which flow does not take place. Of greater (but still limited) practical importance is the limitation of Darcy's equation at very high flow rates where turbulent flow occurs. The upper limit to Darcy's equation is usually identified using Reynolds number, which for flow through porous media is defined as

$$Re = \frac{\rho q d}{\mu} \qquad (23)$$

Various definitions are used for d, the pore size length scale (e.g. mean grain size, d_{10} or $(k/n)^{1/2}$). In spite of these differences Bear

(1979) indicates that "Darcy's law is valid as long as the Reynolds number does not exceed some value between 1 and 10." Departures from linearity are discussed by Bear (1979) but are not used in any modeling of infiltration.

The discussion of flow through porous media thus far has developed Darcy's equation for saturated porous media. Infiltration and the generation of runoff often involve unsaturated flow through porous media. As illustrated in Figure 21 when a porous medium is unsaturated part of the porosity void space is occupied by air. The simplest configuration of saturated and unsaturated conditions is that of an unsaturated zone near the surface and a saturated zone at depth (Figure 27).
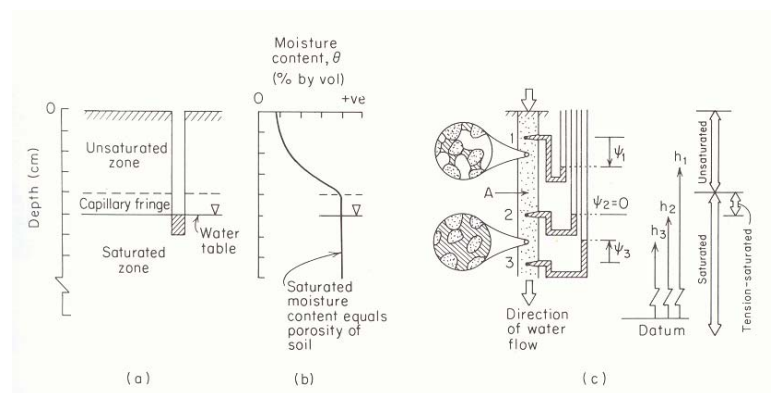
Figure 27. Groundwater conditions near the ground surface. (a) Saturated and unsaturated zones; (b) profile of moisture content versus depth; (c) pressure-head and hydraulic head relationships; insets: water retention under pressure heads less than (top) and greater than (bottom) atmospheric pressure (Freeze/Cherry, Groundwater, © 1979. Electronically reproduced by permission of Pearson Education, Inc., Upper Saddle River, New Jersey).

We commonly think of the water table as being the boundary between them. The water table is defined as the surface on which the fluid pressure p in the pores of a porous medium is exactly atmospheric. The location of this surface is revealed by the level at which water stands in a shallow well open along its length and penetrating the surficial deposits just deeply enough to encounter standing water at the bottom. If p is measured in terms of gage pressure (i.e. relative to atmospheric pressure), then at the water table

p=0. This implies $\psi=0$, and since $h=\psi+z$, the hydraulic head at any point on the water table must be equal to the elevation z of the water table. Positive pressure head occurs in the saturated zone ($\psi > 0$ as indicated by piezometer measurements). Pressure head is zero ($\psi = 0$) at the water table. It follows that pressure head is negative ($\psi < 0$) in the unsaturated zone. This reflects the fact that water in the unsaturated zone is held in the soil pores under tension due to surface-tension forces. A microscopic inspection would reveal a concave meniscus extending from grain to grain across each pore channel (as shown in the upper circular inset in Figure 27c). The radius of curvature on each meniscus reflects the surface tension on that individual, microscopic air-water interface. In reference to this physical mechanism of water retention, negative pressure head is also referred to as tension head or suction head. Above the water table, where $\psi < 0$, piezometers are no longer a suitable instrument for the measurement of h. Instead h must be obtained indirectly from measurements of ψ determined with tensiometers. A tensiometer consists of a porous cup attached to an airtight, water-filled tube. The porous cup is inserted into the soil at the desired depth, where it comes into contact with the soil water and reaches hydraulic equilibrium. The vacuum created at the top of the airtight tube is usually measured by a vacuum gage or pressure transducer attached to the tube above the ground surface, but it can be thought of as acting like an inverted manometer shown for point 1 in the soil in Figure 27c.

Small pores are able to sustain a larger tension head than larger pores, because the surface tension force induced around the pore perimeter is larger relative to the pore cross section area and pressure is force over area. Thus, under hydrostatic conditions (when water is not flowing) water is able to be held higher above the water table in small pores than in larger pores. This effect is illustrated in Figure 27b, and Figure 28 where conceptually (and greatly exaggerated) the height to which water rises in a capillary tube is greater for smaller pores. This leads to the moisture content being a function of the suction head, because as suction increases only the capillary forces in smaller pores can retain water.
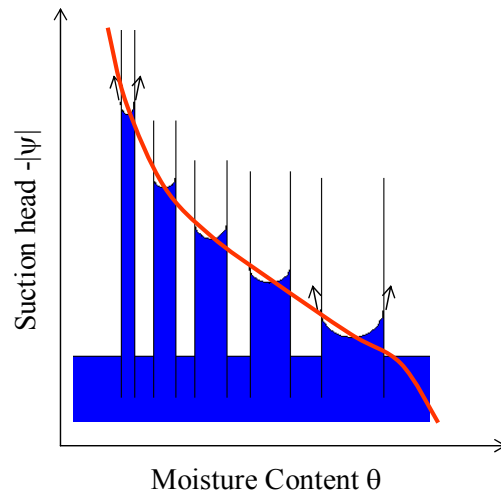
Figure 28. Illustration of capillary rise due to surface tension and relationship between pore size distribution and soil water retention curves.

The flow of water in unsaturated porous media is also governed by Darcy's equation. However, since the moisture content and the size of the pores occupied by water reduces as the magnitude of the suction head is increased (becomes more negative), the paths for water to flow become fewer in number, of smaller cross section and more tortuous. All these effects serve to reduce hydraulic conductivity. Figure 29 illustrates the form of the relationships giving the dependence of suction head and hydraulic conductivity on soil moisture content. This issue is further complicated in that it has been observed experimentally that the $\psi(\theta)$ relationship is hysteretic; it has a different shape when soils are wetting than when they are drying. This also translates into hysteresis in the relationship between hydraulic conductivity and moisture content. The physical processes responsible for hysteresis are discussed by Bear (1979). The curves illustrating the relationship between ψ, θ and K are referred to as *soil water characteristic* curves, or *soil water retention* curves. While hysteresis can have a significant influence on soil-moisture movement, it is difficult to model mathematically and is therefore not commonly incorporated in hydrologic models.
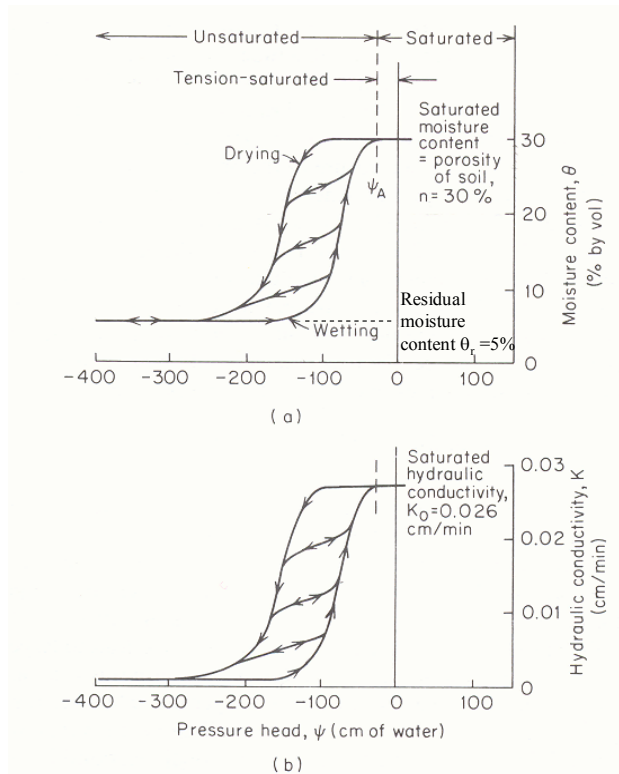
Figure 29. Characteristic curves relating hydraulic conductivity and moisture content to pressure head for a naturally occurring sand soil (Freeze/Cherry, Groundwater, © 1979. Electronically reproduced by permission of Pearson Education, Inc., Upper Saddle River, New Jersey).

Note in Figure 29 that the pressure head is 0 when the moisture content equals the porosity, i.e. is saturated, and that the water content changes little as tension increases up to a point of inflection. This more or less distinct point represents the tension at which significant volumes of air begin to appear in the soil pores and is called the air-entry tension, ψ_a. This retention of soil moisture at (or practically close to) saturation for pressures less than atmospheric gives rise to the capillary fringe illustrated in Figures 12 and 28. The capillary fringe plays an important role in the generation of saturation excess runoff where the water table is close to the surface, and also in the generation of return flow and subsurface storm flow as described above.

In Figure 29 pressure head was given as the independent variable on the x-axis. It is sometimes more convenient to think of moisture

content as the independent variable. Figure 30 gives an example of the soil water characteristic curves with moisture content as the independent variable. This representation has the advantage of avoiding some of the problem of hysteresis, because $K(\theta)$ is less hysteretic than $K(\psi)$ (Tindall et al., 1999).

Note also in Figure 29 that as tension head is increased a point is reached where moisture content is no longer reduced. A certain amount of water can not be drained from the soil, even at high tension head, due to being retained in disconnected pores and immobile films. This is called the *residual moisture content* or in some cases the *irreducible moisture content* θ_r. For practical purpose flow only occurs in soil for moisture contents between saturation, n, and the residual water content θ_r. This range is referred to as the *effective porosity* $\theta_e = n - \theta_r$. When considering flow in unsaturated soil, moisture content is sometimes quantified using the *effective saturation* defined to scale the range from θ_r to n between 0 and 1.

$$S_e = \frac{\theta - \theta_r}{n - \theta_r} \tag{24}$$

The soil water characteristic curves are a unique property of each soil, related to the size distribution and structure of the pore space. For a specific soil the soil water characteristic functions can be determined experimentally through drainage experiments. For practical purposes it is convenient to mathematically represent the characteristic functions using equations and a number of empirical equations have been proposed. Three functional forms proposed by Brooks and Corey (1966), Van Genuchten (1980) and Clapp and Hornberger (1978) are listed. There are no fundamental differences between these equations, they are simply convenient mathematical expressions that approximately fit the empirical shape of many soil characteristic functions.
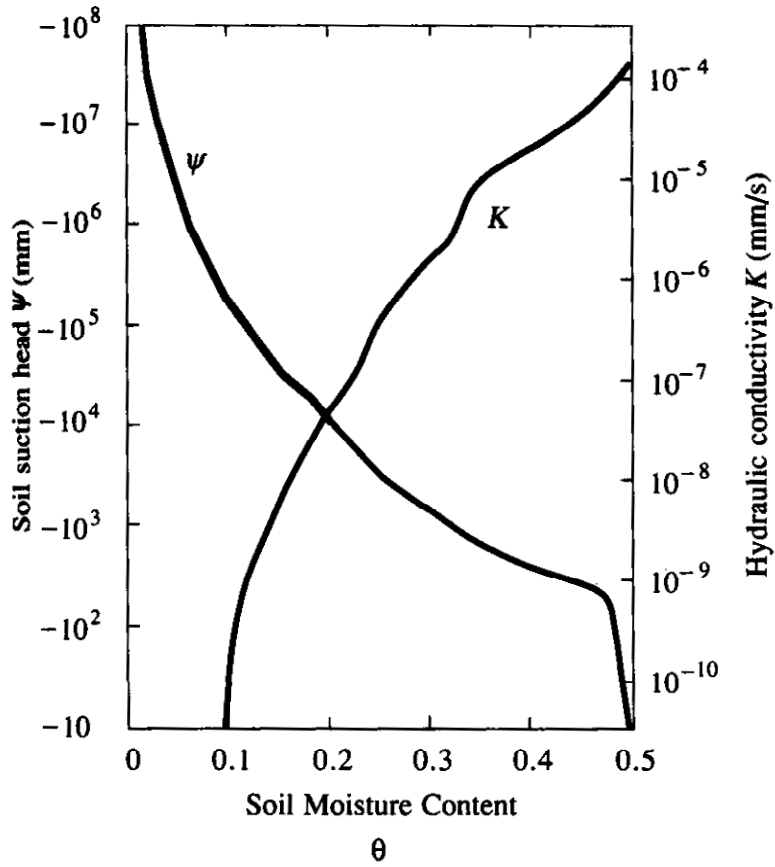
Figure 30. Variation of soil suction head, $|\psi|$, and hydraulic conductivity, K, with moisture content (from Chow et al., 1988).

Brooks and Corey (1966):

$$
\begin{aligned}
|\psi(S_e)| &= |\psi_a| S_e^{-b} \\
K(S_e) &= K_{sat} S_e^c
\end{aligned}
\tag{25}
$$

van Genuchten (1980):

$$
\begin{aligned}
|\psi(S_e)| &= \frac{1}{\alpha}\left(S_e^{-1/m} - 1\right)^{1-m} \\
K(S_e) &= K_{sat} S_e^{1/2}(1 - (1 - S_e^{1/m})^m)^2
\end{aligned}
\tag{26}
$$

Clapp and Hornberger (1978) simplifications of Brooks and Corey functions:

$$| \psi(\theta) | = | \psi_a | \left(\frac{\theta}{n} \right)^{-b}$$

$$K(\theta) = K_{sat} \left(\frac{\theta}{n} \right)^{c}$$

$$(27)$$

In these equations K_{sat} is the saturated hydraulic conductivity and b, c, α and m are fitting parameters. The parameter b is referred to as the pore size distribution index because the pore size distribution determines relationship between suction and moisture content (Figure 28). The parameter c is referred to as the pore disconnectedness index because unsaturated hydraulic conductivity is related to how disconnected and tortuous flow paths become as moisture content is reduced. There are theoretical models that relate the soil water retention and hydraulic conductivity characteristic curves. Two common such models are due to Burdine (1953) and Mualem (1976). The Burdine (1953) model suggests c≈2b+3 in equations (25) and (27). The more recent Mualem (1976) model suggests c≈2b+2.5. The $K(S_e)$ equation due to van Genuchten uses the Mualem theory. The relative merits of these theories are beyond the scope discussed here. The Brooks and Corey (1966) and Clapp and Hornberger (1978) equations apply only for $\psi < \psi_a$ and assume $\theta = n$ for $\psi > \psi_a$, while the van Genuchten (1980) equations provide for a smoother representation of the inflection point in the characteristic curve near saturation. Clapp and Hornberger (1978) and Cosby et al (1984) statistically analyzed a large number of soils in the United States to relate soil moisture characteristic parameters to soil texture class. Parameter values that Clapp and Hornberger (1978) obtained are given in table 1. The Clapp and Hornberger simplification (equation 27) neglects the additional parameter of residual moisture "which generally gives a better fit to moisture retention data" (Cosby et al., 1984) but was adopted in their analysis because "the large amount of variability in the available data suggests a simpler representation." When using values from table 1, one should be aware of this considerable within-soil-type variability as reflected in the standard deviations listed in table 1. Figures 31 and 32 show the characteristic curves for soils with different textures using the parameter values from table 1. The USDA-ARS Salinity Laboratory has developed a software program Rosetta that estimates the soil moisture retention function $\psi(\theta)$ and hydraulic conductivity

See Online Resource

Rosetta soil property program
http://www.ussl.ars.usda.gov/
models/rosetta/rosetta.HTM

See Online Resource

Excel spreadsheet with
table and Figures in
electronic form

function and $K(\theta)$ based upon soil texture class or sand, silt and clay percentages.

Table 1. Clapp and Hornberger (1978) parameters for equation (27) based on analysis of 1845 soils. Values in parentheses are standard deviations.

Soil Texture	Porosity n	K_{sat} (cm/hr)	$\|\psi_a\|$ (cm)	b
Sand	0.395 (0.056)	63.36	12.1 (14.3)	4.05 (1.78)
Loamy sand	0.410 (0.068)	56.16	9 (12.4)	4.38 (1.47)
Sandy loam	0.435 (0.086)	12.49	21.8 (31.0)	4.9 (1.75)
Silt loam	0.485 (0.059)	2.59	78.6 (51.2)	5.3 (1.96)
Loam	0.451 (0.078)	2.50	47.8 (51.2)	5.39 (1.87)
Sandy clay loam	0.420 (0.059)	2.27	29.9 (37.8)	7.12 (2.43)
Silty clay loam	0.477 (0.057)	0.612	35.6 (37.8)	7.75 (2.77)
Clay loam	0.476 (0.053)	0.882	63 (51.0)	8.52 (3.44)
Sandy clay	0.426 (0.057)	0.781	15.3 (17.3)	10.4 (1.64)
Silty clay	0.492 (0.064)	0.371	49 (62.0)	10.4 (4.45)
Clay	0.482 (0.050)	0.461	40.5 (39.7)	11.4 (3.7)

Figure 31. Soil suction head, $|\psi|$, for different soil textures using the Clapp and Hornberger (1978) parameterization (Equation 27).

One can infer from the soil moisture retention curves that as moisture drains from soil under gravitational processes, the hydraulic conductivity is reduced and drainage rate reduced. A point is reached where, for practical purposes, downward drainage has materially ceased. The value of water content remaining in a unit volume of soil after downward gravity drainage has materially ceased is defined as *field capacity*. A difficulty inherent in this definition is that no quantitative specification of what is meant by "materially ceased" is given. Sometimes a definition of drainage for three days following saturation is used. This is adequate for sandy and loamy soils, but is problematic for heavier soils that drain for longer periods.
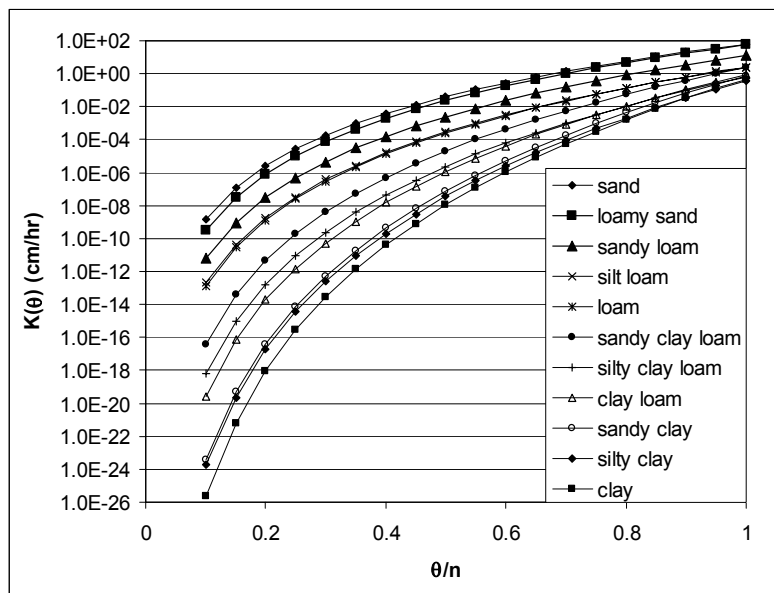
Figure 32. Hydraulic conductivity K(θ) for different soil textures using the Clapp and Hornberger (1978) parameterization (Equation 27).

Because of the difficulty associated with precisely when drainage has materially ceased, a practical approach is to define field capacity as the moisture content corresponding to a specific pressure head. Various studies define field capacity as the moisture content corresponding to a pressure head, ψ, in the range -100 cm to -500 cm with a value of -340 cm being quite common (Dingman, 2002) . The difference between moisture content at saturation and field capacity is referred to as *drainable porosity*, i.e. $n_d = n-\theta(\psi=-100$ cm$)$.

The notion of field capacity is similar to the notion of residual moisture content defined earlier; however some equations (e.g. equation 27) do not use residual moisture content. A distinction in the definitions can be drawn in that residual moisture content is a theoretical value below which there is no flow of water in the soil, i.e. hydraulic conductivity is 0, while field capacity is a more empirical quantity practically defined as the moisture content corresponding to a specific negative pressure head.

In nature, water can be removed from a soil that has reached field capacity only by direct evaporation or by plant uptake. Plants cannot exert suctions stronger than about -15000 cm and when the water content is reduced to the point corresponding to that value on the moisture characteristic curve, transpiration ceases and plants wilt. This water content is called the *permanent wilting point* θ_{pwp}. The difference between the field capacity and permanent wilting point is the water available for plant use, called *plant available water content*, $\theta_a = \theta_{fc} - \theta_{pwp}$. Although most important for irrigation scheduling in agriculture this is relevant for runoff generation processes because during dry spells vegetation may reduce the surface water content to a value between field capacity and permanent wilting point. The antecedent moisture content plays a role in the generation of runoff. Figure 33 shows a classification of water status in soils based on pressure head. Figure 34 shows ranges of porosity, field capacity and wilting point for soils of various textures.
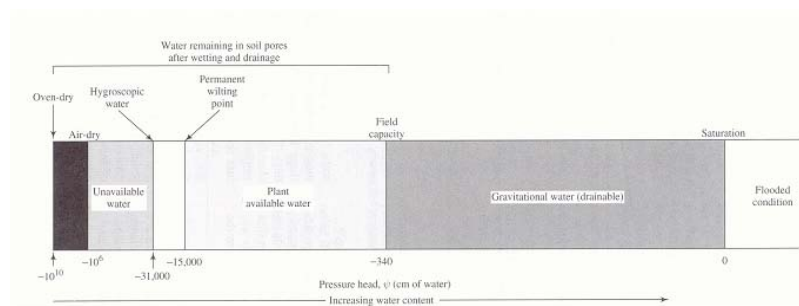
Figure 33. Soil-water status as a function of pressure (tension). Natural soils do not have tensions exceeding about -31000 cm; in this range water is absorbed from the air (Dingman, Physical Hydrology, 2/E, © 2002. Electronically reproduced by permission of Pearson Education, Inc., Upper Saddle River, New Jersey).
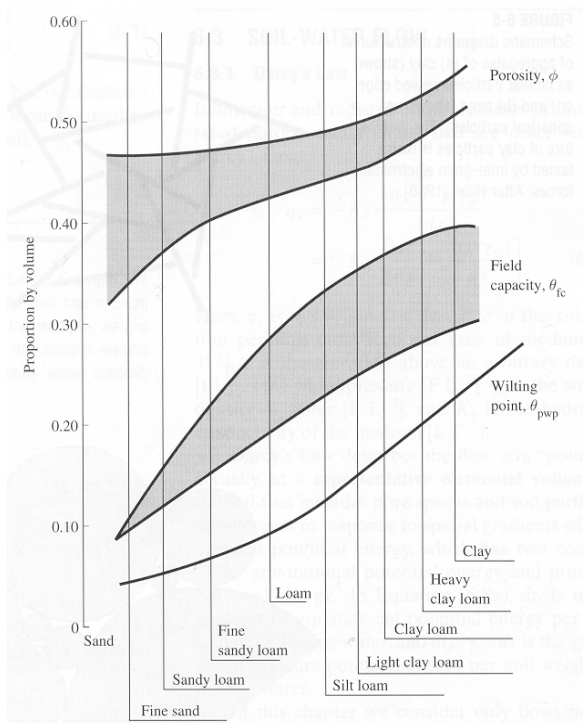
Figure 34. Ranges of porosities, field capacities, and permanent wilting points for soils of various textures (Dingman, Physical Hydrology, 2/E, © 2002. Electronically reproduced by permission of Pearson Education, Inc., Upper Saddle River, New Jersey).

Exercises

1. Infiltration capacity is likely to be larger where:
   A. Hydraulic conductivity is small
   B. Hydraulic conductivity is large

2. Infiltration excess overland flow is likely to be larger where
   A. Hydraulic conductivity is large
   B. Hydraulic conductivity is small

3. Hydraulic conductivity is likely to be large for:
   A. Sandy soils
   B. Clayey soils

4. Porosity is defined as:
   A. Volume of voids/Total volume
   B. Volume of voids/Volume of solids
   C. Volume of water/Volume of solids
   D. Volume of air/Volume of water
   E. Mass of water/Density of soil

5. Volumetric moisture content is defined as:
   A. Volume of air/Volume of water
   B. Mass of water/Density of soil
   C. Volume of water/Total volume
   D. Volume of water/Volume of solids
   E. Volume of voids/Total volume

6. Degree of saturation is defined as:
   A. Volumetric moisture content/Porosity
   B. Volume of water/Volume of voids
   C. Volume of water/Total volume
   D. Volume of water/Volume of solids
   E. Both A and B
   F. Both A and C
   G. Both B and C
   H. A, B, C
   I. B, C, D
   J. A, B, C, D

7. Field and oven-dry weights of a soil sample taken with a 10 cm long by 5 cm diameter cylindrical tube are given in the accompanying table. Assuming ρ_m=2650 kg/m^3 = 2.65 g/cm^3, calculate the volumetric soil moisture content, degree of saturation, bulk density and porosity of those soils.

Field mass	**g**	**302.5**
Oven dry mass	**g**	**264.8**
Bulk Density	**g/cm^3**	
Porosity		
Volumetric soil moisture content		
Degree of saturation		

8. Field and oven-dry weights of a soil sample taken with a 10 cm long by 5 cm diameter cylindrical tube are given in the accompanying table. Assuming ρ_m=2650 kg/m^3 = 2.65 g/cm^3, calculate the volumetric soil moisture content, degree of saturation, bulk density and porosity of those soils.

Field mass	**g**	**390.5**
Oven dry mass	**g**	**274.5**
Bulk Density	**g/cm^3**	
Porosity		
Volumetric soil moisture content		
Degree of saturation		

9. Indicate which (more than one) of the following instruments may be used to measure soil moisture:
   A. Electrical resistance block
   B. Infrared satellite sensor
   C. Capacitance probe
   D. Time domain reflectometry probe
   E. Thermometer
   F. X-Ray sensor
   G. Microwave satellite sensor
   H. Hygrometer
   I. Neutron probe

10. Plot a grain size distribution curve and determine the soil texture for the following soil sieve analysis data.

Diameter (mm)	Percentage passing
50	100
19	100
9.5	100
4.76	98
2	95
0.42	80
0.074	60
0.020	42
0.005	35
0.002	30

11. Plot a grain size distribution curve and determine the soil texture for the following soil sieve analysis data.

Diameter (mm)	Percentage passing
50	100
19	100
9.5	100
4.76	95
2	92
0.42	80
0.074	70
0.020	65
0.005	40
0.002	20

12. Hydraulic conductivity is determined in a Darcy experiment conducted using water at 20 $^\circ$C to be 30 cm/hr. The viscosity of water at 20 $^\circ$C is 1.05 x 10^{-3} N s m^{-2}. Using g=9.81 m/s^2 and ρ_w=1000 kg/m^3 calculate the intrinsic permeability of this material.

13. Following is data from a Darcy experiment using the notation depicted in figure 25. Fill in the blanks and calculate the hydraulic conductivity. The internal diameter of the circular tube used was 10 cm and the length Δl, between piezometers, 40 cm. This experiment is conducted at 20 $^\circ$C.

h_1 (cm)	70
h_2 (cm)	58
z_1 (cm)	50
z_2 (cm)	30
n	0.32
Q (l/hr)	0.5
ψ_1 (cm)	
ψ_2 (cm)	
p_1 (Pa)	
p_2 (Pa)	
dh/dl	
q (cm/hr)	
K (cm/hr)	
k (cm^2)	
V (cm/hr)	
Re	

14. Following is data from a Darcy experiment using the notation depicted in figure 25. Fill in the blanks and calculate the hydraulic conductivity. The internal diameter of the circular tube used was 10 cm and the length Δl, between piezometers, 40 cm. This experiment is conducted at 20 °C.

h_1 (cm)	56
h_2 (cm)	35
z_1 (cm)	50
z_2 (cm)	30
n	0.4
Q (l/hr)	2.2
ψ_1	
ψ_2	
p_1 (Pa)	
p_2 (Pa)	
dh/dl	
q (cm/hr)	
K (cm/hr)	
k (cm^2)	
V (cm/hr)	
Re	

15. Consider the following soil with parameters from Table 1. Evaluate the field capacity moisture content, θ_{fc}, at which pressure head is -340 cm, permanent wilting point moisture content, θ_{fc}, at which the pressure head is -15000 cm and plant available water, θ_a, using the Clapp and Hornberger (1978) soil moisture characteristic parameterization.

Texture	Porosity n	$|\psi_a|$ (cm)	b	θ_{fc}	θ_{pwp}	θ_a
sand	0.395	12.1	4.05			

16. Consider the following soil with parameters from Table 1. Evaluate the field capacity moisture content, θ_{fc}, at which pressure head is -340 cm, permanent wilting point moisture content, θ_{fc}, at which the pressure head is -15000 cm and plant available water, θ_a, using the Clapp and Hornberger (1978) soil moisture characteristic parameterization.

Texture	Porosity n	$|\psi_a|$ (cm)	b	θ_{fc}	θ_{pwp}	θ_a
loamy sand	0.41	9	4.38			

17. Consider the following experimental situation. A and B are vertical tensiometers that measure pore water pressure (tension) relative to atmospheric pressure, at depths 30 and 50 cm below the ground.
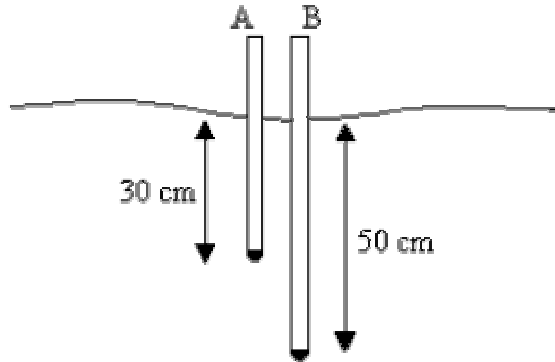
Following are pressure measurements recorded at A and B. Negative denotes suction. Evaluate the pressure head at A and B, and total head at A and B using the surface as a datum. Indicate the direction of flow (i.e. downwards into the ground from A to B, or upwards from B to A).

Pressure at A (Pa)	-4000
Pressure at B (Pa)	-3000
ψ at A (cm)	
ψ at B (cm)	
Total head at A (cm)	
Total head at B (cm)	
Direction of flow	

18. Consider the following experimental situation. A and B are vertical tensiometers that measure pore water pressure (tension) relative to atmospheric pressure, at depths 30 and 50 cm below the ground.

A   B

30 cm

50 cm
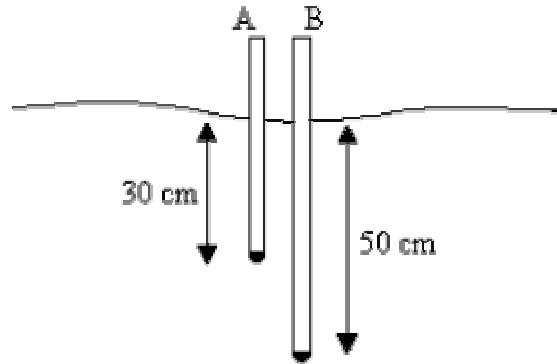
Following are pressure measurements recorded at A and B. Negative denotes suction. Evaluate the pressure head at A and B, and total head at A and B using the surface as a datum. Indicate the direction of flow (i.e. downwards into the ground from A to B, or upwards from B to A).

Pressure at A (Pa)	-5500
Pressure at B (Pa)	-3000
ψ at A (cm)	
ψ at B (cm)	
Total head at A (cm)	
Total head at B (cm)	
Direction of flow	

References

Bear, J., (1979), Hydraulics of Groundwater, McGraw-Hill, New York, 569 p.

Bras, R. L., (1990), Hydrology, an Introduction to Hydrologic Science, Addison-Wesley, Reading, MA, 643 p.

Brooks, R. H. and A. T. Corey, (1966), "Properties of Porous Media Affecting Fluid Flow," J. Irrig. and Drain. ASCE, 92(IR2): 61-88.

Burdine, N. T., (1953), "Relative Permeability Calculations from Pore Size Distribution Data," Petroleum Transactions AIME, 198: 71-78.

Chow, V. T., D. R. Maidment and L. W. Mays, (1988), Applied Hydrology, McGraw Hill, 572 p.

Clapp, R. B. and G. M. Hornberger, (1978), "Empirical Equations for Some Soil Hydraulic Properties," Water Resources Research, 14: 601-604.

Cosby, B. J., G. M. Hornberger, R. B. Clamp and T. R. Ginn, (1984), "A Statistical Exploration of the Relationships of Soil Moisture Characteristics to the Physical Properties of Soils," Water Resources Research, 20(6): 682-690.

Dingman, S. L., (2002), Physical Hydrology, 2nd Edition, Prentice Hall, 646 p.

Freeze, R. A. and J. A. Cherry, (1979), Groundwater, Prentice Hall, Englewood Cliffs, 604 p.

Hillel, D., (1980), Fundamentals of Soil Physics, Academic Press, New York, NY.

Mualem, Y., (1976), "A New Model for Predicting the Hydraulic Conductivity of Unsaturated Porous Media," Water Resources Research, 12(3): 513-522.

Tindall, J. A., J. R. Kunkel and D. E. Anderson, (1999), Unsaturated Zone Hydrology for Scientists and Engineers, Prentice Hall, Upper Saddle River, New Jersey, 624 p.

Van Genuchten, M. T., (1980), "A Closed Form Equation for Predicting the Hydraulic Conductivity of Unsaturated Soils," <u>Soil Sci. Soc. Am. J.</u>, 44: 892-898.

Chapter 5
At a Point Infiltration Models for Calculating Runoff

CHAPTER 5: AT A POINT INFILTRATION MODELS FOR CALCULATING RUNOFF

Infiltration is the movement of water into the soil under the driving forces of gravity and capillarity, and limited by viscous forces involved in the flow into soil pores as quantified in terms of permeability or hydraulic conductivity. The *infiltration rate*, f, is the rate at which this process occurs. The infiltration rate actually experienced in a given soil depends on the amount and distribution of soil moisture and on the availability of water at the surface. There is a maximum rate at which the soil in a given condition can absorb water. This upper limit is called the *infiltration capacity*, f_c. Note that this is a rate, not a depth quantity. It is a limitation on the rate at which water can move into the ground. If surface water input is less than infiltration capacity, the infiltration rate will be equal to the surface water input rate, w. If rainfall intensity exceeds the ability of the soil to absorb moisture, infiltration occurs at the infiltration capacity rate. Therefore to calculate the actual infiltration rate, f, is the lesser of f_c or w. Water that does not infiltrate collects on the ground surface and contributes to surface detention or runoff (Figure 35). The surface overland flow runoff rate, R, is the excess surface water input that does not infiltrate.

$$R = w - f \tag{28}$$

This is also often referred to as *precipitation excess*.

The infiltration capacity declines rapidly during the early part of a storm and reaches an approximately constant steady state value after a few hours (Figure 7). The focus of this section on at a point infiltration models for calculating runoff is on how to calculate runoff accounting for the reduction of infiltration capacity. We use accumulated infiltration depth, F, as an independent variable and write infiltration capacity as a decreasing function $f_c(F)$, then as F increases with time f_c is reduced. f_c may be a gradually decreasing function, or a threshold function, as in the case of saturation excess runoff where there is a finite soil moisture deficit that can accommodate surface water input.

Several processes combine to reduce the infiltration capacity. The filling of fine pores with water reduces capillary forces drawing water into pores and fills the storage potential of the soil. Clay swells as it becomes wetter and the size of pores is reduced. The impact of

raindrops breaks up soil aggregates, splashing fine particles over the surface and washing them into pores where they impede the entry of water. Coarse-textured soils such as sands have large pores down which water can easily drain, while the exceedingly fine pores in clays retard drainage. If the soil particles are held together in aggregates by organic matter or a small amount of clay, the soil will have a loose, friable structure that will allow rapid infiltration and drainage.
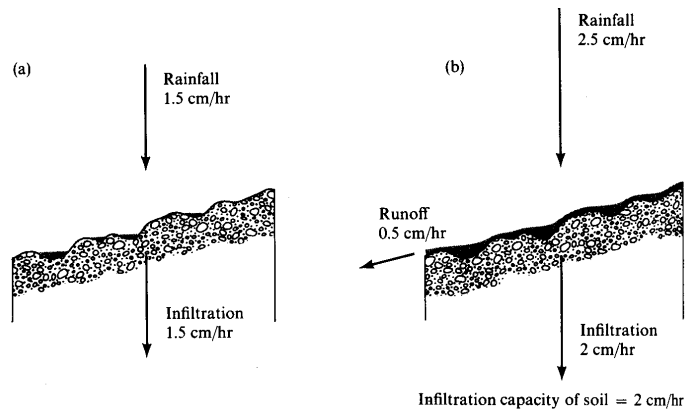
Figure 35. Surface Runoff occurs when surface water input exceeds infiltration capacity. (a) Infiltration rate = rainfall rate which is less than infiltration capacity. (b) Runoff rate = Rainfall intensity – Infiltration capacity (from Water in Environmental Planning, Dunne and Leopold, 1978)

The depth of the soil profile and its initial moisture content are important determinants of how much infiltrating water can be stored in the soil before saturation is reached. Deep, well-drained, coarse-textured soils with large organic matter content will tend to have high infiltration capacities, whereas shallow soil profiles developed in clays will accept only low rates and volumes of infiltration.

Vegetation cover and land use are very important controls of infiltration. Vegetation and litter protect soil from packing by raindrops and provide organic matter for binding soil particles together in open aggregates. Soil fauna that live on the organic matter assist this process by churning together the mineral particles and the organic material. The manipulation of vegetation during land use causes large differences in infiltration capacity. In particular, the stripping of forests and their replacement by crops that do not cover the ground efficiently and do not maintain a high organic content in the soil often lower the infiltration capacity drastically. Soil surfaces trampled by livestock or compacted by vehicles also have reduced

infiltration capacity. The most extreme reduction of infiltration capacity, of course, involves the replacement of vegetation by an asphalt or concrete cover in urban areas. In large rainstorms it is the final, steady state rate of infiltration that largely determines the amount of surface runoff that is generated.

The calculation of infiltration at a point combines the physical conservation of mass (water) principle expressed through the continuity equation with quantification of unsaturated flow through soils, expressed by Darcy's equation. Here we will derive the continuity equation then substitute in Darcy's equation to obtain as a result Richard's equation which describes the vertical movement of water through unsaturated soil. Figure 36 shows a control volume in an unsaturated porous medium. Consider flow only in the vertical direction. The specific discharge across the bottom surface into the volume is denoted as q, and the outflow across the top surface is denoted as q+Δq. The volumetric flux is specific discharge times cross sectional area, $A = \Delta x \cdot \Delta y$. The volume of water in the control volume is the moisture content times the total volume (equation 7), here $V = \Delta x \cdot \Delta y \cdot \Delta z$. Therefore we can write

Change in Storage = (Inflow rate – Outflow rate) x (time interval)

$$\Delta\theta \; \Delta x \; \Delta y \; \Delta z = (q \; \Delta x \; \Delta y - (q+\Delta q) \; \Delta x \; \Delta y) \; \Delta t \qquad (29)$$

Dividing by Δx Δy Δz Δt and simplifying results in

$$\frac{\Delta\theta}{\Delta t} = -\frac{\Delta q}{\Delta z} \qquad (30)$$

Now letting Δz and Δt get smaller and approach 0, as is usual in calculus, we get

$$\frac{\partial\theta}{\partial t} = -\frac{\partial q}{\partial z} \qquad (31)$$

This is the continuity equation in one direction (the vertical direction z). In a more general case where flow can be three dimensional, the continuity equation is obtained in a similar fashion as

$$\frac{\partial\theta}{\partial t} = -\left(\frac{\partial q_x}{\partial x} + \frac{\partial q_y}{\partial y} + \frac{\partial q_z}{\partial z}\right) = -\nabla \bullet \underline{q} \qquad (32)$$

where the operator ∇ is used as shorthand notation for $\left(\dfrac{\partial}{\partial x}, \dfrac{\partial}{\partial y}, \dfrac{\partial}{\partial z}\right)$ and $\underline{q}$ denotes the specific discharge vector (q_x, q_y, q_z) with component in each coordinate direction.
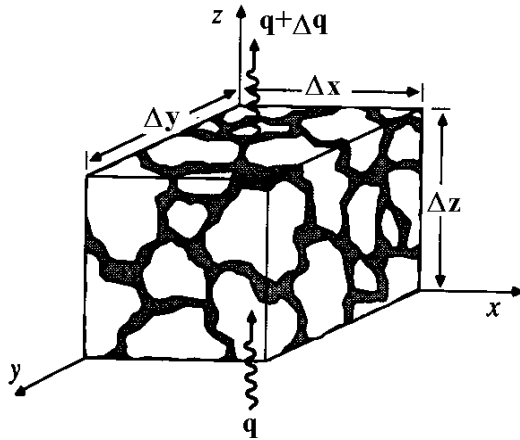
Figure 36. Control volume for development of the continuity equation in an unsaturated porous medium (from Chow et al., 1988).

Substituting Darcy's equation (16) into (31) gives

$$\frac{\partial \theta}{\partial t} = \frac{\partial}{\partial z} K \frac{\partial h}{\partial z} \tag{33}$$

In this equation $h = \psi + z$ (equation 18) resulting in

$$\frac{\partial \theta}{\partial t} = \frac{\partial}{\partial z}\left(K \frac{\partial \psi}{\partial z} + K \right) \tag{34}$$

This equation is known as Richard's equation and it describes the vertical movement of water through unsaturated soil. Although simple appearing, its solution is complicated by the soil moisture characteristic relationships relating moisture content and pressure head $\theta(\psi)$ and Hydraulic conductivity and pressure head or moisture content $K(\psi)$ or $K(\theta)$ discussed above (equations 25, 26, 27 and Figures 29-32). Richard's equation may be written in one of two forms depending on whether we take moisture content, θ, or pressure head, ψ, as the independent variable.

In terms of moisture content, Richard's equation is written

$$\frac{\partial \theta}{\partial t} = \frac{\partial}{\partial z}\left(K(\theta)\frac{\partial \psi(\theta)}{\partial z} + K(\theta) \right)$$

$$= \frac{\partial}{\partial z}\left(K(\theta)\frac{d\psi}{d\theta}\frac{\partial \theta}{\partial z} + K(\theta) \right) \qquad (35)$$

$$= \frac{\partial}{\partial z}\left(D(\theta)\frac{\partial \theta}{\partial z} + K(\theta) \right)$$

In this equation the explicit functional dependence on moisture content, θ, has been shown. The quantity $D(\theta)=K(\theta)\dfrac{d\psi}{d\theta}$ is called the *soil water diffusivity*, because the term involving it is similar to a diffusion term in the diffusion equation. For specific parameterizations of the soil moisture characteristic curves $\psi(\theta)$ and $K(\theta)$, such as equations (25-27), $D(\theta)$ can be derived.

In terms of pressure head, Richard's equation is written

$$\frac{\partial \theta(\psi)}{\partial t} = \frac{d\theta}{d\psi}\frac{\partial \psi}{\partial t} = \frac{\partial}{\partial z}\left(K(\psi)\frac{\partial \psi}{\partial z} + K(\psi) \right)$$

$$C(\psi)\frac{\partial \psi}{\partial t} = \frac{\partial}{\partial z}\left(K(\psi)\frac{\partial \psi}{\partial z} + K(\psi) \right) \qquad (36)$$

As above, in this equation the explicit functional dependence on pressure head, ψ, has been shown. The quantity $C(\psi) = d\theta/d\psi$ is called the *specific moisture capacity*.

Analytic solutions for Richard's equation are known for specific parameterizations of the functions $K(\theta)$ and $D(\theta)$ or $K(\psi)$ and $C(\psi)$ and for specific boundary conditions (see e.g. Philip, 1969; Parlange et al., 1999; Smith et al., 2002). There are also computer codes that implement numerical solutions to Richard's equation. Hydrus 1-D is one such code available from the USDA-ARS Salinity Laboratory (http://www.ussl.ars.usda.gov/models/hydr1d1.HTM) Computational codes based on the moisture content form tend to be better at conserving moisture and dealing with dryer soil conditions. These have problems as saturation is increased because moisture content becomes capped at the porosity and $d\psi/d\theta$ tends to infinity. Computational codes based on the pressure head form are able to

better handle the transition between saturated and unsaturated flow near the water table, but because moisture content is not a specific state variable in their solution, are not as good at conserving mass. Pressure head (and suction) is a continuous function of depth, however in layered soils moisture content is discontinuous at the interface between layers where hydraulic conductivity changes. Computer codes using ψ as the independent variable cope better with these discontinuities. Some approaches to the numerical solution of Richard's equation combine the moisture content and pressure head representations (Celia et al., 1990).

Although Richard's equation is fundamental to the movement of water through unsaturated soil we do not give numerical solutions here, because these are complex and require detailed soils data that are usually not available. Instead we analyze the development of soil moisture versus depth profiles more qualitatively to develop the empirical models used to calculate infiltration.

Consider a block of soil that is homogeneous with water table at depth and initially hydrostatic conditions above the water table (Figure 37). Hydrostatic conditions mean that water is not moving, so in Darcy's equation (16), q=0, dh/dz=0 and therefore the hydraulic head h is constant. Because pressure head ψ is 0 at the water table equation (18) implies that $\psi = -z$ where z is the height above the water table. This gives initial moisture content at each depth z

$$\theta(z) = \theta(\psi = -z) \tag{37}$$

from the soil moisture retention characteristic.

Beginning at time t=0, liquid water begins arriving at the surface at a specified surface water input rate w. This water goes into storage in the layer, increasing its water content. The increase in water content causes an increase in hydraulic conductivity according to the hydraulic conductivity – water content relation for the soil (equations 25, 26, 27). Also because the water content is increased, the absolute value of the negative pressure head is reduced according to the soil moisture characteristic and a downward hydraulic gradient is induced. This results in a flux out of the surface layer in to the next layer down. This process happens successively in each layer as water input continues, resulting in the successive water content profiles at times t_1, t_2 and t_3 shown in Figure 37.
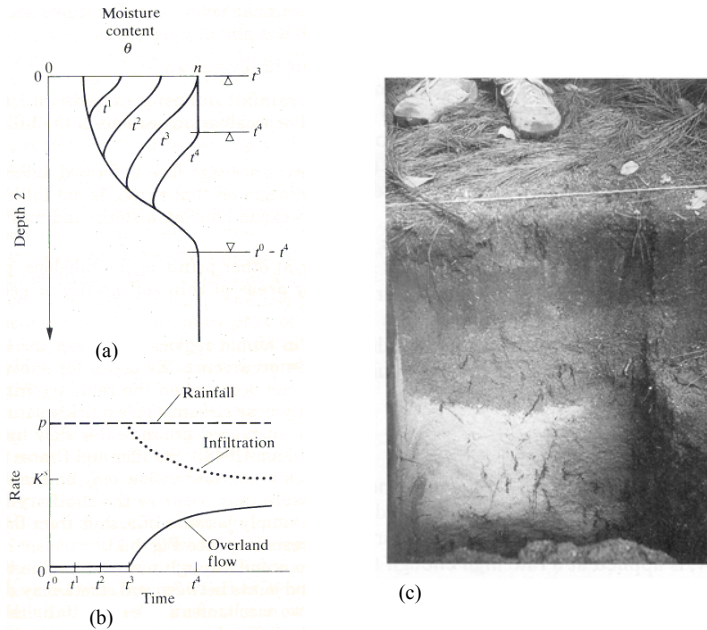
Figure 37. Infiltration excess runoff generation mechanism. (a) Moisture content versus depth profiles and (b) Runoff generation time series. (Bras, Hydrology: An introduction to Hydrologic Science, © 1990. Electronically reproduced by permission of Pearson Education, Inc., Upper Saddle River, New Jersey) (c) Wetting front in a sandy soil exposed after intense rain (Dingman, Physical Hydrology, 2/E, © 2002. Electronically reproduced by permission of Pearson Education, Inc., Upper Saddle River, New Jersey).

Note that the downward hydraulic gradient inducing infiltration is from a combination of the effect of gravity, quantified by the elevation head, and capillary surface tension forces, quantified by the pressure head (negative due to suction) being lower at depth due to lower moisture content. Now if water input rate is greater than the saturated hydraulic conductivity (i.e. $w > K_{sat}$), at some point in time the water content at the surface will reach saturation. At this time the infiltration capacity drops below the surface water input rate and runoff is generated. This is indicated in Figure 37 as time t_3 and is called the *ponding time*. After ponding occurs, water continues to infiltrate and a zone of saturation begins to propagate downward into the soil, as show for t_4 in Figure 37. This wave of soil moisture propagating into the soil (from t_1 to t_4) is referred to as a wetting front. After ponding the infiltration rate is less than the water input

rate and the excess water accumulates at the surface and becomes infiltration excess runoff. As time progresses and the depth of the zone of saturation increases, the contribution of the suction head to the gradient inducing infiltration is reduced, so infiltration capacity is reduced.

The time series of water input, infiltration and surface runoff during this process is depicted in Figure 37b, which shows a reduction in infiltration with time and a corresponding increase in runoff. The necessary conditions for the generation of runoff by the infiltration excess mechanism are (1) a water input rate greater than the saturated hydraulic conductivity of the soil, and (2) a surface water input duration longer than the required ponding time for a given initial soil moisture profile and water input rate.

Now consider a similar situation, but with the water table nearer to the surface as depicted in Figure 38.
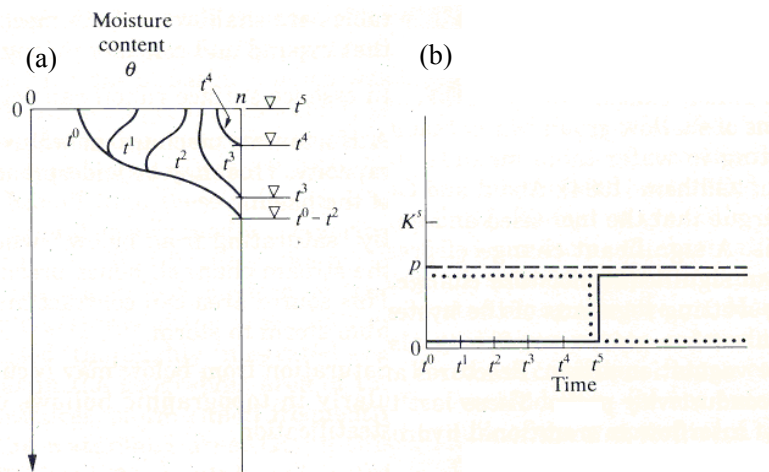
Figure 38. Saturation excess runoff generation mechanism. (a) Moisture content versus depth profiles, and (b) Runoff generation time series. (Bras, Hydrology: An introduction to Hydrologic Science, © 1990. Electronically reproduced by permission of Pearson Education, Inc., Upper Saddle River, New Jersey)

If initial conditions are hydrostatic the initial moisture content is again given by (37). At each depth z, the soil moisture deficit, below saturation is therefore $n-\theta(z)$. Integrating this from the water table to the surface we obtain the total soil moisture deficit as

$$D = \int_0^{z_w} (n - \theta(z))dz \qquad (38)$$

This defines the total amount of water that can infiltrate into a soil profile. Surface water input to a situation like this again (similar to the infiltration excess case) results in soil moisture profiles at times t_1, t_2, t_3, and t_4, depicted in Figure 38a. However, even if $w < K_{sat}$, a point in time is reached where the accumulated surface water input is equal to D. At this time the soil profile is completely saturated and no further water can infiltrate. Infiltration capacity goes to zero, and all surface water input becomes runoff. This is the saturation excess runoff generation mechanism. The time series of surface water input, infiltration and surface runoff for this mechanism are depicted in Figure 38b.

Note that the infiltration excess and saturation excess mechanisms are not mutually exclusive. One or the other could occur in a given situation given different initial depths to the water table and surface water input rates.

Green–Ampt Model

The Green – Ampt (1911) model is an approximation to the infiltration excess process described above and depicted in Figure 37. In Figure 37 successive soil moisture profiles were shown as curves, with moisture content gradually reducing to the initial conditions below the wetting front. The Green – Ampt model approximates the curved soil moisture profiles, that result in practice, and from solution to Richard's equation, as a sharp interface with saturation conditions, $\theta = n$, above the wetting front and initial moisture content, $\theta = \theta_o$, below the wetting front (Figure 39). The initial moisture content is assumed to be uniform over depth. Let L denote the depth to the wetting front. Denote the difference between initial and saturation moisture contents as $\Delta\theta = n - \theta_o$. Then the depth of infiltrated water following initiation of infiltration is

$$F = L \Delta\theta \qquad (39)$$

The datum for the definition of hydraulic head is taken as the surface and an unlimited supply of surface water input is assumed, but with small ponding depth, so the contribution to hydraulic gradient from the depth of ponding at the surface is neglected. Immediately below

the wetting front, at depth just greater than L, the soil is at its initial unsaturated condition, with corresponding suction head $|\psi_f|$. The hydraulic head difference driving infiltration, measured from the surface to just below the wetting front is therefore

$$h = -(L + |\psi_f|) \tag{40}$$

The hydraulic gradient is obtained by dividing this head difference by the distance L between the surface and the wetting front to obtain

$$\frac{dh}{dz} = -\frac{L + |\psi_f|}{L} \tag{41}$$
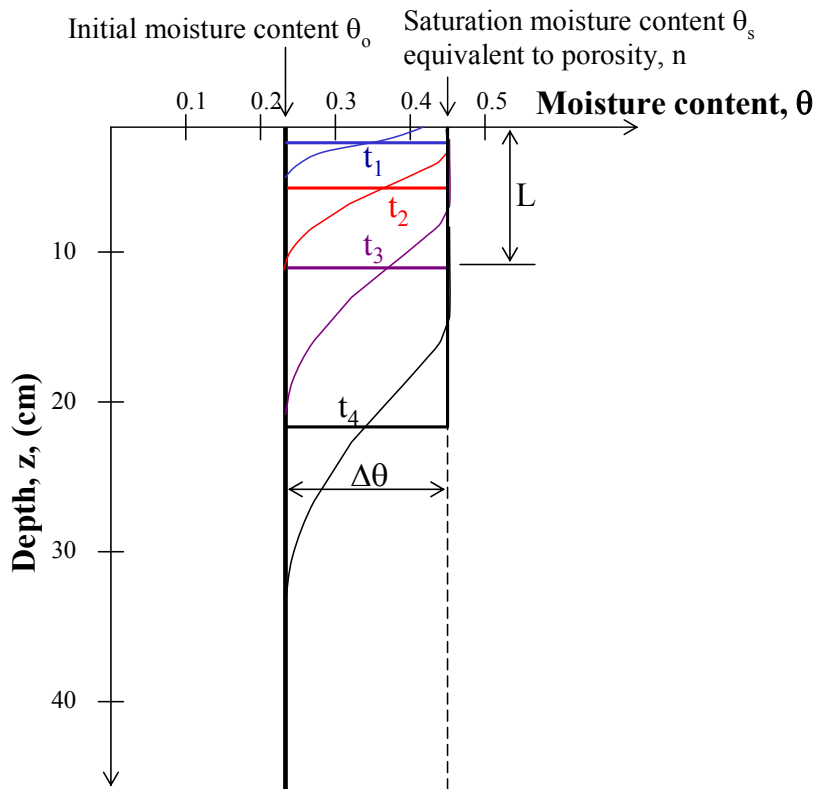
Figure 39. Green–Ampt model idealization of wetting front penetration into a soil profile.

Using this in Darcy's equation (16) gives the infiltration capacity as

$$f_c = K_{sat} \frac{L + |\psi_f|}{L} = K_{sat}\left(1 + \frac{|\psi_f|}{L}\right)$$

$$= K_{sat}\left(1 + \frac{|\psi_f|\Delta\theta}{F}\right) = K_{sat}\left(1 + \frac{P}{F}\right) \tag{42}$$

where in the third expression (39) has been used to express $L = F/\Delta\theta$. This provides an expression for the reduction in infiltration capacity as a function of infiltrated depth $f_c(F)$. The parameters involved are K_{sat} and the product $P = |\psi_f|\Delta\theta$. Using the soil moisture characteristic ψ_f may be estimated as

$$\psi_f = \psi(\theta_o) \tag{43}$$

Values for θ_o may be estimated from field capacity θ_{fc}, or wilting point θ_{pwp}, depending on the antecedent conditions. Rawls et al. (1993) recommended evaluating $|\psi_f|$ from the air entry pressure as

$$|\psi_f| = \frac{2b+3}{2b+6}|\psi_a| \tag{44}$$

where $|\psi_a|$ and b are from table 1. The latter simpler approach appears to be justified for most hydrologic purposes (Dingman, 2002). Table 2 gives Green-Ampt infiltration parameters for soil texture classes reported by Rawls et al. (1983).

Given a surface water input rate of w, the cumulative infiltration prior to ponding is F = wt. Ponding occurs when infiltration capacity decreases to the point where it equals the water input rate, $f_c = w$. Setting $f_c = w$ in (42) and solving for F one obtains the cumulative infiltration at ponding

Green-Ampt cumulative infiltration at ponding:
$$F_p = \frac{K_{sat}|\psi_f|\Delta\theta}{(w - K_{sat})} \tag{45}$$

The time to ponding is then

Green-Ampt time to ponding:
$$t_p = F_p/w = \frac{K_{sat}|\psi_f|\Delta\theta}{w(w - K_{sat})} \tag{46}$$

Table 2. Green – Ampt infiltration parameters for various soil classes (Rawls et al., 1983). The numbers in parentheses are one standard deviation around the parameter value given.

Soil Texture	Porosity n	Effective porosity θ_e	Wetting front soil suction head $|\psi_f|$ (cm)	Hydraulic conductivity K_{sat} (cm/hr)
Sand	0.437 (0.374-0.500)	0.417 (0.354-0.480)	4.95 (0.97-25.36)	11.78
Loamy sand	0.437 (0.363-0.506)	0.401 (0.329-0.473)	6.13 (1.35-27.94)	2.99
Sandy loam	0.453 (0.351-0.555)	0.412 (0.283-0.541)	11.01 (2.67-45.47)	1.09
Loam	0.463 (0.375-0.551)	0.434 (0.334-0.534)	8.89 (1.33-59.38)	0.34
Silt loam	0.501 (0.420-0.582)	0.486 (0.394-0.578)	16.68 (2.92-95.39)	0.65
Sandy clay loam	0.398 (0.332-0.464)	0.330 (0.235-0.425)	21.85 (4.42-108.0)	0.15
Clay loam	0.464 (0.409-0.519)	0.309 (0.279-0.501)	20.88 (4.79-91.10)	0.1
Silty clay loam	0.471 (0.418-0.524)	0.432 (0.347-0.517)	27.30 (5.67-131.50)	0.1
Sandy clay	0.430 (0.370-0.490)	0.321 (0.207-0.435)	23.90 (4.08-140.2)	0.06
Silty clay	0.479 (0.425-0.533)	0.423 (0.334-0.512)	29.22 (6.13-139.4)	0.05
Clay	0.475 (0.427-0.523)	0.385 (0.269-0.501)	31.63 (6.39-156.5)	0.03

⊠ See Online Resource

Excel spreadsheet with table in electronic form

To solve for the infiltration that occurs after ponding with the Green Ampt model, recognize that infiltration rate is the derivative of cumulative infiltration, and is limited by the infiltration capacity

$$f(t) = \frac{dF}{dt} = f_c(t) \tag{47}$$

Here the functional dependence on time is explicitly shown. Now using (42) the following differential equation is obtained

$$\frac{dF}{dt} = K_{sat}(1 + \frac{P}{F}) \tag{48}$$

Using separation of variables this can be integrated from any initial cumulative infiltration depth F_s at time t_s to a final cumulative infiltration depth F at time t

Green-Ampt infiltration under ponded conditions:

$$t - t_s = \frac{F - F_s}{K_{sat}} + \frac{P}{K_{sat}} \ln\left(\frac{F_s + P}{F + P}\right) \tag{49}$$

There is no explicit expression for F from this equation. However by setting $t_s = t_p$, and $F_s = F_p$ this equation can be solved numerically for F given any arbitrary t (greater than t_p) to give the cumulative infiltration as a function of time.

An important concept that emerges from the Green – Ampt model is that infiltration capacity during a storm decreases as a function of cumulative infiltrated depth. This provides for a decrease in infiltration capacity and increase in runoff ratio with time, consistent with empirical observations. The dependence on cumulative infiltrated depth means that cumulative infiltrated depth may be treated as a state variable and that variable rainfall rates, and hence variable infiltration rates, and consequent variability in the rate at which infiltration capacity is reduced, is modeled quite naturally using the Green – Ampt model. This is referred to as the infiltrability-depth approximation (IDA) (Smith et al., 2002).

In the Horton and Philip infiltration models discussed below the decrease in infiltration capacity is modeled explicitly as a function of time rather than cumulative infiltrated depth. Alternative equivalent solution procedures can be developed using the time compression approach (Mein and Larson, 1973) or the infiltrability-depth approximation. Here the infiltrability-depth approximation is used, because this provides a more natural and physically sound basis for understanding and using this approach.

Horton Model

The Horton infiltration capacity formulation (Horton, 1939; although apparently first proposed by others Gardner and Widstoe, 1921) has an initial infiltration capacity value f_0, for dry or pre-storm conditions. Once surface water input and infiltration commences,

this decreases in an exponential fashion to a steady state infiltration capacity, f_1.

$$f_c(t) = f_1 + (f_0 - f_1)e^{-kt} \qquad (50)$$

Here k is a rate parameter quantifying the rate at which infiltration capacity decreases with time. Eagleson (1970) showed that Horton's equation can be derived from Richard's equation by assuming that K and D are constants independent of the moisture content of the soil. Under these conditions equation (35) reduces to

$$\frac{\partial \theta}{\partial t} = D \frac{\partial^2 \theta}{\partial z^2} \qquad (51)$$

which is the standard form of a diffusion equation and may be solved to yield the moisture content as a function of time and depth. Horton's equation results from solving for the rate of moisture diffusion at the soil surface under specific initial and boundary conditions.

Figure 40 shows the Horton infiltration equation as applied to a given rainfall event. It may be argued that at point t_1 where surface water input rate first exceeds infiltration capacity; the actual infiltration capacity will be larger than that given by $f_c(t_1)$ in the Figure. This is because $f_c(t_1)$ assumes that the infiltration rate has decayed from f_0 due to increased soil moisture from the water that has infiltrated. The cumulative depth of infiltration that has contributed to soil moisture is given by the area under the $f_c(t)$ curve between time 0 and t_1. This is less than the maximum that would have infiltrated were the surface saturated with an unlimited supply of moisture. To account for this discrepancy, the time compression approach (Mein and Larson, 1973) illustrated in Figure 40, was developed. This can be viewed as a shifting of the $f_c(t)$ curve to the right, but is more fundamentally a recasting of equation (50) in terms of cumulative infiltrated depth, F, rather than t, using the infiltrability-depth approximation. Under conditions of unlimited surface water input, the cumulative infiltration up to time t is expressed as

$$F = \int_0^t f_c(t)dt = f_1 t + \frac{(f_0 - f_1)}{k}(1 - e^{-kt}) \qquad (52)$$

Now eliminating t between equation (50) and (52) (by solving (50) for t and substituting in (52)) results in

$$F = \frac{f_0 - f_c}{k} - \frac{f_1}{k} \ln\left(\frac{f_c - f_1}{f_0 - f_1}\right) \qquad (53)$$

This is an implicit equation that, given F, can be solved for f_c, i.e. it is an implicit function $f_c(F)$.
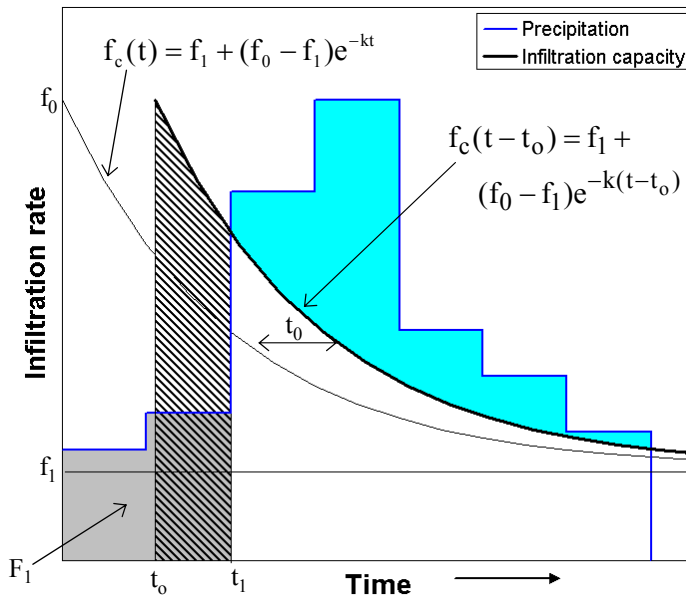
Figure 40. Partition of surface water input into infiltration and runoff using the Horton infiltration equation. Ponding starts at t1. The cumulative depth of water that has infiltrated up to this time is the area F1 (shaded gray). This is less than the maximum possible infiltration up to t1 under the fc(t) curve. To accommodate this the fc(t) curve is shifted in time by an amount to so that the cumulative infiltration from to to t1 (hatched area) equals F1. Runoff is precipitation in excess of fc(t-to) (blue area).

Given a surface water input rate of w, the cumulative infiltration prior to ponding is $F = wt$. Ponding occurs when infiltration capacity decreases to the point where it equals the water input rate, $f_c = w$. Setting $f_c = w$ in (53) one obtains the cumulative infiltration at ponding

Horton cumulative infiltration at ponding:

$$F_p = \frac{f_0 - w}{k} - \frac{f_1}{k} \ln\left(\frac{w - f_1}{f_0 - f_1}\right) \tag{54}$$

The time to ponding is then

Horton time to ponding:

$$t_p = F_p/w = \frac{f_0 - w}{kw} - \frac{f_1}{kw} \ln\left(\frac{w - f_1}{f_0 - f_1}\right) \tag{55}$$

To solve for the infiltration that occurs after ponding with the Horton model, recognize that infiltration rate under ponded conditions is given by f_c, but with the time origin shifted so that the cumulative infiltration F (equation 52) matches the initial cumulative infiltration F_s at an initial time t_s. From (52) t_o is solved implicitly in

$$F_s = f_1(t_s - t_0) + \frac{(f_0 - f_1)}{k}(1 - e^{-k(t_s - t_0)}) \tag{56}$$

Then cumulative infiltration F at any time t (t>t_s) can be obtained from

Horton infiltration under ponded conditions:

$$F = f_1(t - t_0) + \frac{(f_0 - f_1)}{k}(1 - e^{-k(t - t_0)}) \tag{57}$$

Philip Model

Philip (1957; 1969) solved Richard's equation under less restrictive conditions (than used by Eagleson (1970) to obtain Horton's equation) by assuming that K and D can vary with the moisture content θ. Philip employed the Boltzmann transformation $B(\theta) = zt^{-1/2}$ to convert (35) into an ordinary differential equation in B, and solved this equation to yield an infinite series for cumulative infiltration F(t). Approximating the solution by retaining only the first two terms in the infinite series results in

$$F(t) = S_p\, t^{1/2} + K_p\, t \tag{58}$$

where S_p is a parameter called *sorptivity*, which is a function of the soil suction potential and K_p is a hydraulic conductivity. Differentiating with respect to time t, we get

$$f_c(t) = \frac{1}{2} S_p t^{-1/2} + K_p \qquad (59)$$

As time increases the first term will decrease to 0 in the limit and $f_c(t)$ will converge to K_p. $\rightarrow \infty$, $f_c(t)$ tends to K_p. The two terms in Philip's equation represent the effects of soil suction head and gravity head respectively. As with Horton's equation, this equation can also be recast, using the infiltrability-depth approximation, in terms of cumulative infiltrated depth, F, rather than t, by eliminating t between equations (58) and (59).

$$f_c(F) = K_p + \frac{K_p S_p}{\sqrt{S_p^2 + 4K_p F} - S_p} \qquad (60)$$

In Philip's equation S_p is theoretically related to the wetting front suction (and hence to the initial water content of the soil) and to K_{sat}, and K_p is related to K_{sat}. Rawls et al. (1993; citing Youngs, 1964) suggested that S_p is given by

$$S_p = (2K_{sat} \Delta\theta \,|\, \psi_f \,|)^{1/2} \qquad (61)$$

with $|\psi_f|$ from (43) or (44) and $\Delta\theta = n - \theta_o$, the difference between porosity and initial moisture content. Rawls et al. (1993; citing Youngs, 1964) reports K_p ranging from $K_{sat}/3$ to K_{sat} with K_{sat} the preferred value. $K_p = K_{sat}$ is consistent with the reasoning of the Green – Ampt approach and true for an asymptotic infiltration capacity. However Dingman (2002; citing Sharma et al., 1980) reports that for short time periods smaller values of K_p, generally in the range between 1/3 and 2/3 of K_{sat} better fit measured values.

As for the Horton model, given a surface water input rate of w, the cumulative infiltration prior to ponding is F = wt. Ponding occurs when infiltration capacity decreases to the point where it equals the water input rate, i.e. $f_c = w$. Setting $f_c = w$ in (60) one obtains the cumulative infiltration at ponding

Philip cumulative infiltration at ponding:

$$F_p = \frac{S_p^2(w - K_p/2)}{2(w - K_p)^2} \tag{62}$$

The time to ponding is then

Philip time to ponding:

$$t_p = F_p/w = \frac{S_p^2(w - K_p/2)}{2w(w - K_p)^2} \tag{63}$$

Again, as for the Horton model, to solve for the infiltration that occurs after ponding, recognize that infiltration rate under ponded conditions is given by f_c, but with the time origin shifted so that the cumulative infiltration F (equation 58) matches the initial cumulative infiltration F_s at an initial time t_s. From (58) t_o is solved to be

$$t_0 = t_s - \frac{1}{4K_p^2}\left(\sqrt{S_p^2 + 4K_pF_s} - S_p\right)^2 \tag{64}$$

Then cumulative infiltration F at any time t (t>t_s) can be obtained from

Philip infiltration under ponded conditions:

$$F = S_p(t - t_0)^{1/2} + K_p(t - t_0) \tag{65}$$

Working with at a point infiltration models

In many practical applications the parameters in the Green – Ampt model (K_{sat} and P), Horton model (f_0, f_1 and k) and Philip model (S_p and K_p) are treated simply as empirical parameters whose values are those that best fit infiltration data, or as fitting parameters in relating measured rainfall to measured runoff. The equations (42), (53) and (60) provide different, somewhat physical, somewhat empirical representations of the tendency for infiltration capacity to be reduced in response to the cumulative infiltrated depth.

The functions $f_c(F)$ derived above provide the basis for the calculation of runoff at a point, given a time series of surface water inputs, and the soil conditions, quantified in terms of infiltration model parameters. The problem considered is: Given a surface water input hyetograph, and the parameters of an infiltration

equation, determine the ponding time, the infiltration after ponding occurs, and the runoff generated. The process is illustrated in Figure 41. A discrete representation is used for the surface water input using the time average surface water input in each time interval as input to the calculations. This is the typical way that a precipitation hyetograph is represented. There is flexibility to have the time interval as small as required to represent more detail in the input and output. The output is the runoff generated from excess surface water input over the infiltration capacity integrated over each time interval. Infiltration capacity decreases with time due to its dependence on the cumulative infiltrated depth F, which serves as a state variable through the calculations.
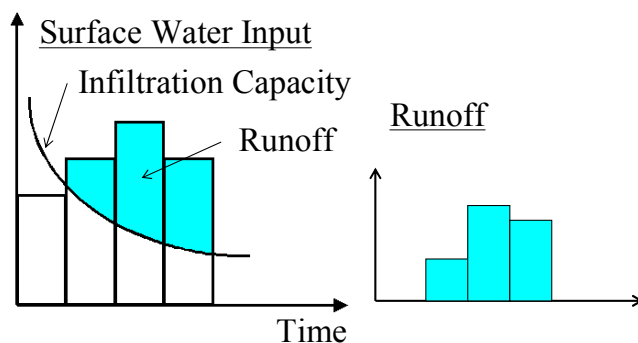
Figure 41. Pulse runoff hyetograph obtained from surface water input hyetograph and variable infiltration capacity.

Figure 42 presents a flow chart for determining infiltration and runoff generated under variable surface water input intensity. Consider a series of time intervals of length Δt. Interval 1 is designated as the interval from $t=0$ to $t=\Delta t$, interval 2 from $t=\Delta t$ to $t=2\Delta t$ and so on. In general interval i is from $t=(i-1)\Delta t$ to $t=i\Delta t$. The surface water input intensity during the interval is denoted w_t and is taken as constant throughout the interval. The cumulative infiltration depth at the beginning of the interval, representing the initial state, is designated as F_t. The infiltration capacity at the beginning of the interval is then obtained from one of equations (42, 53, 60), corresponding to the Green-Ampt, Horton or Philip models as $f_c(F_t)$. The goal is to, given the infiltrated depth, F_t, at the beginning of a time interval and water input, w_t, during the interval, calculate infiltration f_t during the interval and hence $F_{t+\Delta t}$ at the end of the interval, together with any runoff r_t generated during the time interval. The calculation is initialized with F_0 at the beginning of a storm and proceeds from step to step for the full duration of the

surface water input hyetograph. There are three cases to be considered: (1) ponding occurs throughout the interval; (2) there is no ponding throughout the interval; and (3) ponding begins part-way through the interval. The infiltration capacity is always decreasing or constant with time, so once ponding is established under a given surface water input intensity, it will continue. Ponding cannot cease in the middle of an interval. However ponding may cease at the end of an interval when the surface water input intensity changes. The equations used, based on those derived above, are summarized table 3.

The three infiltration models presented are three of the most popular from a number of at a point infiltration models used in hydrology. Fundamentally there are no advantages of one over the other. The Green-Ampt model provides a precise solution to a relatively crude approximation of infiltration in terms of a sharp wetting front. The Horton model can be justified as a solution to Richard's equation under specific (and practically limiting) assumptions. The Philip model has less limiting assumptions (than Horton) but is a series approximation solution to Richard's equation. Infiltration is a complex process subject to the vagaries of heterogeneity in the soil and preferential flow (as illustrated in Figure 5). Practically, infiltration capacity has the general tendency to decrease with the cumulative depth of infiltrated water and these models provide convenient empirical, but to some extent justifiable in terms of the physical processes involved, equations to parameterize this tendency. The choice of which model to use in any particular setting often amounts to a matter of personal preference and experience and may be based on which one fits the data best, or for which one parameters can be obtained. The Green-Ampt model is popular because Green-Ampt parameters based upon readily available soil texture information has been published (table 2 Rawls et al., 1983). Certain infiltration capacity instruments (Guelph permeameter) have been designed to report their results in terms of parameters for the Philip model.

Three examples, one for each of the models are given to illustrate the procedures involved in calculating runoff using these models. These examples all use the same rainfall input and are designed to produce roughly the same output so that differences between the models can be compared. The examples follow the procedure given in the flow chart (Figure 42) and use the equations summarized in table 3 that were derived above.

Initialize: at $t = 0$, $F_t = 0$

A Calculate infiltration capacity f_c from F_t, column 1 of table.

Is $f_c \leq w_t$

$f_c \leq w_t$

$f_c > w_t$

B Ponding occurs throughout interval: $F_{t+\Delta t}$ calculated using infiltration under ponded conditions equations with $t_s = t$ and $F_s = F_t$. Column 3.

C No ponding at the beginning of the interval. Calculate tentative values
$$F'_{t+\Delta t} = F_t + w_t \Delta t$$
f_c from $F'_{t+\Delta t}$ and column 1.

Is $f'_c \leq w_t$

$f'_c \leq w_t$

$f'_c > w_t$

D Ponding starts during the interval. Solve for F_p from w_t, column 2.
$$\Delta t' = (F_p - F_t)/w_t$$
$F_{t+\Delta t}$ calculated using infiltration under ponded conditions equations with $t_s = t + \Delta t'$ and $F_s = F_p$. Column 3.

E No ponding throughout interval
$$F_{t+\Delta t} = F'_{t+\Delta t}$$

F Infiltration is $f_t = F_{t+\Delta t} - F_t$

Runoff generated is $r_t = w_t \Delta t - f_t$

G Increment time $t = t + \Delta t$

Figure 42. Flow chart for determining infiltration and runoff generated under variable surface water input intensity.

Table 3. Equations for variable surface water input intensity infiltration calculation.

	Infiltration capacity	Cumulative infiltration at ponding	Cumulative infiltration under ponded conditions
Green-Ampt Parameters K_{sat} and P	$f_c = K_{sat}\left(1 + \dfrac{P}{F}\right)$	$F_p = \dfrac{K_{sat}P}{(w - K_{sat})}$ $w > K_{sat}$	$t - t_s = \dfrac{F - F_s}{K_{sat}} + \dfrac{P}{K_{sat}}\ln\left(\dfrac{F_s + P}{F + P}\right)$ Solve implicitly for F
Horton Parameters k, f_o, f_1.	$F = \dfrac{f_o - f_c}{k} - \dfrac{f_1}{k}\ln\left(\dfrac{f_c - f_1}{f_o - f_1}\right)$ Solve implicitly for f_c given F	$F_p = \dfrac{f_o - w}{k} - \dfrac{f_1}{k}\ln\left(\dfrac{w - f_1}{f_o - f_1}\right)$ $f_c < w < f_o$	Solve first for time offset t_o in $F_s = f_1(t_s - t_o) + \dfrac{(f_o - f_1)}{k}(1 - e^{-k(t_s - t_o)})$ then $F = f_1(t - t_o) + \dfrac{(f_o - f_1)}{k}(1 - e^{-k(t - t_o)})$
Philip Parameters K_p and S_p	$f_c(F) = K_p + \dfrac{K_p S_p}{\sqrt{S_p^2 + 4K_p F} - S_p}$	$F_p = \dfrac{S_p^2(w - K_p/2)}{2(w - K_p)^2}$ $w > K_p$	Solve first for time offset to in $t_o = t_s - \dfrac{1}{4K_p^2}\left(\sqrt{S_p^2 + 4K_p F_s} - S_p\right)^2$ then $F = S_p(t - t_o)^{1/2} + K_p(t - t_o)$

Example 1. Green-Ampt. A rainfall hyetograph is given in column 2 of table 4. If this rain falls on a sandy loam of with initial moisture content equal to the field capacity, determine the runoff hyetograph using the Green – Ampt approach.

Solution. The solution is shown in table 4. From table 2, for a sandy loam, K_{sat} = 1.09 cm/h, n=0.453, θ_e = 0.412 and $|\psi_f|$=11.01 cm. From table 1, $|\psi_a|$=21.8 cm and b=4.9. Table 1 gives different values for K_{sat} and n. It is unclear which values are best to use and the K_{sat} values differ by an order of magnitude. This sort of uncertainty is not uncommon. For the purposes of this example we use the K_{sat} and n values from table 2 because these have been developed specifically for the Green-Ampt model.

The effective porosity, θ_e, reported in table 2 suggests a residual moisture content (see equation 24) θ_r=n-θ_e=0.453-0.412=0.041. The concepts of residual moisture content and field capacity are similar (as noted earlier). The residual moisture content could be used with equations (25) or (26) to obtain moisture content corresponding to a negative pressure head that defines field capacity. However this would be inconsistent because the parameters in table 1 are from fits of the simplified Brooks and Corey functions, that do not contain θ_r as a parameter, as expressed in equation (27), to data.

We invert equation (27) to

$$\theta = n\left(\frac{|\psi|}{|\psi_a|}\right)^{-1/b}$$

and use as a definition of field capacity the moisture content corresponding to pressure head ψ = -340 cm in this equation to obtain θ_{fc} = 0.259. This value is larger than θ_r consistent with field capacity being a moisture content reached after about 3 days of drainage as opposed to residual moisture content being a moisture content below which flow in the soil is not possible.

$|\psi_f|$ could also have been estimated from equation (44) which would give a different value to what we obtained from table 2. This is another not uncommon uncertainty in estimation of parameters. Here for the purposes of this example we use the value from table 2.

We now have the information necessary to calculate the P parameter,
$P = |\psi_f|(n-\theta_{fc}) = 2.14$ cm.

The time interval is 15 minutes, $\Delta t = 0.25$ h. Column 2 shows the incremental rainfall in each time interval. The rainfall intensity in column 3 is found from column 2 by dividing by Δt (0.25 h).

With this information we now work through the flowchart (Figure 42). Initially $F = 0$, so $f_c = \infty$ (from 42) and ponding does not occur at time 0. Hence we move from box A to box C in the flowchart:

$$F'_{t+\Delta t} = F_t + w_t\Delta t = 0 + 0.3 = 0.3\,\text{cm}$$

This is the preliminary cumulative infiltration under the assumption of no ponding. The corresponding value of $f'_{t+\Delta t}$ is (from 42)

$$f'_{t+\Delta t} = K_{sat}\left(1 + \frac{P}{F}\right) = 1.09\left(1 + \frac{2.14}{0.3}\right) = 8.867\,\text{cm}/\text{h}$$

as shown in column 7 of the table. This value is greater than w_t; therefore no ponding occurs during this interval and moving on to box E the cumulative infiltration is set to the preliminary value $F_{t+\Delta t} = F'_{t+\Delta t}$ as shown in column 11. Box F gives the infiltration (column 13) and runoff (column 14). The calculation then proceeds to box G where time is incremented and back to box A for the next time step. The same sequence is followed for the first three time steps where it is found that ponding does not occur up to 0.75 hours of rainfall.

During the fourth time interval (starting at 0.75 hours)

$$f'_{t+\Delta t} = K_{sat}\left(1 + \frac{P}{F}\right) = 1.09\left(1 + \frac{2.14}{1.8}\right) = 2.386\,\text{cm}/\text{h}$$

as shown in column 7 of the table. This value is less that $w_t=2.4$ cm/h for the interval from 0.75 to 1 h so ponding starts during this interval. Following the preliminary infiltration rate calculation in box C the calculation proceeds to box D. The cumulative infiltration at ponding is given by (45, also table 3 column2)

$$F_p = \frac{K_{sat} P}{(w - K_{sat})} = \frac{1.09 \times 2.14}{2.4 - 1.09} = 1.781 \text{ cm}$$

The partial time interval required for ponding is

$$\Delta t' = (F_p - F_t)/w_t = (1.781 - 1.2)/2.4 = 0.242 \text{ h.}$$

Ponding therefore starts at $0.75 + 0.242 = 0.992$ h as shown in column 9. Infiltration under ponded conditions occurs from 0.992 h to 1.0 h. The cumulative infiltration at the end of this interval is obtained by solving equation (49, column3 table 3) for F. Define the function

$$g(F) = t - t_s - \frac{F - F_s}{K_{sat}} - \frac{P}{K_{sat}} \ln\left(\frac{F_s + P}{F + P}\right)$$

and solve numerically for $g(F) = 0$. This is accomplished easily using the Solver function in Excel, or using a numerical solution method such as Newton Rhapson (Gerald, 1978). $g(F)$ is shown in column 12. This results in

$$F_{t+\Delta t} = 1.79995 \text{ cm.}$$

(This numerical precision is not warranted but is retained here for clarity to indicate that this number is less than 1.8.) The infiltration in this time interval is therefore (column 13)

$$f_t = F_{t+\Delta t} - F_t = 1.79995 - 1.2 = 0.59995 \text{ cm}$$

The rainfall is 0.6 cm so the runoff generated is $0.6 - 0.59995 = 0.00005$ cm (column 14). Practically this runoff is 0.

At the start of the fifth time interval (time = 1 h) the cumulative infiltration is 1.79995 cm. This leads to an infiltration capacity

$$f_c = K_{sat}\left(1 + \frac{P}{F}\right) = 1.09\left(1 + \frac{2.14}{1.79995}\right) = 2.386 \text{ cm/h}$$

This is already less than the rainfall rate (2.8 cm/h) for the fifth time interval so the calculation proceeds through box B on the flowchart. The procedure is exactly the same as for box D, except that the starting values F_s and t_s are taken as the beginning of the time step

values (columns 8 and 10). There is no need to solve for the time when ponding starts during the interval. Numerical solution of g(F) = 0 is used to obtain $F_{t+\Delta t}$ given in column 11.

Similarly, at the start of the sixth time interval (time=1.25 h) the cumulative infiltration is 2.354 cm which with equation (42) leads to f_c = 2.081 cm/h (column 5), already less than the rainfall rate (3.2 cm/h) so the calculation proceeds through box B on the flowchart to obtain the cumulative infiltration reported in column 11 and infiltration and runoff reported in columns 13 and 14.

During the seventh time interval (starting at time =1.5 h) the rainfall rate reduces to 1.6 cm/h. At the start of this interval the cumulative infiltration is 2.851 cm and using equation (42) the infiltration capacity is 1.908 cm/h (column 5). This is more than the rainfall rate, so in this time interval ponding ceases and all rainfall infiltrates (at least initially). The calculation enters box C of the flowchart and the preliminary cumulative infiltration at the end of the time interval is calculated (column 6)

$$F_{t+\Delta t}' = F_t + w_t \Delta t = 2.851 + 0.4 = 3.251 \text{cm}$$

Using this value in equation (42) gives (column 7) f_c'=1.808 cm/h. This is more than the rainfall rate so no ponding in this interval is confirmed, and the calculation proceeds through box E, F, G, resulting in no runoff being generated.

During the eighth time interval (starting at time =1.75 h) the rainfall rate increases to 2.4 cm/h. At the start of this interval the cumulative infiltration is 3.251 cm and using equation (42) (or recognizing the result from above) the infiltration capacity (column 5) is f_c=1.808 cm/h. This is less than the rainfall rate, so ponding occurs again in this time interval, starting at the beginning of the time interval, and the calculation proceeds through box B similar to the fifth and sixth time intervals above, with infiltration and runoff given in columns 13 and 14.

The last time interval (starting at time = 2.00 h) is similar with ponding throughout the interval. Figure 43 illustrates the rainfall hyetograph, infiltration capacity and runoff generated from this example.
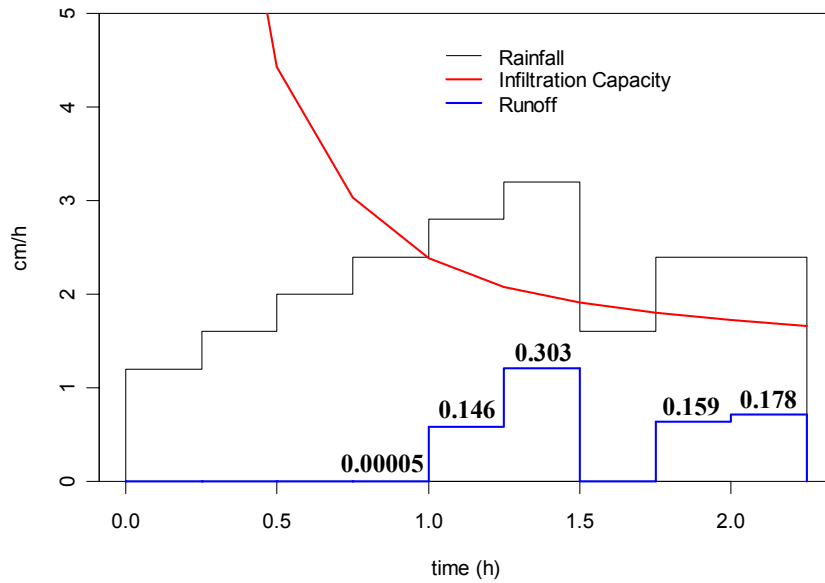
Figure 43. Rainfall Hyetograph, Infiltration Capacity and Runoff Generated in Example 1. Numbers are infiltration in cm in each interval.

Table 4. Calculation of runoff using the Green–Ampt infiltration equation.

Column	1	2	3	4	5	6	7	8	9	10	11	12	13	14
	Time	Incremental Rainfall	Rainfall Intensity	F_t	f_c	F'	f_c'	F_p or F_s	dt'	t_s	$F_{t+\Delta t}$	g(F)	**Infiltration**	**Runoff**
	(h)	(cm)	(cm/h)	(cm)	(cm/h)	(cm)	(cm/h)	(cm)	(h)	(h)	(cm)		**(cm)**	**(cm)**
	0	0.3	1.2	0	∞	0.300	8.867				0.300		**0.300**	**0.000**
	0.25	0.4	1.6	0.300	8.867	0.700	4.423				0.700		**0.400**	**0.000**
	0.50	0.5	2	0.700	4.423	1.200	3.034				1.200		**0.500**	**0.000**
Ponding	0.75	0.6	2.4	1.200	3.034	1.800	2.386	1.781	0.242	0.992	1.79995	0.000	**0.59995**	**0.00005**
	1.00	0.7	2.8	1.800	2.386			1.800	0.000	1.000	2.354	0.000	**0.554**	**0.146**
	1.25	0.8	3.2	2.354	2.081			2.354	0.000	1.250	2.851	0.000	**0.497**	**0.303**
Ponding	1.50	0.4	1.6	2.851	1.908	3.251	1.808				3.251		**0.400**	**0.000**
	1.75	0.6	2.4	3.251	1.808			3.251	0.000	1.750	3.692	0.000	**0.441**	**0.159**
	2.00	0.6	2.4	3.692	1.722			3.692	0.000	2.000	4.114	0.000	**0.422**	**0.178**

Example 2. Horton. Assume the same rainfall hyetograph as for example 1 falls on a soil with Horton infiltration parameters, $f_o = 6$ cm/h, $f_1 = 1$ cm/h, $k = 2$ h^{-1}. Determine the runoff hyetograph using the Horton approach.

Solution. The solution is shown in table 5. Column 2 of table 5 shows the incremental rainfall and column 3 shows rainfall intensity. The solution follows the flowchart in Figure 42. After initializing (F=0) the infiltration capacity needs to be calculated (Box A) by solving equation (53, also given in table 3 column 1) implicitly. Define the function

$$g(f_c) = F - \frac{f_0 - f_c}{k} + \frac{f_1}{k} \ln\left(\frac{f_c - f_1}{f_0 - f_1}\right)$$

This can be solved for $g(f_c) = 0$ using the Solver function in Excel or a numerical solution method such as Newton Rhapson. $g(f_c)$ is shown in column 5. The result for F=0 is $f_c = 6$ shown in column 6. This is greater than the rainfall intensity (column 3) so ponding does not occur at time 0. We now move from box A in the flowchart (Figure 42) to box C:

$$F'_{t+\Delta t} = F_t + w_t \Delta t = 0 + 0.3 = 0.3 \, \text{cm} \quad \text{(column 7)}$$

This is the preliminary cumulative infiltration under the assumption of no ponding. The corresponding value of f'_c is obtained solving equation (53, given in table 3 column 1) implicitly again, this time showing $g(f'_c)$ in column 8 and the solution $f'_c = 5.5$ cm/h in column 9. This value is greater than w_t; therefore no ponding occurs during this interval and moving on to box E the cumulative infiltration is set to the preliminary value $F_{t+\Delta t} = F'_{t+\Delta t}$ as shown in column 15. Box F gives the infiltration (column 16) and runoff (column 17). The calculation then proceeds to box G where time is incremented and back to box A for the next time step. The same sequence is followed for the first four time steps where it is found that ponding does not occur up to 1.0 hours of rainfall.

During the fifth time interval (starting at 1.0 hours) when in box C we obtain $f'_c = 2.327$ cm/h as shown in column 9 of the table. This

value is less that w_t=2.8 cm/h for the interval 1 to 1.25 h so ponding starts during this interval. The calculation therefore proceeds to box D. The cumulative infiltration at ponding is given by equation (54, table 3 column 3)

$$F_p = \frac{f_0 - w}{k} - \frac{f_1}{k} \ln\left(\frac{w - f_1}{f_0 - f_1}\right) = \frac{6 - 2.8}{2} - \frac{1}{2}\ln\left(\frac{2.8 - 1}{6 - 1}\right) = 2.111 \, cm$$

(column 10)

The partial time interval required for ponding is

$$\Delta t' = (F_p - F_t)/w_t = (2.111 - 1.8)/2.8 = 0.111 \text{ h. (column 11)}$$

Ponding therefore starts at $1.0 + 0.111 = 1.111$ h as shown in column 12. Infiltration under ponded conditions occurs from 1.111 h to 1.25 h. The cumulative infiltration at the end of this interval is obtained by solving (56) for t_o implicitly then (57) for F (table 3, column 3). Define the function

$$h(t_0) = F_s - f_1(t_s - t_0) - \frac{(f_0 - f_1)}{k}(1 - e^{-k(t_s - t_0)})$$

and solve numerically for $h(t_0) = 0$. $h(t_0)$ is shown in column 14. This results in t_o=0.6 h (column 13) which in (57) gives

$$F_{t+\Delta t} = 2.468 \text{ cm. (column 15)}$$

The infiltration in this time interval is therefore (column 16)

$$f_t = F_{t+\Delta t} - F_t = 2.468 - 1.8 = 0.668 \text{ cm}$$

The rainfall is 0.7 cm so the runoff generated is 0.7-0.668 = 0.032 cm (column 17).

At the start of the sixth time interval (time = 1.25 h) the cumulative infiltration is 2.468 cm. This leads to an infiltration capacity solved for implicitly in equation (53, column 1 table 3) of 2.363 cm/h shown in column 6. This is already less than the rainfall rate (3.2 cm/h) for the sixth time interval so the calculation proceeds through box B on the flowchart. The procedure is exactly the same as for box D, except that the starting values F_s and t_s are taken as the beginning of the time step values (columns 10 and 12). There is no need to solve for the time when ponding starts during the interval. Numerical

solution of $h(t_0) = 0$ results in the same t_o as in the previous time step. t_o only increases following infiltration under non ponded conditions. Equation (57, table 3 column 3) is used to obtain $F_{t+\Delta t}$ given in column 15.

During the seventh time interval (starting at time =1.5 h) the rainfall rate reduces to 1.6 cm/h. At the start of this interval the cumulative infiltration is 2.986 cm and solving (53) implicitly the infiltration capacity is 1.827 cm/h (column 5). This is more than the rainfall rate, so in this time interval ponding ceases and all rainfall at the beginning of this time step infiltrates. The calculation enters box C of the flowchart and the preliminary cumulative infiltration at the end of the time interval is calculated (column 7)

$$F'_{t+\Delta t} = F_t + w_t \Delta t = 2.986 + 0.4 = 3.386 cm$$

Using this value in equation (53) gives (column 9) $f_c' = 1.510$ cm/h. This is less than the rainfall rate so ponding occurs part of the way through this interval, as was the case during the fifth time interval. The calculation proceeds through boxes D, F and G as for the fifth time interval. The time offset t_o solution to $h(t_0) = 0$ (column 14) increases (slightly) from what it was previously.

During the eighth time interval (starting at time =1.75 h) the rainfall rate increases to 2.4 cm/h. At the start of this interval the cumulative infiltration is 3.383 cm and using equation (53) the infiltration capacity (column 6) is $f_c = 1.512$ cm/h. This is less than the rainfall rate, so ponding occurs again in this time interval, starting at the beginning of the time interval and the calculation proceeds through box B similar to the sixth time interval above, with infiltration and runoff given in columns 16 and 17.

The last time interval (starting at time = 2.00 h) is similar, with ponding throughout the interval. Figure 44 illustrates the rainfall hyetograph, infiltration capacity and runoff generated from this example.
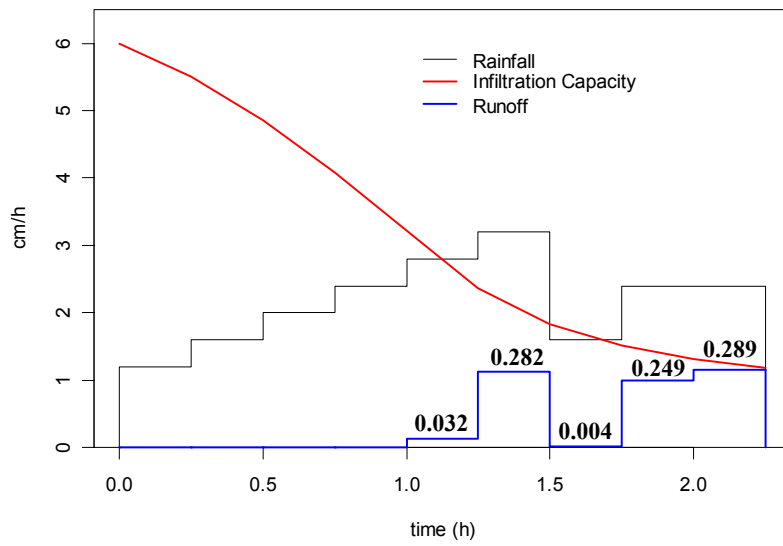
Figure 44. Rainfall Hyetograph, Infiltration Capacity and Runoff Generated in Example 2. Numbers are infiltration in cm in each interval.

Table 5. Calculation of runoff using the Horton infiltration equation.

Column 1	2	3	4	5	6	7	8	9	10	11	12	13	14	15	16	17
	Incremental Rainfall	Rainfall Intensity														
Time	Rainfall	Intensity	F_t	$g(f_c)$	f_c	F'	$g(f_c')$	f_c'	F_p or F_s	dt'	t_s	t_o	$h(t_o)$	$F_{t+\Delta t}$	**Infiltration**	**Runoff**
(h)	(cm)	(cm/h)	(cm)		(cm/h)	(cm)		(cm/h)	(cm)	(h)	(h)	(h)		(cm)	**(cm)**	**(cm)**
0	0.3	1.2	0	0	6	0.300	8E-08	5.504						0.300	**0.300**	0.000
0.25	0.4	1.6	0.300	8E-08	5.504	0.700	4E-07	4.859						0.700	**0.400**	0.000
0.50	0.5	2	0.700	4E-07	4.859	1.200	2E-07	4.083						1.200	**0.500**	0.000
0.75	0.6	2.4	1.200	2E-07	4.083	1.800	2E-07	3.214						1.800	**0.600**	0.000
1.00	0.7	2.8	1.800	2E-07	3.214	2.500	3E-07	2.327	2.111	0.111	1.111	0.600	0.000	2.468	**0.668**	0.032
1.25	0.8	3.2	2.468	8E-07	2.363				2.468	0.000	1.250	0.600	0.000	2.986	**0.518**	0.282
1.50	0.4	1.6	2.986	3E-07	1.827	3.386	8E-07	1.510	3.260	0.171	1.671	0.611	0.000	3.383	**0.396**	0.004
1.75	0.6	2.4	3.383	6E-07	1.512				3.383	0.000	1.750	0.611	0.000	3.734	**0.351**	0.249
2.00	0.6	2.4	3.734	3E-07	1.311				3.734	0.000	2.000	0.611	0.000	4.045	**0.311**	0.289

Ponding Ponding

Example 3. Philip. A rainfall hyetograph is given in column 2 of table 6. If this rain falls on a sandy loam, determine the runoff hyetograph using the Philip approach.

Solution. The solution is shown in table 6. From table 2, for a sandy loam, K_{sat} = 1.09 cm/h, θ_e = 0.412 and $|\psi_f|$ =11.01 cm. Assuming $\Delta\theta = \theta_e$ in equation (61) we get

Excel spreadsheet used in Example 3.

$$S_p = (2K_{sat}\Delta\theta\,|\psi_f\,|)^{1/2}$$
$$= (2\times1.09\times0.412\times11.01)^{1/2} = 3.14\,\mathrm{cm\,h}^{-1/2}$$

Take K_p =K_{sat}/2 = 0.545 cm/h in the middle of the range from 1/3 K_p to 2/3 K_{sat} suggested by Sharma (1980). The solution follows the flowchart in Figure 42. Initially F=0, so f_c = ∞ (from 60) and ponding does not occur at time 0. The calculation moves from box A to box C in the flowchart.

$$F'_{t+\Delta t} = F_t + w_t\Delta t = 0 + 0.3 = 0.3\,\mathrm{cm} \qquad \text{(column 6)}$$

This is the preliminary cumulative infiltration under the assumption of no ponding. The corresponding value of f'_c is calculated using equation (60, table 3 column 1)

$$f_c\,(F) = K_p + \frac{K_p S_p}{\sqrt{S_p^2 + 4K_p F} - S_p}$$
$$= 0.545 + \frac{0.545\times3.14}{\sqrt{3.14^2 + 4\times0.545\times0.3} - 3.14} = 17.29\,\mathrm{cm/h}$$

as shown in column 7 of the table. This value is greater than w_t; therefore no ponding occurs during this interval and moving on to box E the cumulative infiltration is set to the preliminary value $F_{t+\Delta t} = F'_{t+\Delta t}$ as shown in column 12. Box F gives the infiltration (column 13) and runoff (column 14). The calculation then proceeds to box G where time is incremented and back to box A for the next time step. The same sequence is followed for the first four time steps where it is found that ponding does not occur up to 1.0 hours of rainfall.

During the fifth time interval (starting at 1.00 hours) when in box C we obtain

$$f_c (F) = K_p + \frac{K_p S_p}{\sqrt{S_p^2 + 4K_p F} - S_p}$$

$$= 0.545 + \frac{0.545 \times 3.14}{\sqrt{3.14^2 + 4 \times 0.545 \times 2.5} - 3.14} = 2.765 \, cm/h$$

as shown in column 7 of the table. This value is less that w_t=2.8 cm/h for the interval 1.0 to 1.25 h so ponding starts during this interval. The calculation therefore proceeds to box D. The cumulative infiltration at ponding F_p is given by (62, table 3, column 2)

$$F_p = \frac{S_p^2(w - K_p/2)}{2(w - K_p)^2} = \frac{3.14^2(2.8 - 0.545/2)}{2(2.8 - 0.545)^2} = 2.458 \, cm$$

The partial time interval required for ponding is

$$\Delta t' = (F_p\text{-}F_t)/w_t = (2.458 - 1.8)/2.8 = 0.235 \, h.$$

Ponding therefore starts at $1.0 + 0.235 = 1.235$ h as shown in column 10. Infiltration under ponded conditions occurs from 1.235 h to 1.25 h. The cumulative infiltration at the end of this interval is obtained by solving (64, table 3 column 3) for t_o then (65, table 3 column 3) for F.

$$t_0 = t_s - \frac{1}{4K_p^2}\left(\sqrt{S_p^2 + 4K_p F_s} - S_p\right)^2$$

$$= 1.235 - \frac{1}{4 \times 0.545^2}\left(\sqrt{3.14^2 + 4 \times 0.545 \times 2.458} - 3.14\right)^2$$

$$= 0.749$$

$$F = S_p(t - t_0)^{1/2} + K_p(t - t_0)$$

$$= 3.14 \times (1.25 - 0.749)^{1/2} + 0.545 \times (1.25 - 0.749)$$

$$= 2.4997 \, cm$$

This result is practically equivalent, but numerically slightly less than the cumulative rainfall of 2.5 cm up to this point. The infiltration in this time interval is therefore (column 13)

$$f_t = F_{t+\Delta t} - F_t = 2.4997 - 1.8 = 0.6997 \text{ cm}$$

The rainfall is 0.7 cm so the runoff generated is 0.7-0.6997 = 0.0003 cm (column 14), which is practically 0. The precision carried here is only for clarity in the calculations.

At the start of the sixth time interval (time = 1.25 h) the cumulative infiltration is 2.4997 cm. This leads to an infiltration capacity

$$
\begin{aligned}
f_c\,(F) &= K_p + \frac{K_p S_p}{\sqrt{S_p^2 + 4K_p F} - S_p} \\
&= 0.545 + \frac{0.545 \times 3.14}{\sqrt{3.14^2 + 4 \times 0.545 \times 2.4997} - 3.14} \\
&= 2.766 \text{ cm/h}
\end{aligned}
$$

This is already less than the rainfall rate (3.2 cm/h) for the sixth time interval so the calculation proceeds through box B on the flowchart. The procedure is exactly the same as for box D, except that the starting values F_s and t_s are taken as the beginning of the time step values (columns 8 and 10). There is no need to solve for the time when ponding starts during the interval.

During the seventh time interval (starting at time =1.5 h) the rainfall rate reduces to 1.6 cm/h. At the start of this interval the cumulative infiltration is 3.135 cm and using equation (60, table 3 column 1) the infiltration capacity is 2.359 cm/h (column 5). This is more than the rainfall rate, so in this time interval ponding ceases and all rainfall infiltrates (at least initially). The calculation enters box C of the

flowchart and the preliminary cumulative infiltration at the end of the time interval is calculated (column 6)

$$F'_{t+\Delta t} = F_t + w_t \Delta t = 3.135 + 0.4 = 3.535 \text{ cm}$$

Using this value in equation (60, table 3 column 1) gives (column 7) $f_c' = 2.177$ cm/h. This is more than the rainfall rate so no ponding in this interval is confirmed, and the calculation proceeds through box E, F, G, resulting in no runoff being generated.

During the eighth time interval (starting at time =1.75 h) the rainfall rate increases to 2.4 cm/h. At the start of this interval the cumulative infiltration is 3.535 cm and using equation (60, table 3 column 1) (or recognizing the result from above) the infiltration capacity (column 5) is $f_c = 2.177$ cm/h. This is less than the rainfall rate, so ponding occurs again, starting at the beginning of the time interval and the calculation proceeds through box B similar to the sixth time interval above, with infiltration and runoff given in columns 13 and 14.

The last time interval (starting at time = 2.00 h) is similar with ponding throughout the interval. Figure 45 illustrates the rainfall hyetograph, infiltration capacity and runoff generated from this example.
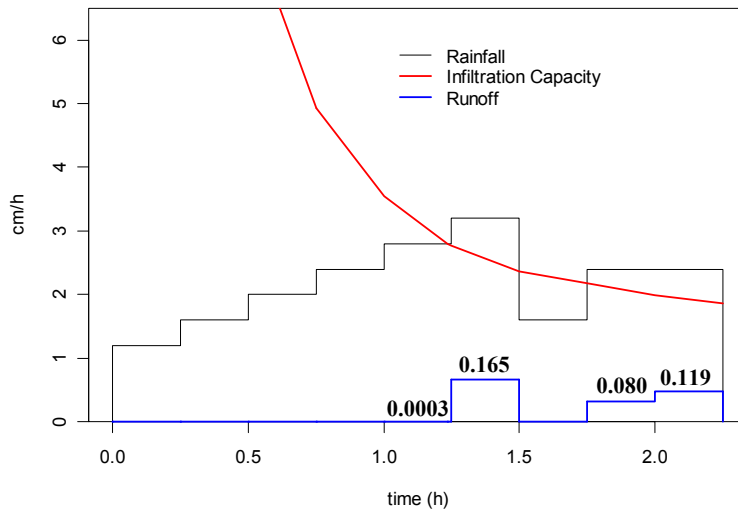

Figure 45. Rainfall Hyetograph, Infiltration Capacity and Runoff Generated in Example 3. Numbers are infiltration in cm in each interval.

Table 6. Calculation of runoff using the Philip infiltration equation.

Column 1	2	3	4	5	6	7	8	9	10	11	12	13	14
Time	Incremental Rainfall	Rainfall Intensity	F_t	f_c	F'	f_c'	F_p or F_s	dt'	t_s	t_o	$F_{t+\Delta t}$	**Infiltration**	**Runoff**
(h)	(cm)	(cm/h)	(cm)	(cm/h)	(cm)	(cm/h)	(cm)	(h)	(h)	(h)	(cm)	**(cm)**	**(cm)**
0	0.3	1.2	0	∞	0.300	17.294					0.300	**0.300**	**0.000**
0.25	0.4	1.6	0.300	17.294	0.700	7.8711					0.700	**0.400**	**0.000**
0.50	0.5	2	0.700	7.8711	1.200	4.9218					1.200	**0.500**	**0.000**
0.75	0.6	2.4	1.200	4.9218	1.800	3.5417					1.800	**0.600**	**0.000**
1.00	0.7	2.8	1.800	3.5417	2.500	2.7655	2.458	0.235	1.235	0.749	2.4997	**0.6997**	**0.0003**
1.25	0.8	3.2	2.4997	2.7657			2.4997	0.000	1.250	0.749	3.135	**0.635**	**0.165**
1.50	0.4	1.6	3.135	2.359	3.535	2.1771					3.535	**0.400**	**0.000**
1.75	0.6	2.4	3.535	2.1771			3.535	0.000	1.750	0.822	4.055	**0.520**	**0.080**
2.00	0.6	2.4	4.055	1.9936			4.055	0.000	2.000	0.822	4.536	**0.481**	**0.119**

Ponding

Empirical and index methods

The Horton, Philip and Green-Ampt at a point infiltration models attempt to represent the physics of the infiltration process described by Richard's equation, albeit in a simplified way (although given the examples above it may not seem so simple). In many situations the data does not exist to support application of one of these approaches, or spatial variability over a watershed makes this impractical. Empirical and index methods are therefore still rather commonly used in practice, despite being lacking in theoretical basis.

The ϕ Index. The ϕ index method requires that a rainfall hyetograph and streamflow hydrograph are available. First baseflow needs to be separated from streamflow to produce the direct runoff hydrograph. Various methods for baseflow separation are illustrated in Figure 46. These are acknowledged as empirical and somewhat arbitrary. The ϕ index is that constant rate of abstractions (in/h or cm/h) that will yield an excess rainfall hyetograph (ERH) with a total depth equal to the depth of direct runoff over the watershed. The volume of loss is distributed uniformly across the storm pattern as shown in Figure 47. The ϕ index determined from a single storm is not generally applicable to other storms, and unless it is correlated with basin parameters other than runoff, it is of little value (Viessman et al., 1989).

(a) Straight line method.
(b) Fixed base method.
(c) Variable slope method.
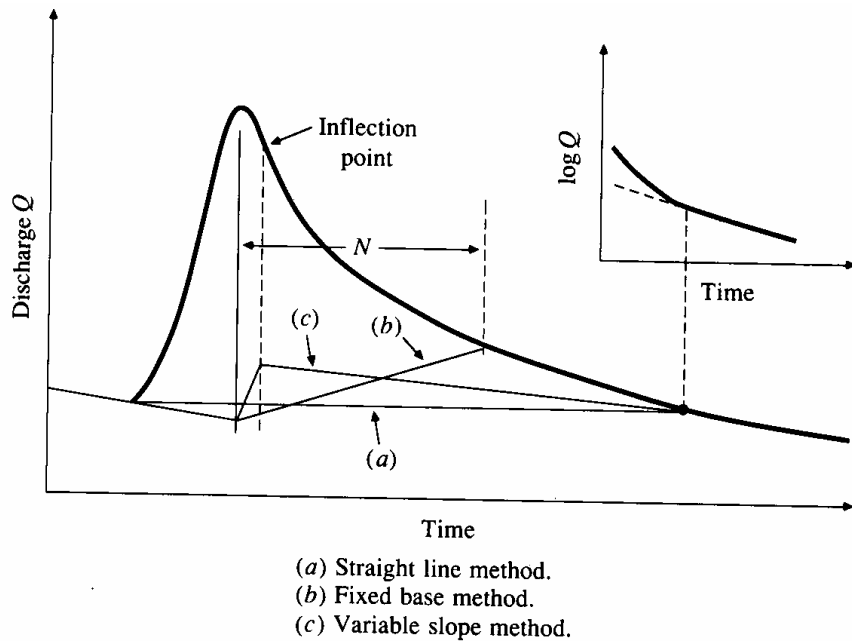
Figure 46. Baseflow Separation Techniques (from Chow et al, 1988). Linsley et al. (1982) suggest as a rule of thumb N=0.2A, for A in square miles and N in days for the fixed base method (b).
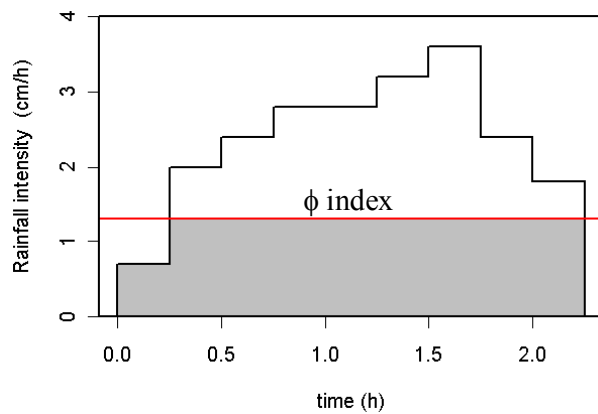
Figure 47. Representation of a φ index.

Runoff Coefficients. Abstractions may also be accounted for by means of runoff coefficients. The most common definition of a runoff coefficient is that it is the ratio of the peak rate of direct runoff to the average intensity of rainfall in a storm. Because of

highly variable rainfall intensity, this value is difficult to determine from observed data. A runoff coefficient can also be defined to be the ratio of runoff to rainfall over a given time period. These coefficients are most commonly applied to storm rainfall and runoff, but can also be used for monthly or annual rainfall and streamflow data.

The SCS Method. The following description follows Chow et al. (1988). The Soil Conservation Service (1972) developed a method for computing abstractions from storm rainfall. For the storm as a whole, the depth of excess precipitation or direct runoff R is always less than or equal to the depth of precipitation P; likewise, after runoff begins, the additional depth of water retained in the watershed, F_a, is less than or equal to some potential maximum retention S. There is some amount of rainfall I_a (initial abstraction) for which no runoff will occur, so the potential runoff is P-I_a. The hypothesis of the SCS method is that the ratios of the two actual to the two potential quantities are equal, that is,

$$\frac{F_a}{S} = \frac{R}{P - I_a} \tag{66}$$

From the continuity principle

$$P = R + I_a + F_a \tag{67}$$

Combining (66) and (67) to solve for R gives

$$R = \frac{(P - I_a)^2}{P - I_a + S} \tag{68}$$

which is the basic equation for computing the depth of excess rainfall or direct runoff from a storm by the SCS method.

By study of results from many small experimental watersheds, an empirical relation was developed

$$I_a = 0.2 \, S \tag{69}$$

On this basis

$$R = \frac{(P - 0.2S)^2}{P + 0.8S} \tag{70}$$

Plotting data for P and R from many watersheds, the SCS found
curves of the type shown in Figure 48. To standardize these curves, a
dimensionless curve number CN is defined such that $0 \leq CN \leq 100$.
For impervious and water surfaces CN = 100; for natural surfaces
CN < 100.

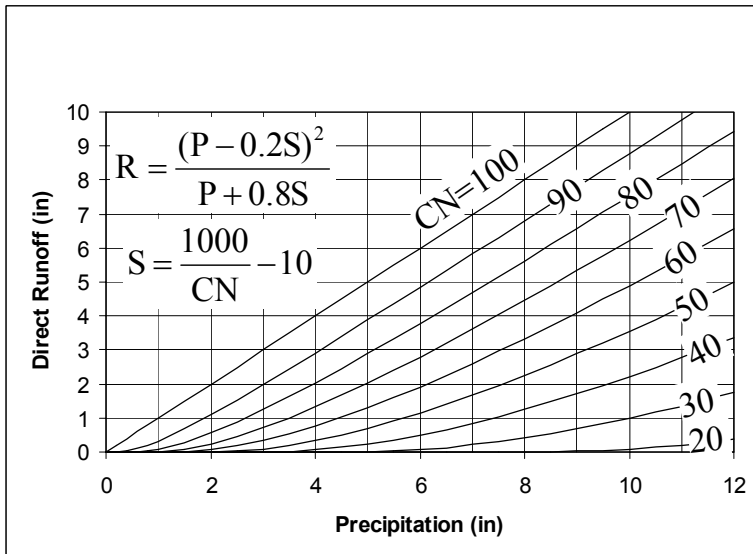Figure 48. Solution to the SCS runoff equations.

The curve number and S are related by

$$S = \frac{1000}{CN} - 10 \tag{71}$$

where S is in inches. The curve numbers shown in Figure 48 apply
for *normal antecedent moisture conditions* (AMC II).

For dry conditions (AMC I) or wet conditions (AMC III), equivalent curve numbers can be computed by

$$CN(I) = \frac{4.2CN(II)}{10 - 0.058CN(II)} \qquad (72)$$

and

$$CN(III) = \frac{23CN(II)}{10 + 0.13CN(II)} \qquad (73)$$

The range of antecedent moisture conditions for each class is shown in table 7. Curve numbers have been tabulated by the Soil Conservation Service on the basis of soil type and land use. Four soil groups are used:

Group A: Low runoff potential. Soils having high infiltration capacity even if thoroughly wetted, such as deep sand, deep loess, aggregated silts.

Group B: Soils having moderate infiltration capacity if thoroughly wetted, such as shallow loess, aggregated silts.

Group C: Soils having low infiltration capacity if thoroughly wetted, such as clay loams, shallow sandy loam, soils low in organic content and soils usually high in clay.

Group D: High runoff potential. Soils having very low infiltration capacity if thoroughly wetted consisting chiefly of soils that swell significantly when wet, heavy plastic clays, and certain saline soils.

The values of CN for various land uses on these soil types are given in table 8. For a watershed made up of several soil types and land uses a composite average CN is customarily used, despite the nonlinearity of (71) and (70). The SCS curve number methods are empirical and limited in their physical basis, but are often used in practice due to the availability of CN values in soils maps and databases such as STATSGO (USDA-NRCS Soil Survey Division).

Table 7. Classification of antecedent moisture classes (AMC) for the SCS method of rainfall abstraction.

| AMC group | Total 5-day antecedent rainfall (in) | |
	Dormant Season	Growing Season
I	Less than 0.5	Less than 1.4
II	0.5 to 1.1	1.4 to 2.1
III	Over 1.1	Over 2.1

Table 8. Runoff curve numbers for selected agricultural, suburban and urban land uses.

| Land Use Description | Hydrologic Soil Group | | | |
	A	B	C	D
Cultivated land: without conservation treatment	72	81	88	99
with conservation treatment	62	71	787	81
Pasture or range land: poor condition[1]	68	79	86	89
good condition[1]	39	61	74	80
Meadow: good condition	30	58	71	78
Wood or forest land: thin stand, poor cover, no mulch	45	66	77	83
good cover[2]	25	55	70	77
Open Spaces, lawns, parks, golf courses, cemeteries, etc.				
good condition: grass cover on 75% or more of the area	39	61	74	80
fair condition: grass cover on 50% to 75% of the area	49	69	79	84
Commercial and business areas (85% impervious)	89	92	94	95
Industrial districts (72% impervious)	81	88	91	93
Residential				
Average lot size Average % impervious				
1/8 acre or less 65	77	85	90	92
1/4 acre 38	61	75	83	87
1/3 acre 30	57	72	81	87
1/2 acre 25	54	70	80	85
1 acre 20	51	68	79	84
Paved parking lots, roofs, driveways, etc.	98	98	98	98
Streets and roads:				
paved with curbs and storm sewers	98	98	98	98
gravel	76	85	89	91
dirt	72	82	87	89

1. Poor and good condition here refers to hydrologic condition. Poor is highly grazed or compacted with low infiltrability, good is less disturbed with higher infiltrability.
2. Good cover is protected from grazing ant litter and brush cover soil

Antecedent Precipitation Index.

Antecedent precipitation methods have been empirically devised to account for the fact that the quantity of runoff from a storm depends on the moisture conditions of the catchment at the beginning of the storm. The precipitation summed over a past period of time is used as a surrogate for soil moisture. The Antecedent Precipitation Index I is computed at the end of each day t from

$$I_t = k \, I_{t-1} + P_t \tag{73}$$

where P_t is the precipitation during day t and k is a recession factor (typically in the range 0.85 to 0.98) representing a logarithmic decrease in soil moisture with time during periods of no precipitation. Infiltration equations based on the antecedent precipitation index take the form

$$f_c = f_1 + (f_0 - f_1)e^{-bI} \tag{74}$$

In antecedent precipitation index methods k, f_0, f_1, and b are empirically or statistically derived coefficients that may vary with season and soil type. Linsley et al. (1982) give further details of this method which has limited physical basis, but given here because it may still be encountered in use in certain situations.

Exercises

1. Consider a silty clay loam soil with the following properties:

Porosity	0.477
Air entry tension ψ_a (cm)	35.6
Pore size distribution index b	7.75
Residual moisture content θ_r	0.15

    Hydrostatic conditions exist over a water table 1.5 m deep.

    a) Calculate the **suction** and **moisture content** at depths of **0.5 m** and **1.25 m**, using the Brooks and Corey soil moisture characteristic equations as well as the Clapp and Hornberger simplifications.
    b) Plot a graph of the **soil moisture content** as a function of depth.
    c) Calculate the **soil moisture deficit**, i.e. the amount of water that could infiltrate before the occurrence of saturation excess runoff. Use the Brooks and Corey soil moisture characteristic equations

2. Consider a silty clay loam soil with the following properties

Porosity	0.477
K_{sat} (cm/h)	0.612
Air entry tension ψ_a (cm)	35.6
Pore size distribution index b	7.75
Initial moisture content	0.3

    a) Calculate ψ_f (cm) according to the Green – Ampt model.
    b) Given precipitation at a rate of 2 cm/h calculate the cumulative infiltration at ponding, F_p (cm), and time to ponding, t_p (h).
    c) Assume that this rainfall of 2 cm/h persists for 3 hours. Calculate the runoff produced in cm.
    d) Calculate the infiltration capacity, f_c (cm/h), at the end of this 3 hour period.

3. Consider a soil with the following properties pertaining to Philip's Infiltration Equation

   Sorptivity, S_p in Philip's equation ($cm/h^{0.5}$)　　　　2.5
   Conductivity, K_p in Philip's equation (cm/h)　　　0.4

   a) Given precipitation at a rate of 2 cm/h calculate the cumulative infiltration at ponding, F_p (cm), and time to ponding, t_p (h).
   b) Calculate the time compression time offset, t_o (h):
   c) Assume that this rainfall of 2 cm/h persists for 3 hours. Calculate the runoff produced in cm:
   d) Calculate the infiltration capacity, f_c (cm/h), at the end of this 3 hour period using the cumulative infiltrated depth F (equation 60).
   e) Calculate the infiltration capacity, f_c (cm/h), at the end of this 3 hour period using equation (59) with $t-t_o$ substituted for t.

4. Consider a soil with infiltration governed by the Horton equation with parameters

   f_o = 4 cm/h
   f_1 = 1 cm/h
   k = 1.3 h^{-1}

   a) Given precipitation at a rate of 2 cm/h calculate the cumulative infiltration at ponding, F_p (cm), and time to ponding t_p (h).
   b) Calculate the time compression time offset, t_o (h).
   c) Assume that this rainfall of 2 cm/h persists for 3 hours. Calculate the runoff produced in cm.
   d) Calculate the infiltration capacity, f_c (cm/h), at the end of this 3 hour period using the cumulative infiltrated depth F (implicit equation 53).
   e) Calculate the infiltration capacity, f_c (cm/h), at the end of this 3 hour period using equation (50) with $t-t_o$ substituted for t.

5. Consider a soil with properties

   Porosity　　　　0.477
   K_{sat} (cm/h)　　0.612
   $|\psi_a|$ (cm)　　　35.6
   b　　　　　　7.75

   a) Use equation (44) to evaluate $|\psi_f|$ from the air entry pressure.
   b) Use the Clapp and Hornberger (1978) simplifications of Brooks and Corey functions (equation 27) to evaluate the

moisture content at field capacity defined as moisture content when $\psi = -340$ cm.

c) Assume field capacity initial conditions to evaluate the Green-Ampt parameter $P = |\psi_f| \Delta\theta$.

d) Use the Green-Ampt model (equation 42) to plot a graph of infiltration capacity as a function of infiltrated volume for this soil.

e) Given the following rainfall hyetograph calculate the ponding, infiltration and runoff generated in each time step.

Time (hours)	0-1	1-2	2-3	3-4
Rainfall intensity (cm/hr)	1	2	4	1.4

6. Consider a soil with properties

Porosity	0.477
K_{sat} (cm/h)	0.612
$|\psi_f|$ (cm)	145.2
Initial moisture content θ_o	0.3

a) Estimate $K_p = K_{sat}/2$ and S_p from equation (61).

b) Use the Philip model (equation 60) to plot a graph of infiltration capacity as a function of infiltrated volume for this soil.

c) Given the following rainfall hyetograph calculate the ponding, infiltration and runoff generated in each time step.

Time (hours)	0-1	1-2	2-3	3-4
Rainfall intensity (cm/hr)	1	2	4	1.4

7. Consider the following storm:

Time (hours)	0-0.5	0.5-1	1-1.5
Rainfall intensity (cm/hr)	5	3	1.5

Horton's equation is applicable with f_o = 6 cm/h, f_1 = 1.06 cm/h and k = 2.3 h^{-1} .

a) Plot a graph of infiltration capacity as a function of infiltrated volume for this soil.

b) Determine the infiltration and runoff generated in each half hour increment. Plot your results. State the total depths of runoff and infiltration. Indicate the times when there is ponding.

8. Consider the following rainfall-runoff data on a watershed with area 0.2 mi^2.

Time (h)	1	2	3	4	5	6	7
Rainfall rate (in/h)	1.05	1.28	0.8	0.75	0.7	0.6	0
Direct runoff (cfs)	0	30	60	45	30	15	0

a) Calculate the volume of direct runoff from this watershed in ft^3. Do this by summing the cfs flows and multiplying by the number of seconds in an hour (3600).

b) Calculate the per unit area depth of direct runoff by dividing your answer in (a) by the basin area. Express your answer in inches. (There are 5280 ft to a mile and 12 in to a foot).

c) Calculate the total storm infiltration loss by subtracting the direct runoff (from b) from the total number of inches of precipitation.

d) Referring to figure 47 apportion this loss over the time steps where there is precipitation to estimate a ϕ-index from this storm. [Hint. In some time steps the rainfall rate will be less than the ϕ-index. You need to accommodate this in your calculations recognizing that in these cases the infiltration is the lesser of rainfall rate and ϕ-index.]

e) Determine the rainfall excess generated in each time step.

9. Compute the runoff from a 7 in rainfall on a watershed that has hydrologic soil groups that are 40% group A, 40% group B, and 20% group C interspersed throughout the watershed. The land use is 90% residential area that is 30% impervious and 10% paved roads with curbs. Assume AMC II conditions.

a) Report the average curve number.

b) Report the runoff in inches.

References

Bras, R. L., (1990), <u>Hydrology, an Introduction to Hydrologic Science</u>, Addison-Wesley, Reading, MA, 643 p.

Celia, M. A., E. T. Bouloutas and R. L. Zarba, (1990), "A General Mass-Conservative Numerical Solution for the Unsaturated Flow Equation," <u>Water Resour. Res.</u>, 26(7): 1483-1496.

Chow, V. T., D. R. Maidment and L. W. Mays, (1988), <u>Applied Hydrology</u>, McGraw Hill, 572 p.

Dingman, S. L., (2002), <u>Physical Hydrology</u>, 2nd Edition, Prentice Hall, 646 p.

Dunne, T. and L. B. Leopold, (1978), <u>Water in Environmental Planning</u>, W H Freeman and Co, San Francisco, 818 p.

Eagleson, P. S., (1970), <u>Dynamic Hydrology</u>, McGraw-Hill Book Company, 462 p.

Gardner, W. and J. A. Widstoe, (1921), "Movement of Soil Moisture," <u>Soil Sci.</u>, 11: 215-232.

Gerald, C. F., (1978), <u>Applied Numerical Analysis</u>, 2nd Edition, Addison Wesley, Reading, Massachusetts, 518 p.

Green, W. H. and G. Ampt, (1911), "Studies of Soil Physics. Part I - the Flow of Air and Water through Soils," <u>J. Agric. Sci</u>, 4: 1-24.

Horton, R. E., (1939), "Approach toward a Physical Interpretation of Infiltration Capacity," <u>Proc. Soil Sci. Soc. Am.</u>, 23(3): 399-417.

Linsley, R. K., M. A. Kohler and J. L. H. Paulhus, (1982), <u>Hydrology for Engineers</u>, 3rd Edition, McGraw-Hill, New York, 508 p.

Mein, R. G. and C. L. Larson, (1973), "Modeling Infiltration During a Steady Rain," <u>Water Resources Research</u>, 9: 384-394.

Parlange, J.-Y., W. L. Hogarth, D. A. Barry, M. B. Parlange, R. Haverkamp, P. J. Ross, T. S. Steenhuis, D. A. DiCarlo and G. Katul, (1999), "Analytical Approximation to the Solutions of Richards' Equation with Applications to Infiltration, Ponding, and Time

Compression Approximation," <u>Advances in Water Resources</u>, 23: 189-194.

Philip, J. R., (1957), "The Theory of Infiltration: 1. The Infiltration Equation and Its Solution," <u>Soil Sci.</u>, 83(5): 345-357.

Philip, J. R., (1969), "Theory of Infiltration," in <u>Advances in Hydroscience</u>, Edited by V. t. Chow, Vol 5, Academic Press, New York, p.215-297.

Rawls, W. J., L. R. Ahuja, D. L. Brakensiek and A. Shirmohammadi, (1993), "Infiltration and Soil Water Movement," in <u>Handbook of Hydrology, Chapter 5</u>, Edited by D. R. Maidment, McGraw-Hill, New York.

Rawls, W. J., D. L. Brakensiek and N. Miller, (1983), "Green-Ampt Infiltration Parameters from Soils Data," <u>J Hydraul. Div. Am. Soc. Civ. Eng.</u>, 109(1): 62-70.

Sharma, M. L., G. A. Gander and G. C. Hunt, (1980), "Spatial Variability of Infiltration in a Watershed," <u>Journal of Hydrology</u>, 45: 101-122.

Smith, R. E., K. R. J. Smettem, P. Broadbridge and D. A. Woolhiser, (2002), <u>Infiltration Theory for Hydrologic Applications</u>, Water Resources Monograph 15, American Geophysical Union, Washington, DC, 212 p.

Soil Conservation Service, (1972), "Hydrology," Section 4 in <u>National Engineering Handbook</u>, U.S. Dept of Agriculture, Washington, DC.

USDA-NRCS Soil Survey Division, <u>National Statsgo Database</u>, <u>http://www.ftw.nrcs.usda.gov/stat_data.html</u>.

Viessman, W., G. L. Lewis and J. W. Knapp, (1989), <u>Introduction to Hydrology</u>, 3rd Edition, Harper & Row.

Youngs, E. G., (1964), "An Infiltration Method Measuring the Hydraulic Conductivity of Unsaturated Porous Materials," <u>Soil Science</u>, 97: 307-311.

Chapter 6
Simulation of Runoff Generation
in Hydrologic Models

CHAPTER 6: SIMULATION OF RUNOFF GENERATION IN HYDROLOGIC MODELS

The sections above have focused on understanding the rainfall-runoff processes. This understanding forms the basis for a number of numerical models that represent runoff process in a conceptual way and are used to continuously simulate runoff generation in a research or operational setting. The essential feature of a simulation model is that it produces an output or series of outputs in response to an input or series of inputs. In the case of a rainfall-runoff model the inputs are characteristics of the watershed being modeled, such as drainage area and channel network geometry (size and length), topography, soil and land use characteristics and a time series of surface water input. The output is a time series of streamflow at an outlet location. Lumped models treat a whole catchment, or a significant portion of it, as a single unit, with inputs, internal state variables and outputs representing the hydrologic processes over the catchment as a whole. Distributed models divide the catchment into a number of sub areas; simulate each of them, and the interactions between them separately, maintaining different state variables for each model element, then combine the outputs to obtain catchment response. The distinction between lumped and distributed may amount to one of scale. A lumped model can be applied over a set of small watersheds that comprise a catchment to obtain a distributed model. However there is also often a difference in representation of the processes between lumped and distributed models, with distributed models being based more on the basic physical equations used to describe the processes involved and taking advantage of physically measurable attributes of the watershed, whereas lumped models use a more conceptual representation of the rainfall runoff process. There is a vast literature on hydrologic modeling that we do not address here (see Freeze and Harlan, 1969; Beven, 1989; Beven and Binley, 1992; Grayson et al., 1992a; Grayson et al., 1992b; Beven, 2000 and the descriptions in a number of hydrology texts), but we do review two of the more prominent rainfall runoff models.

TOPMODEL is a rainfall-runoff model (Beven and Kirkby, 1979) that takes advantage of topographic information (specific catchment area and wetness index) related to runoff generation, although Beven et al. (1995) prefer to consider TOPMODEL as not a hydrological modeling package, but rather a set of conceptual tools that can be used to reproduce the hydrological behavior (in particular the dynamics of surface or subsurface contributing areas) of catchments

in a distributed or semi-distributed way. The National Weather Service River Forecast System (NWSRFS) is another such model that is more conceptual in nature involving the accounting for water storage in a number of conceptual stores representing the hydrologic state of components of the watershed involved in rainfall-runoff processes. In this section we review some of the key ideas in these models as they are related to rainfall runoff processes so that the users of these models can appreciate the physical basis for conceptual process representations that these models use.

TOPMODEL

TOPMODEL is fully described by Beven et al. (1995). Streamflow is separated into surface runoff generated by surface water input on saturated contributing areas and subsurface downhill flow comprising baseflow and return flow. TOPMODEL uses four basic assumptions to relate down slope flow from a point to discharge at the catchment outlet.

A1. The dynamics of the saturated zone are approximated by successive steady state representations.

A2. The recharge rate r [m/hr] (equation 2) entering the water table is spatially homogeneous.

A3. The effective hydraulic gradient of the saturated zone is approximated by the local topographic surface gradient S (tanβ is the notation most common in TOPMODEL descriptions).

A4. The effective down slope transmissivity T of a soil profile at a point is a function of the soil moisture deficit at that point. This is commonly based on an exponential decrease of hydraulic conductivity with depth, but Ambroise et al. (1996) generalized this to also include linear and parabolic relationships.

Assuming steady state with spatially homogeneous recharge rate (A1 and A2), the down slope subsurface flow rate per unit contour width is given as (equation 2, Figure 49)

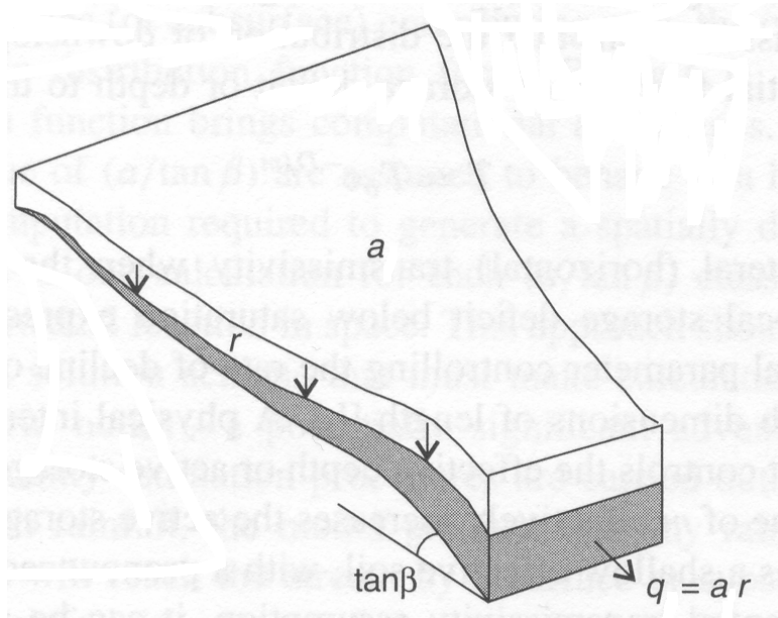$$q = r \, a \qquad\qquad\qquad (75)$$

Figure 49. Definition of the upslope area draining through a point within a catchment (from Beven, 2000).

Assuming an exponential decrease of hydraulic conductivity with depth, z,

$$K(z) = K_o e^{-fz} \tag{76}$$

and soil moisture deficit quantified in terms of the depth to the water table z_w the down slope transmissivity of the saturated part of the soil profile below the water table is

$$T(z_w) = \int_{z_w}^{\infty} K(z)dz = \int_{z_w}^{\infty} K_0 e^{-fz}dz = \frac{K_0}{f} e^{-fz_w} = T_0 e^{-fz_w} \tag{77}$$

Here K_o is the hydraulic conductivity at the surface and f sensitivity a parameter that quantifies how rapidly hydraulic conductivity decreases with depth. $T_o = K_o/f$ is the transmissivity of the soil profile. If an effective porosity θ_e is assumed, the soil moisture deficit D [m] can be approximated (equation 38) as

$$D = \theta_e z_w \tag{78}$$

This assumes moisture content at the residual moisture content above the water table. Equation (77) can then be written in terms of soil moisture deficit rather than depth to the water table as

$$T(D) = T_0 e^{-f z_w} = T_0 e^{-f D/\theta_e} = T_0 e^{-D/m} \qquad (79)$$

where $m = \theta_e / f$. Some descriptions of TOPMODEL take equation (79) as the starting point for assumption A4, with m a parameter controlling the rate of decline of transmissivity with increasing soil moisture deficit, while other TOPMODEL descriptions start from assuming (76).

Now assuming (A3) that the hydraulic gradient is equal to the local surface slope

$$q = T(D) S = T_0 e^{-D/m} S \qquad (80)$$

By combining (75) and (80) it is possible to calculate the local soil moisture deficit D

$$r\, a = T(D) S = T_0 e^{-D/m} S \qquad (81)$$

therefore

$$D = -m \ln\!\left(\frac{r\, a}{T_0 S} \right) \qquad (82)$$

This is the soil moisture deficit that results from the depth to the water table naturally adjusting so that transmissivity of the soil profile below the water table is equal to the lateral drainage of steady state recharge from the hillslope above. Under steady state drainage, r is also the per unit area baseflow discharge from the watershed, so equation (82) provides the capability to calculate soil moisture deficit at each point in a watershed based on the overall moisture condition of the watershed as expressed by baseflow r and the topographic and soils parameters a, T_o and S. TOPMODEL uses a series of steady state representations (A1) to represent the dynamics of soil moisture deficit D over a watershed using equation (82). Equation (82) may be written

$$D = -m\ln(r) - m\ln\left(\frac{a}{T_oS}\right)$$

$$= -m\ln(r) + m\ln(T_o) - m\ln\left(\frac{a}{S}\right) \tag{83}$$

$$= -m\ln(r) - m\gamma = -m\ln(r) + m\ln(T_o) - m\lambda$$

where we have denoted

$$\lambda = \ln\left(\frac{a}{S}\right) \quad \text{and} \quad \gamma = \ln\left(\frac{a}{T_oS}\right) \tag{84}$$

λ is a topographic wetness index that quantifies the dependence of soil moisture deficit on topographic parameters a and S. γ is a soil and topographic wetness index that quantifies the dependence of soil moisture deficit on soil and topographic parameters T_o, a and S. λ and γ are sometimes referred to as similarity indices because of the assumption that all locations with the same λ or γ have equivalent hydrologic behavior, in terms of soil moisture deficit and generation of runoff by saturation excess. A further consequence of this similarity is that the specific spatial locations of points with a specific λ or γ do not matter. The probability distribution as represented for example using a histogram is sufficient to describe the hydrologic response of a watershed using TOPMODEL.

The mean catchment soil moisture deficit $\overline{D}$ is obtained by spatially averaging (82) over the entire area A of the catchment.

$$\overline{D} = \frac{1}{A}\int -m\ln\left(\frac{ra}{T_oS}\right)dA = -m\ln(r) - m\overline{\gamma}$$

$$= -m\ln(r) + m\overline{\ln(T_o)} - m\overline{\lambda} \tag{85}$$

where the over bar is used to denote spatial averaging. Subtracting equation (85) from (83) one obtains

$$D = \overline{D} - m(\gamma - \overline{\gamma}) \tag{86}$$

for the case where T_o is spatially variable, and

$$D = \overline{D} - m(\lambda - \overline{\lambda}) = \overline{D} - m\left(\ln(a/S) - \overline{\lambda}\right) \tag{87}$$

for the case where T_o is assumed to be spatially constant. This explicitly establishes the basis for the topographic wetness index $\ln(a/S)$.

Equations (86) and (87) provide a way to calculate the soil moisture deficit D at each point in a catchment given the average soil moisture deficit, a soil parameter m, and the difference between the average topographic index and the local topographic index (λ or γ). m can be estimated from soil characteristics or calibrated based on the catchment recession curve. λ or γ can be estimated from a topographic map (and a map of soil characteristics in the case of γ), and we can keep track of $\overline{D}$ by water balance accounting. If D is less than 0, the soil is completely saturated and any rain on the surface will become overland flow by the process of saturation excess runoff generation. TOPMODEL therefore, through the topographic index, provides an explicit modeling of the saturation excess runoff process. This is the key distinguishing feature of TOPMODEL.

In equations (75) and (81) the rate of recharge to the water table, r, was assumed to be spatially homogeneous. With the steady state assumption, integrating this over the watershed, the subsurface response per unit area is also r. This can be expressed in terms of the average deficit by replacing D in equation (81) with (86) or (87) to obtain

$$r = e^{-\overline{D}/m}e^{-\overline{\gamma}} = T_0 e^{-\overline{D}/m}e^{-\overline{\lambda}} \tag{88}$$

This is the mean subsurface discharge from the watershed. The last expression above is for the case when T_o is spatially constant. Thus in TOPMODEL the subsurface flow is controlled by the soil characteristics T_o and m, topography (λ or γ) and the average saturation deficit of the catchment. Equation (88) gives the drainage rate of basin average soil moisture as an exponential function of the soil moisture deficit. During periods where there is no precipitation integration of this equation describes the recession curve. This property provides a way to estimate the parameter m from analysis of baseflow recession curves. This is not all of TOPMODEL, but is a summary of the main conceptual points. Added to the components above are other standard components of the water budget: interception, infiltration excess runoff generation, evapotranspiration,

snowmelt and channel routing. Several computer model implementations of TOPMODEL exist that incorporate the runoff generation components described above with representation of these other processes to provide a complete continuous simulation modeling capability.

Example 4. This example focuses only on the runoff generation aspects of TOPMODEL that can be fairly easily calculated using a Geographic Information System (GIS). Consider the Spawn Creek watershed shown in Figure 50, with parameters K_o=10 m/hr, f=5 m^{-1}, θ_e=0.2.
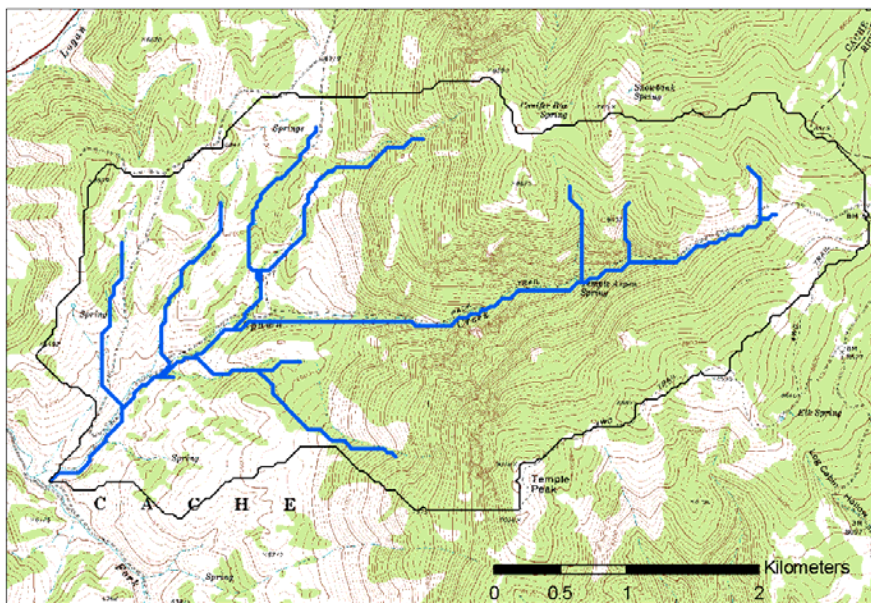
Figure 50. Channel network and drainage area delineated from a digital elevation model of the Spawn Creek area in Logan Canyon UT.

Here we assume that K_o is spatially uniform. Assume that the baseflow prior to a rainfall is Q_b = 0.8 m^3/s. We want to calculate the saturated area using TOPMODEL, and the quantity of runoff from 25 mm of rainfall. As part of calculating this we will also calculate the expansion of the saturated area during the rainfall and the map these areas. GIS methods are beyond the scope of this module, but the relatively simple capability used here can be readily applied using ArcGIS and the TauDEM software (Tarboton, 2002). Figure 50 shows the channel network and drainage area delineated from a digital elevation model of the Spawn Creek area in Logan Canyon UT. Although this is real terrain the rest of the parameters

used in this example are synthetic, for illustration purposes, and not related to physical conditions in this watershed.

This example watershed was delineated using TauDEM software with a 30 m grid digital elevation model from the National Elevation Dataset. The watershed as delineated comprises 15890 grid cells. The drainage area is therefore A=15893 x 30 x 30 = 14,303,700 m^2 = 14.3 km^2. The per unit area baseflow is therefore r=Q_b/A = 0.8/14,301,000 = 5.59 x 10^{-8} m/s. Multiplying by the number of seconds in an hour r = 5.59 x 10^{-8} m/s x 3600 s/hr = 0.0002 m/hr = 0.2 mm/hr. GIS methods were used to calculate the slope, specific catchment area and wetness index ln(a/S) for each grid cell in this area as illustrated in Figure 51.

Note that there are a few gaps in the grid where wetness index has been calculated. These are locations where the slope S is 0 and ln(a/S) is therefore mathematically undefined. These locations need to be treated separately. In TOPMODEL theory the depth to the water table is based on the adjustment of lateral transmissivity to balance the drainage from upslope under a topographic drainage. Where there is no topographic gradient (slope is 0) there can be no lateral soil moisture drainage in the theory, so these grid cells are always saturated. There are 81 grid cells with 0 slopes. Averaging ln(a/S) over the non zero slope grid cells we obtain $\bar{\lambda}$=6.9. The transmissivity parameter is $T_o = K_o$/f = 10/5 = 2 m^2/hr and m = θ_e/f = 0.2/5 = 0.04 m^{-1}. The average soil moisture deficit is evaluated using equation (85)

$$\bar{D} = -m \ln(r) + m \overline{\ln(T_o)} - m \bar{\lambda}$$

$$= -0.04 \ln(0.0002) + 0.04 \ln(2) - 0.04 \times 6.9 = 0.092 \text{ m}$$

The soil moisture deficit at each location may then be evaluated using equation (87).

$$D = \bar{D} - m\left(\ln(a/S) - \bar{\lambda}\right) = 0.092 - 0.04 \times (\ln(a/S) - 6.904)$$

Equivalently one could have computed D directly using equation (82) without the intermediate steps of evaluating $\bar{\lambda}$ and $\bar{D}$. Figure 52 shows a map of D.
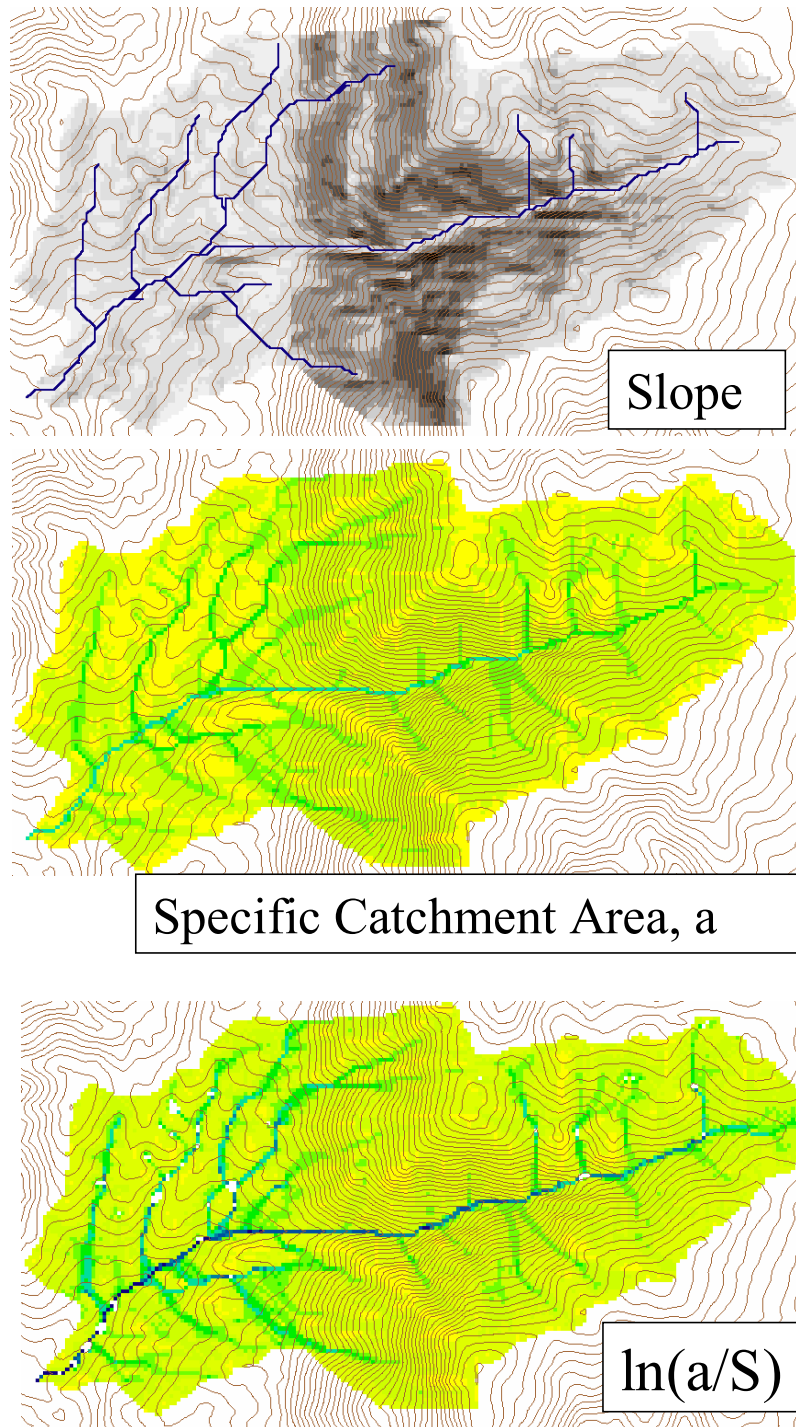
Figure 51. Slope, Specific Catchment Area and Wetness Index for Spawn Creek.
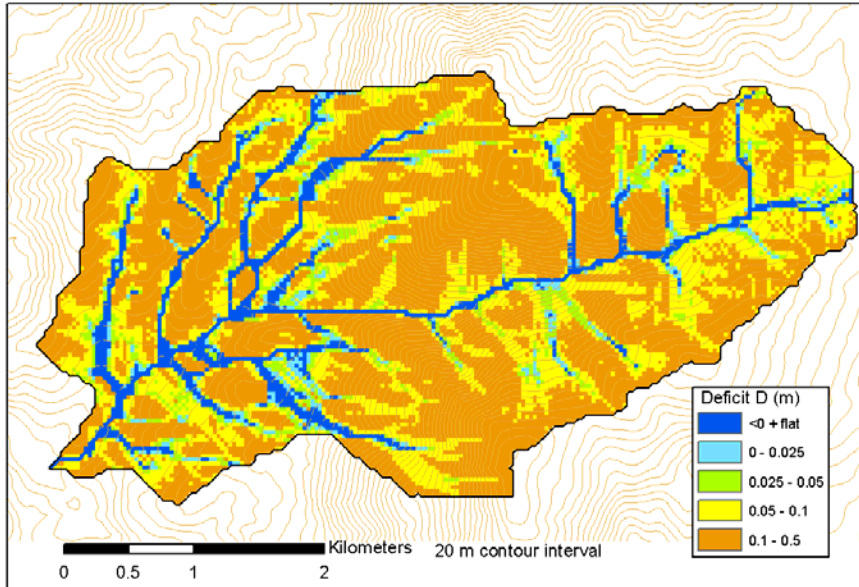
Figure 52. Soil Moisture Deficit for Spawn Creek calculated using TOPMODEL.

At the average soil moisture deficit calculated above, the dark blue shaded areas in figure 52 are already saturated and will generate saturation excess from any surface water input. There are 1246 grid cells with $D \leq 0$ which when combined with the 81 flat grid cells gives a saturated area of $(1246+81)$ x 30 x 30 = 1,194,300 m^2 = 1.2 km^2 or 1.2/14.3 = 8.3% of the watershed. The lighter blue areas have soil moisture deficit less than 0.025 m = 25 mm so will become saturated during 25 mm of surface water input. There are 546 grid cells in the range $0 < D \leq 0.025$ m that have an area 546 x 30 x 30 = 491,400 m^2 or 3.4% of the watershed. The green, yellow and brown areas require surface water inputs greater than 25 mm to generate runoff by saturation excess, but may generate runoff by infiltration excess depending upon the surface water input rate and infiltration capacity and could be calculated using the Horton, Philip or Green-Ampt model described above (examples 1-3). Considering only the runoff due to saturation excess from the 25 mm of surface water input, 25 mm of runoff is generated over 8.3% of the watershed. Over 3.4% of the watershed something between 0 and 25 mm of runoff is generated. This is evaluated using the GIS raster calculator functionality evaluating 0.025 - D and averaging this for the grid cells for which $0 < D \leq 0.025$ m. The result is 0.0113 m = 11.3 mm. The total basin runoff volume is therefore:

0.025 x 1,194,300 + 0.0113 x 491,400 = 35,410 m^3

The corresponding per unit area runoff depth is:

35,410/14,303,700 = 0.0025 m = 2.5 mm.

This represents a runoff ratio of 2.5/25 = 0.1 or 10%.

National Weather Service River Forecast System

The Sacramento Soil Moisture Accounting model has become a major tool in the National Weather Service River Forecast System (NWSRFS). The model is based on the generalized hydrologic model (Burnash et al., 1973) depicted in Figure 53 intended to represent significant hydrologic processes in the headwaters of a watershed in a conceptual manner. It is beyond the scope here to describe the model completely, but we present a brief overview of the key ideas involved in the representation of rainfall – runoff processes.
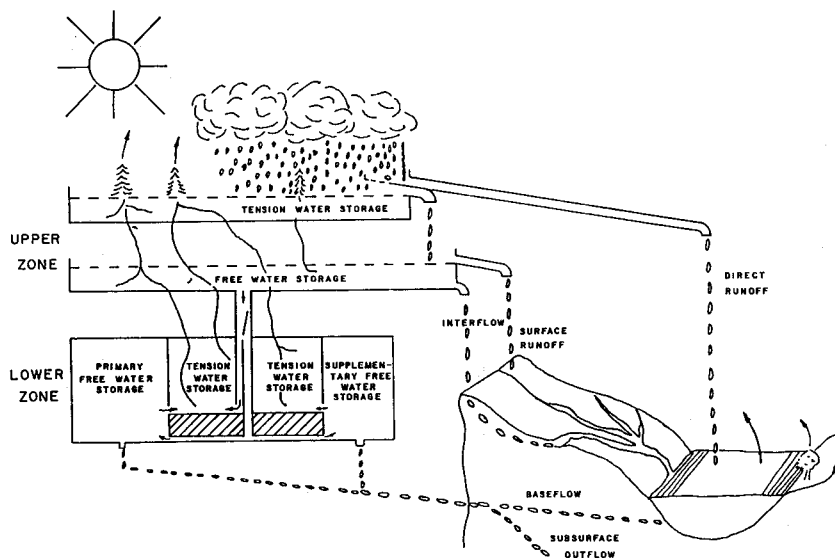

Figure 53. Generalized Hydrologic Model that serves as the basis for the National Weather Service River Forecast System (from Burnash et al., 1973).

In the Sacramento model incoming rainfall is distributed between interception, impervious areas such as lakes and streams and water input to the upper zone. The upper zone consists of interception storage, tension water storage, representing water held by capillary forces and free water storage that supplies percolation to the lower zone as well as interflow and surface water runoff. Model

parameters, which need to be user supplied or calibrated, govern the rate of water movement between the zones and the capacity of the storage zones. Surface runoff occurs when the upper zone capacity is completely filled, due to precipitation rate being in excess of the percolation rate for sufficient time.

To represent the spatial variability of infiltration capacity a linear cumulative distribution function shown as a line from the origin to point b in Figure 54 is used. The position of this line is varied, by varying the value of b, as a function of the ratio of moisture in the lower-zone storage (LZS) to the nominal capacity of this zone (LZSN). The net infiltration to the lower zone is the hatched trapezoid of Figure 54, and is a function of the current soil moisture ratio (LZS/LZSN) and the supply rate X. Interflow is calculated by a similar process. Line B of Figure 54 divides the rainfall excess triangle into two portions, surface runoff and interflow. The position of line B is fixed by multiplying b by a factor c which is greater than 1 and is also a function of LZS/LZSN. The fraction of interflow increases as soil moisture increases.
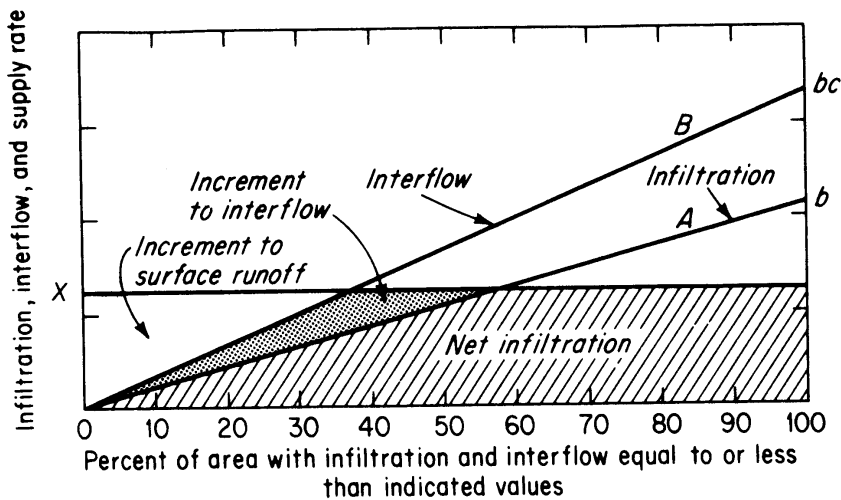
Figure 54. Infiltration–interflow function used in the Sacramento Model (from Linsley et al., 1982).

A complete flow diagram depicting all the processes represented is shown in Figure 55. There are a large number of parameters representing the storage capacities of the various stores and characterizing the rates of flow between these stores. These parameters need to be estimated for each specific watershed through calibration that takes measured precipitation inputs and minimizes a

measure of the difference between modeled and observed streamflow. Considerable research on parameter optimization exists and the reader is referred to recent papers in this area for a perspective on the methods available (e.g. Beven and Binley, 1992; Kuczera, 1997; Gupta et al., 1998; Beven, 2000).
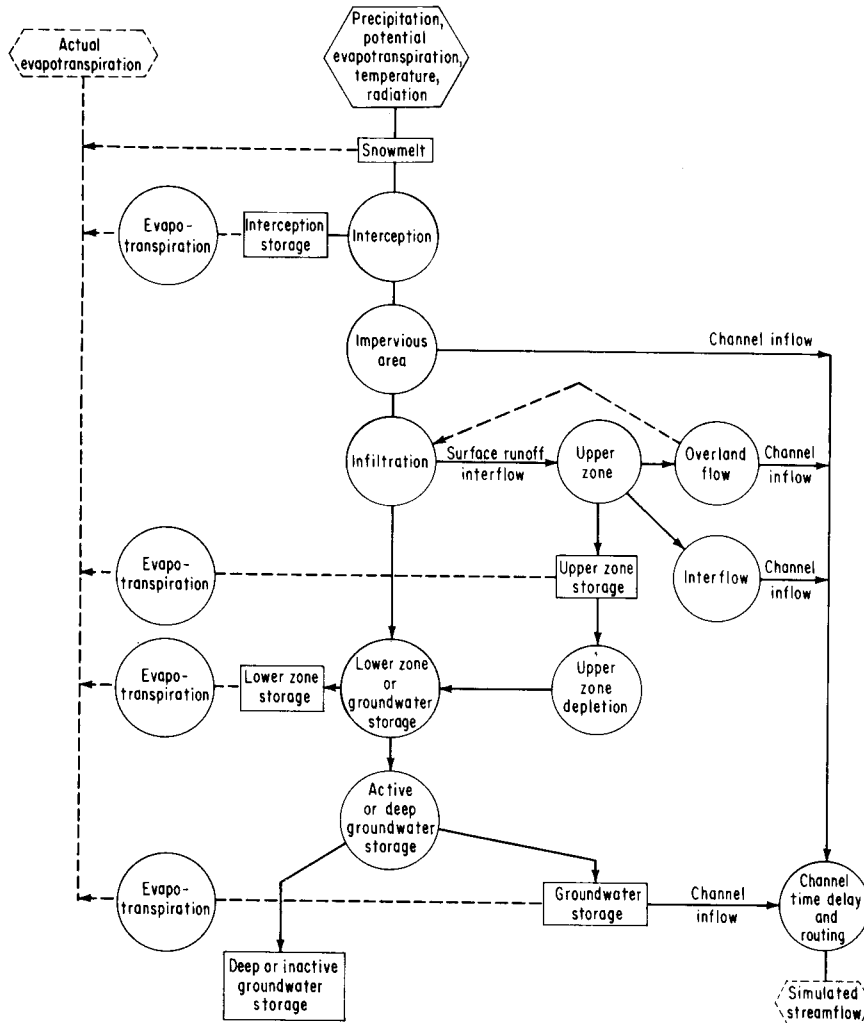

Figure 55. Flow diagram of the Sacramento Model (from Linsley et al., 1982).
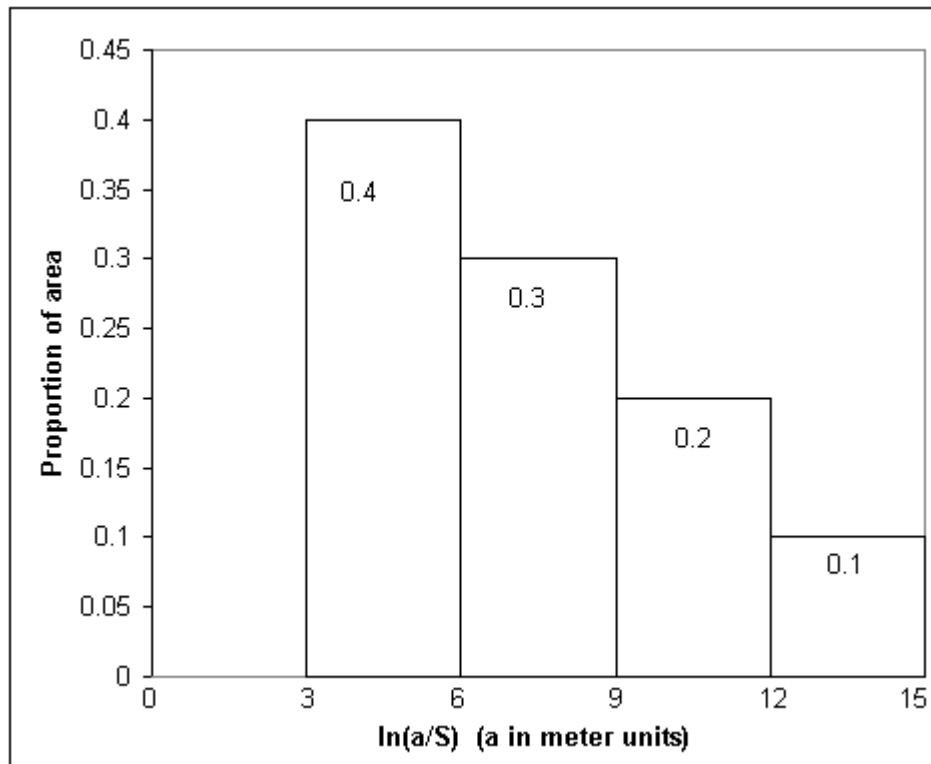
Exercises

1. The probability distribution of wetness index represented by a histogram is sufficient to describe the hydrologic response of a watershed using TOPMODEL. Consider a watershed that has TOPMODEL wetness index $\ln(a/S)$ distributed according to the histogram shown

The watershed has TOPMODEL parameters: Spatially homogeneous $K_o= 4$ m/hr, $f= 2$ m^{-1}, antecedent baseflow $Q_b = 12$ m^3/s, drainage area $= 400$ km^2, effective porosity of unsaturated zone $= 0.2$.

a) Estimate the TOPMODEL $\bar{\lambda}$ parameter for this watershed by averaging the histogram above.

b) Estimate the recharge parameter r by dividing baseflow by the drainage area and expressing the result in m/hr.

c) In TOPMODEL locations with wetness index $\ln(a/S)$ greater than a threshold are saturated to the surface. This threshold can be obtained from setting D=0 in equation (82) or (83) and solving for $\ln(a/S)$. Report the threshold $\ln(a/S)$ above which saturation occurs for the antecedent conditions given.

d) The fraction of watershed that is initially saturated is obtained by integrating the histogram over values larger than the threshold determined in (c). Report the fraction of watershed that is initially saturated.

e) Following infiltration of rainfall the saturated area expands to encompass all locations where D was less than the rainfall. Use equation (82) or (83) to determine the threshold $\ln(a/S)$ corresponding to D=0.025 m (25mm).

f) Integrate the histogram over values larger than the threshold determined in (e) to determine the fraction of watershed that is saturated at the end of a 25 mm rainstorm.

g) Estimate the volume of runoff from 25 mm of rain, by summing the runoff from the initially saturated area and the area that becomes saturated during the storm. Report your answer on a per unit total area basis.

h) Equation (88) gives the baseflow in terms of average soil moisture deficit $\overline{D}$. This decreases by 25 mm due to infiltration during the storm and this equation may be used to calculate the corresponding increase in r which corresponds to an increase in baseflow. Use equation (88) to determine the baseflow that you expect after the direct runoff hydrograph from the 25 mm of rainfall has receded. Report your result in m^3/s.

See Online Resource

Take the Final Exam!

References

Ambroise, B., K. J. Beven and J. Freer, (1996), "Toward a Generalization of the Topmodel Concepts: Topographic Indices of Hydrological Similarity," <u>Water Resources Research</u>, 32(7): 2135-2145.

Beven, K., (1989), "Changing Ideas in Hydrology - the Case of Physically-Based Models," <u>Journal of Hydrology</u>, 105: 157-172.

Beven, K. and A. Binley, (1992), "The Future of Distributed Models: Model Calibration and Uncertainty Prediction," <u>Hydrological Processes</u>, 6: 279-298.

Beven, K., R. Lamb, P. Quinn, R. Romanowicz and J. Freer, (1995), "Topmodel," Chapter 18 in <u>Computer Models of Watershed Hydrology</u>, Edited by V. P. Singh, Water Resources Publications, Highlands Ranch, Colorado, p.627-668.

Beven, K. J., (2000), <u>Rainfall Runoff Modelling: The Primer</u>, John Wiley, Chichester.

Beven, K. J. and M. J. Kirkby, (1979), "A Physically Based Variable Contributing Area Model of Basin Hydrology," <u>Hydrological Sciences Bulletin</u>, 24(1): 43-69.

Burnash, R. J. C., R. L. Ferral and R. A. Maguire, (1973), "A Generalized Streamflow Simulation System: Conceptual Models for Digital Computers," Joint Federal State River Forecast Center, Sacramento, CA.

Freeze, R. A. and R. L. Harlan, (1969), "Blueprint for a Physically-Based, Digitally Simulated Hydrologic Response Model," <u>Journal of Hydrology</u>, 9: 237-258.

Grayson, R. B., I. D. Moore and T. A. McMahon, (1992a), "Physically Based Hydrologic Modeling 1. A Terrain-Based Model for Investigative Purposes," <u>Water Resources Research</u>, 28(10): 2639-2658.

Grayson, R. B., I. D. Moore and T. A. McMahon, (1992b), "Physically Based Hydrologic Modeling 2. Is the Concept Realistic," <u>Water Resources Research</u>, 28(10): 2659-2666.

Gupta, H. V., S. Sorooshian and P. O. Yapo, (1998), "Toward Improved Calibration of Hydrologic Models: Multiple and Noncommensurable Measures of Information," <u>Water Resources Research</u>, 34(4): 751-763.

Kuczera, G., (1997), "Efficient Subspace Probabilistic Parameter Optimization for Catchment Models," <u>Water Resources Research</u>, 33(1): 177-185.

Linsley, R. K., M. A. Kohler and J. L. H. Paulhus, (1982), <u>Hydrology for Engineers</u>, 3rd Edition, McGraw-Hill, New York, 508 p.

Tarboton, D. G., (2002), "Terrain Analysis Using Digital Elevation Models (Taudem)," Utah Water Research Laboratory, Utah State University, http://www.engineering.usu.edu/dtarb.

APPENDICES

SYMBOLS AND NOTATION

GLOSSARY

SYMBOLS AND NOTATION

Physical constants

g: acceleration due to gravity, g= 9.81 m/s^2, 32.2 ft/s^2.

ρ_{water}: density of water at 4°C, ρ_{water}= 1000 kg/m^3, 62.5 lb/ft^3.

μ_{water}: dynamic viscosity of water, μ_{water}= 1.05×10^{-3} N.s/m^2.

Math constants

e: natural logarithm base, e= 2.718281828459…

π: ratio of a circle circumference to its diameter,
π= 3.14159265358979…

Notation

For each quantity the dimensions are given in terms of the fundamental dimensions of length, L, time, T, mass, M, and force, F.

A: area, either drainage area or flow cross sectional area [L^2]

a: specific catchment area [L]

C(ψ): specific moisture capacity, dθ/dψ [1/L]

D(θ): soil water diffusivity [L^2/T]

d: effective grain diameter [L]

D: soil moisture deficit [L]

$\overline{D}$: catchment mean soil moisture deficit [L]

E: evapotranspiration rate [L/T]

F: cumulative depth of infiltrated water [L]

f: infiltration rate [L/T]

f$_1$: steady state infiltration capacity parameter in Horton's equation [L/T]

F$_a$: depth of water retained in watershed, SCS method [L]

f$_c$: infiltration capacity [L/T]

f$_o$: initial infiltration capacity parameter in Horton's equation [L/T]

F$_p$: cumulative depth of infiltration at ponding [L]

f$_t$: infiltration rate at time t [L/T]

h: hydraulic head [L]

I$_a$: initial abstraction, SCS method [L]

I$_t$: Antecedent precipitation index at day t [L]

K(θ): hydraulic conductivity as a function of θ [L/T]

K: hydraulic conductivity [L/T]

k: intrinsic permeability [L^2]

k: recession factor parameter in Horton's equation [1/T]

k: recession factor parameter in antecedent precipitation index [Unitless]

K$_p$: hydraulic conductivity parameter in Philip's equation [L/T]

K_{sat}: saturated hydraulic conductivity [L/T]

L: depth to the wetting front [L]

M_m: mass of mineral grains [M]

$M_{s\ dry}$: mass of soil sample when dry [M]

$M_{s\ wet}$: mass of soil sample when wet [M]

n: porosity of soil [Unitless]

P: precipitation rate [L/T]

P: precipitation depth [L]

P: Combined moisture content difference and wetting front suction
   product Green-Ampt model parameter [L]

p: pressure [F/L^2]

P_t: precipitation at day t [L]

Q: flow rate, discharge [L^3/T]

Q: runoff rate [L/T]

q: lateral moisture flux across a unit contour width [L^2/T]

q: specific discharge [L/T]

q_{cap}: lateral flow capacity of soil profile [L^2/T]

r: runoff [L/T]

R_e: Reynold's number [Unitless]

S: potential maximum retention, SCS method [L]

S: tan(β), slope [Unitless]

S_d: degree of saturation [Unitless]

S_e: effective saturation [Unitless]

S_p: sorptivity in Philip's equation [L/T$^{0.5}$]

T: transmissivity [L^2/T]

T_o: transmissivity of a saturated soil profile [L^2/T]

t_p: time to ponding [T]

v: flow velocity [L/T]

V_a: volume of air in a soil sample [L^3]

V_m: volume of mineral grains [L^3]

V_s: total volume of a soil sample [L^3]

V_w: volume of water in a soil sample [L^3]

w: relative wetness of soil [Unitless]

w: surface water input [L/T]

z: depth below soil surface [L]

z_w: depth of water table [L]

$\Delta\theta$: difference between initial and saturated moisture contents
   [Unitless]

γ: soil topographic wetness index [ln(T/L)]

λ: topographic wetness index [ln(L)]

θ: volumetric moisture content [Unitless]

θ_a: plant available moisture content [Unitless]

θ_e: effective porosity [Unitless]

θ_{fc}: field capacity [Unitless]

θ_o: initial moisture content [Unitless]

θ_{pwp}: permanent wilting point [Unitless]

θ_r: residual or irreducible moisture content [Unitless]

ρ_b: bulk density of soil [M/L^3]

ρ_m: mineral density of soil particles [M/L^3]

$\psi(\theta)$: pressure head as a function of moisture content [L]

ψ: pressure head [L]

ψ_a: air entry head [L]

ψ_f: suction head [L]

GLOSSARY

Anisotropic medium

A medium having properties that vary depending on the direction of measurement. An example would be hydraulic conductivity that may be different in a vertical and lateral direction due to layering and alignment of the soil grains.

Antecedent moisture conditions

Soil-moisture content preceding a given storm.

Baseflow

Stream discharge derived from groundwater seepage; a time-based definition relating to runoff sustained without precipitation, largely composed of groundwater; outflow from extensive groundwater aquifers, which are recharged by water percolating down through the soil mantle to the water table (Butler, 1957; Langbein and Iseri, 1960; Tischendorf, 1969).

Bulk density

The dry density of the soil; the mass of the solid mineral and organic components of soil divided by the total volume.

Capillary fringe

The unsaturated zone containing water in direct hydraulic contact with the water table, and held above the water table by capillary forces (Butler, 1957) resulting in a negative pressure potential in the soil matrix (Hillel, 1971).

Contributing area

The area upslope of any point on a watershed or topographic surface; the area of a catchment contributing to storm runoff (Betson, 1964), dimensioned as $[L^2]$.

Darcy's Law

An experimentally-derived relationship stating that rate of fluid flow through a permeable medium is directly proportional to the hydraulic gradient and to the hydraulic conductivity. It is valid only for flow velocities within the laminar range. Being originally stated for saturated flow, it was extended by Richards in 1931 to

embrace unsaturated flow. (Swatzendruber, 1960; Hillel, 1971; Wind, 1972).

Depression storage

The volume of water, forming part of surface detention, which is contained in small natural depression in the land surface during or shortly after rainfall, none of which runs off (Horton, 1933; Horton, 1935; Langbein and Iseri, 1960; Tischendorf, 1969).

Distributed hydrologic model

A hydrologic model that allows for spatial variability of model parameters and inputs. The spatial resolution of distributed parameters and inputs depends on available physical data.

Drainable porosity

The difference between moisture content at saturation and at field capacity; quantifies the porosity of the soil that gravity drains within a time frame of a few days. Quantitatively, it is defined as porosity minus the field capacity moisture content corresponding to a pressure head between -100 and -500 cm.

Elevation head

The elevation above an arbitrary horizontal datum, also called gravitational head.

Field Capacity

The moisture content remaining in soil after a few days of gravity drainage. Quantitatively, it is defined as the moisture content corresponding to a pressure head between -100 and -500 cm.

Hydraulic conductivity

A coefficient of proportionality describing the rate at which water can move through a porous medium under a hydraulic gradient. A function of both the porous medium and fluid properties. Hydraulic conductivity depends upon the pore geometry determined by soil texture and structure and the fluid viscosity and density. The hydraulic conductivity is at its maximum when the soil is saturated and decreases with decreasing water content or increasing water tension.

Hydraulic head

The equivalent height of a liquid column corresponding to a given pressure (Hillel, 1971); usually called simply "head" of the fluid (Dingman, 2002). Hydraulic head is measured with respect

to an arbitrary horizontal datum and is the sum of pressure head and elevation head.

Hydraulic gradient

The gradient of hydraulic head that induces flow of water, expressed as head drop per unit distance in the direction of flow.

Hydrograph

A graph or table of stream discharge versus time.

Hyetograph

A graph or table of water input (rainfall or snowfall) or runoff generated versus time.

Hysteresis

A phenomenon that occurs during the draining and wetting of soils whereby the relationship between soil moisture content and negative pressure head depends upon the history of drying and wetting.

Infiltration capacity, f_c

The maximum rate at which a given soil can absorb falling rain (or melting snow), when it is in a specified condition (Horton, 1933; Horton, 1941).

Infiltration excess overland flow

Overland flow that occurs when the infiltration capacity drops below the water input rate from rainfall or snowmelt.   Also known as Hortonian overland flow and saturation from above.

Infiltration rate, f

The volume rate of the passage of water through the surface of the soil, via pores or small opening, into the soil (Horton, 1933; Horton, 1941).

Interception

Water retained in the vegetation canopy for some period, however short, after rain has struck the vegetative material above the soil surface (Tischendorf, 1969).

Interflow

An intermediate component of runoff, between overland flow and groundwater flow.   Interflow is made up of subsurface flow,

which never reaches the water table but instead returns to form surface runoff (Amerman, 1965).

Intrinsic permeability

A property of a porous medium which determines the ease with which a fluid will move through the matrix. Intrinsic permeability depends on the pore geometry determined by soil texture and structure. It does not contain any fluid properties so is more general than hydraulic conductivity because it applies to the flow of all fluids through the porous medium. It is equal to Nd^2 where N is a pore shape factor and d is a pore size scale measure (such as the average pore diameter or grain size).

Kinetic energy

The energy associated with the motion of a substance (Serway, 1998). For fluid flow kinetic energy is proportional to the square of the velocity.

Lateral moisture flux [L²/T]

The flow rate in a lateral or horizontal direction through a soil profile. This is normalized by the corresponding width so is expressed as volume per unit width per time. This is integrated over the full depth of the soil profile conducting flow laterally.

Lateral flow capacity [L²/T]

The capacity of a soil profile to conduct flow in a lateral or horizontal direction. When lateral flow is driven by the hydraulic gradient this maximum capacity is generally slope or topographic gradient times the transmissivity.

Lumped hydrologic model

A hydrologic model with spatially averaged parameters and inputs. Lumped model parameters often must be developed through optimization or calibration rather than calculating directly from field measurements or existing data.

Manometer

A device for measuring pressure, one end of a U-shaped tube containing liquid is open to the atmosphere, and the other end is connected to a system of unknown pressure.

Overland flow

Part of streamflow which originates from rain which fails to infiltrate the soil surface at any point as it flows over the land

surface to stream channels (Langbein and Iseri, 1960; Tischendorf, 1969; Hewlett and Nutter, 1970).

Partial area concept

Storm runoff generated by only a part of the surface of a catchment (Betson, 1964).

Piezometer

A tube used to measure the head of fluids of constant density. The hydraulic head at any "point" in a ground-water or porous medium flow can be measure as the height above the selected arbitrary datum to which water rises in a tube connecting the "point" to the atmosphere.

Ponding time

Time to the first occurrence of ponding from the beginning of a surface water input event (such as a rainstorm).

Porosity

The volume of voids or pore spaces in a soil or rock expressed as a fraction of the bulk volume.

Potential energy

Gravitational potential energy, is the energy of an object resulting from its position in a gravitational field.

Precipitation excess

The surface water input that does not infiltrate and ponds on the surface contributing to depression storage or overland flow runoff.

Pressure head

The equivalent height of a liquid column corresponding to a given pressure. Pressure head is measured relative to the height at which pressure is measured and is pressure divided by the weight density of water.

Return flow

Infiltrated water which returns to the land surface after having flowed for some distance in the subsurface.

Runoff

Overland and subsurface flow components that contribute to the quickflow in a stream, leaving a watershed within a time scale of about a day following surface water input. Runoff is also used to refer to all water leaving a watershed, the sum of quick flow, base flow and groundwater outflow.

Saturation excess overland flow

Surface runoff occurring when the soil is saturated. This is also called the Dunne mechanism or saturation from below and occurs most commonly in humid and vegetated areas with shallow water tables, where infiltration capacities of the soil surface are high relative to normal rainfall intensities. Saturation excess overland flow is most common on near-channel wetlands (Betson, 1964; Dunne and Black, 1970).

Soil particle density

The weighted average density of the mineral grains making up the soil; mass of the soil divided by the volume of mineral grains (Dingman, 2002).

Soil texture

The classification of a soil based on the distribution of particle sizes within the soil. Clay is defined as particles with diameter less than 0.002 mm. Silt has a particle diameter range from 0.002 mm to 0.05 mm and sand has particle diameter range from 0.05 to 2 mm. The USDA soil texture triangle assigns names, such as sandy loam, silty clay loam, sandy clay based upon the relative fractions of particles in these size ranges.

Soil water diffusivity

A property that quantifies the flux of water per unit gradient of water content. This is a quantity that appears in Richard's equation describing the flow of water in unsaturated soil.

Sorptivity

A parameter expressing the macroscopic balance between capillary forces pulling water in to a soil and hydraulic conductivity that limits the flow rate. This parameter appears in Philip's solution to Richards equation for unsaturated flow and is the proportionality constant in the expression indicating that in the absence of other forces the quantity of water absorbed is proportional to the square root of time.

Specific catchment area

Contributing area per unit contour width; dimensioned as [L].

Specific discharge

The volume rate of flow per unit area through a porous medium.

Specific moisture capacity

A parameter representing the rate of change of soil moisture content with respect to pressure head, that appears in Richard's equation.

Subsurface runoff

The movement of subsurface storm water within the soil layers to stream channels at a rate more rapid than the usual groundwater flow (Hursch, 1936).

Subsurface stormflow

The part of streamflow which derives from the lateral subsurface flow of water which discharges into the stream channel so quickly as to become part of the stream flow associated directly with a given rainstorm.

Surface detention

That portion of rainwater, other than depression storage, which remains in temporary storage on the land surface as it moves downslope by overland flow and either runs off, is evaporated or is infiltrated after the rain ends (Horton, 1933; Horton, 1937; Butler, 1957; Chow, 1964).

Surface runoff

The stream outflow from a region.

Tensiometer

A device used to directly measure the capillary tension of soil moisture under field conditions; as explained in Dingman (2002), a tensiometer "consists of a hollow metal tube, of which one end is closed off by a cup of porous ceramic material and the other end is fitted with a removable airtight seal. A manometer, vacuum gage, or pressure transducer is attached to the end of the tube. The tube is completely filled with water and inserted into the soil to the depth of the measurement. Since the water in the tube is initially at a pressure somewhat above atmospheric, there is a pressure-induced flow through the porous cup into the soil

that continues until the tension inside the tube equals that in the
soil. When this equilibrium is reached, the manometer or gage
gives the tension in the tube and in a roughly spherical region
immediately surrounding the cup."

Throughfall

The portion of rainfall which penetrates the vegetation and
reaches the surface through spaces in the vegetative canopy and
as drip from leaves, twigs and stems. Throughfall is precipitation
that is not retained as interception.

Throughflow

Downslope flow of water occurring physically within the soil
profile, usually under unsaturated conditions except close to
flowing streams, occurring where permeability decreases with
depth (Kirkby and Chorley, 1967).

Topmodel

An approach for predicting saturation overland flow based on the
idea that
the location and size of zones of surface saturation that generate
saturation overland flow can be predicted based on the
distributed topographic attributes and soil properties of a
catchment (Beven and Kirkby, 1979).

Topographic wetness index

The ration of specific catchment area to slope or its natural
logarithm, denoted $\ln(a/S)$, or $\ln(a/\tan\beta)$. The topographic
wetness index quantifies the dependence of soil moisture deficit
on catchment area and slope. The probability distribution of the
topographic index can be used to describe the hydrologic
response of watersheds.

Transmissivity

The integral over soil depth of hydraulic conductivity. If the soil
is relatively homogenous and flow paths are horizontal,
transmissivity may be defined as the depth times the hydraulic
conductivity.

Variable source area

That portion of a watershed contributing to saturation excess
overland flow.

Viscosity

Used in fluid flow to characterize the degree of internal friction in the fluid. This internal friction or viscous force is associated with the resistance of two adjacent layers of the fluid against moving relative to each other (Serway, 1998).

Volumetric soil moisture content

The ratio of water volume to soil volume (Dingman, 2002).

References

Amerman, C. R., (1965), "The Use of Unit-Source Watershed Data for Runoff Prediction.," <u>Water Resources Research</u>, 1(4): 499-508.

Betson, R. P., (1964), "What Is Watershed Runoff?," <u>Journal of Geophysical Research</u>, 68: 1541-1552.

Beven, K. J. and M. J. Kirkby, (1979), "A Physically Based Variable Contributing Area Model of Basin Hydrology," <u>Hydrological Sciences Bulletin</u>, 24(1): 43-69.

Butler, S. S., (1957), <u>Engineering Hydrology</u>, Prentice-Hall, New Jersey, 356 p.

Chow, V. T., ed. (1964), <u>Handbook of Applied Hydrology</u>, McGraw-Hill, New York.

Dingman, S. L., (2002), <u>Physical Hydrology</u>, 2nd Edition, Prentice Hall, 646 p.

Dunne, T. and R. D. Black, (1970), "An Experimental Investigation of Runoff Production in Permeable Soils," <u>Water Resources Research</u>, 6(2): 478-490.

Hewlett, J. D. and W. L. Nutter, (1970), "The Varying Source Area of Streamflow from Upland Basins," <u>Symposium on Interdisciplinary Aspects of Watershed Management</u>, Montana, p.65-83.

Hillel, D., (1971), <u>Soil and Water: Physical Principles and Processes</u>, Academic Press, New York and London, 288 p.

Horton, R. E., (1933), "The Role of Infiltration in the Hydrological Cycle," <u>Trans. Am. Geophys. Union</u>, 14: 446-460.

Horton, R. E., (1935), "Surface Runoff Phenomena - Part I. Analysis of the Hydrograph," Horton Hydrological Laboratory, Vorheesville, New York.

Horton, R. E., (1937), "Hydrologic Interrelations of Water and Soils," Proc. Soil Sci. Soc. Am, 1: 401-429.

Horton, R. E., (1941), "An Approach toward a Physical Interpretation of Infiltration Capacity," Proc. Soil Sci. Soc. Am, 5: 399-417.

Hursch, C. R., (1936), "'Storm-Water and Absorption', in 'Discussion on List of Terms with Definitions; Report of the Committee on Absoption and Transpiration'," Trans. Am. Geophys. Union, 17: 301-302.

Kirkby, M. J. and R. J. Chorley, (1967), "Throughflow, Overland Flow and Erosion," Bull. Intern. Assoc. Sci. Hydrology, 12.

Langbein, W. B. and K. T. Iseri, (1960), "General Introduction and Hydrologic Definitions: Manual of Hydrology. Part I: General Surface-Water Techniques," Water Supply Paper 1541-A, US Geological Survey.

Serway, R. A., ed. (1998), Principles of Physics, Saunders College Publishing.

Swatzendruber, D., (1960), "Water Flow through a Soil Profile as Affected by the Least Permeable Layer," J. Geophys. Res., 65: 4037-4042.

Tischendorf, W. G., (1969), "Tracing Stormflow to Varying Source Area in Small Forested Watershed in the Southeastern Piedmont," Thesis, University of Georgia.

Wind, G. P., (1972), "A Hydraulic Model for the Simulation of Non-Hysteretic Vertical Unsaturated Flow of Moisture in Soils," J. Hydrology, 15: 227-246.